LR 25048
JANUARY 1972

VOLUME I

FINAL REPORT

CHARACTERISTICS OF HINGELESS ROTORS WITH HUB MOMENT FEEDBACK CONTROLS INCLUDING EXPERIMENTAL ROTOR FREQUENCY RESPONSE

W.A. KUCZYNSKI
G.J. SISSINGH

Submitted to: U.S. Army Air Mobility Research
and Development Laboratory
Ames Directorate
Moffett Field, California

PHASE 2: CONTRACT NAS 2-5419

LOCKHEED-CALIFORNIA COMPANY • BURBANK, CALIFORNIA
A DIVISION OF LOCKHEED AIRCRAFT CORPORATION

FOREWORD

This document has been prepared for the U. S. Army Air Mobility Research and Development Laboratory in fulfillment of Phase 2 of the Lockheed/AMRDL High Advance Ratio Research Program (Contract NAS2-5419). The report is composed of two volumes; Volume 1 constitutes the program final report and Volume 2 serves as a data report.

The authors gratefully acknowledge the support of the many AMRDL and Lockheed personnel who participated in the program. Particular thanks are extended to the AMRDL project engineer Mr. David Sharpe and his associate Dr. Robert Ormiston who offered valuable technical suggestions.

SUMMARY

The second phase of the Lockheed/AMRDL High Advance Ratio Research Program has recently been completed. The study had as its primary objectives

- the investigation of the dynamic characteristics of hingeless rotors with hub moment feedback controls and
- the acquisition of experimental hingeless rotor transfer functions.

The experimental model was composed of the Phase 1 direct swashplate control rotor equipped with an electrical first order lag hub moment feedback control system. Direct control of the rotor by positioning the swashplate was maintained so that the system could be operated in either open loop or closed loop modes.

An extensive test program was conducted in the AMRDL 7 x 10 foot wind tunnel at Moffett Field, California. Rotor transfer functions were calculated from data acquired during open loop frequency response tests. The transfer functions are linear and present the rotor longitudinal and lateral frequency responses to collective pitch, longitudinal cyclic pitch, and lateral cyclic pitch. They were determined for advance ratios ranging from 0 to 1.44 and rotor flapping frequencies from 1.3Ω to 2.32Ω. (The Lock number of the tested rotor was 5.0.) Excitation frequencies up to 24 Hz were considered resulting in nondimensional frequency ratios as high as $\omega/\Omega = 4.4$. The experimental curves reveal that the response of rotor peaks when the excitation frequency is in resonance with the first flap mode rotating natural frequency. Since the excitation originates in stationary coordinates the increased response occurs twice, when $\frac{\omega}{\Omega} \simeq P\text{-}1$ and $\frac{\omega}{\Omega} \simeq P\text{+}1$. No other significant rotor response characteristic which can be definitely associated with the involvement of other rotor modes (e.g., 1st inplane, 2nd flap, etc.) was detected. The rotor transfer functions also show that within the tested advance ratio range the damping of the blade flapping motion increases with

μ. This is indicated by a reduction (with increased μ) in both the relative peaking of the rotor response and the frequency at which the maximum response occurs.

A thorough experimental stability analysis of the rotor and control system was conducted. A classical frequency-analysis approach was employed wherein closed loop stability margins were determined from open loop transfer functions. Through the use of an on-line transfer function analyzer, the experimental closed loop stability of the system was always known before any loop was actually closed. The end results of the analysis show that the stability of the total system is reduced by increases in advance ratio (μ), control system gain (A) and control system time constant (1/L). The intermediate results also indicate that the primary pitch loop is the least stable of the four loops which comprise the system. It is, in fact, less stable than the total closed loop system. Since the pitch and roll loops are coupled through the rotor the implication is that for the system tested, rotor pitch/roll coupling is stabilizing.

Closed loop steady state tests were conducted at the completion of the stability investigations. When the time constants of the control filters were infinite (i.e., L = 0) and the phase angles Δ and Γ equal to 0 deg the rotor moment responses to steady θ_o and α disturbances were zero. The rotor also exhibited only longitudinal response to θ_{long} and lateral response to θ_{lat}. These characteristics

$$\left.\begin{aligned} \frac{\partial M_R}{\partial \alpha} &= \frac{\partial L_R}{\partial \alpha} = 0 \\ \frac{\partial M_R}{\partial \theta_o} &= \frac{\partial L_R}{\partial \theta_o} = 0 \\ \frac{\partial M_R}{\partial \theta_{long}} &= \frac{\partial L_R}{\partial \theta_{lat}} = 2K_\beta \\ \frac{\partial M_R}{\partial \theta_{lat}} &= \frac{\partial L_R}{\partial \theta_{long}} = 0 \end{aligned}\right\} \quad \begin{aligned} L &= 0 \\ \Delta &= 0 \text{ deg} \\ \Gamma &= 0 \text{ deg} \end{aligned}$$

are independent of μ, p, γ and A for A $\neq$ 0 providing the system is stable.

If $L \neq 0$ these excellent response characteristics are compromised. The control system can no longer completely alleviate the rotor response to θ_o and α disturbances. Further pitch/roll coupling is generated by all excitations and the magnitudes of the response derivatives become functions of γ, p, μ and the ratio A/L. Closed loop frequency response tests indicate that the first order lag hub moment feedback control system is an effective gust alleviation device for steady state and very low frequency ($\omega/\Omega < .1$) external disturbances. It is also capable of automatically decoupling the rotor pitching and rolling responses to similar low frequency longitudinal and lateral control commands. However, as the excitation frequencies increase, the system tends to become totally ineffective and may even be deteriorating. The data show that within a certain frequency range extreme pitch/roll coupling is generated and the magnitude of the closed loop rotor response to collective pitch is amplified above the similar open loop response. These characteristics clearly identify the need for control system optimization with respect to transient response criteria.

Several open loop tests were conducted to determine rotor steady state response derivatives similar to those obtained during the Phase I program. A higher rotor speed was considered in order to achieve a lower nondimensional flapping frequency. Moment and lift derivatives with respect to α, θ_o, θ_s and θ_c were determined at 1200 rpm ($P = 1.17$) for advance ratios from 0.07 to 0.44.

The theoretical analysis conducted in support of the program was based upon the rigid blade flapping model described in Reference 1 coupled with appropriate control system and cyclic pitch actuator equations of motion. The mathematical model and methods by which the equations of motion were solved are fully described in Section 7. Since the rotor represents the only component of the system which is not exactly described mathematically the applicability of the theoretical approach is demonstrated by comparing a limited number of theoretical and experimental rotor transfer functions. The results

of the correlation show that the theoretical rotor frequency response compares very well with test results, particularly at low rotor rotational speeds. The slight disagreements in the magnitudes of the responses are consistent with the results of Reference 1.

TABLE OF CONTENTS

Section		Page
	FOREWORD	iii
	SUMMARY	v
	LIST OF FIGURES	xi
	LIST OF TABLES	xv
1	INTRODUCTION	1
2	SYMBOLS	7
3	MODEL DESCRIPTION	11
4	DATA ACQUISITION	15
	INSTRUMENTATION	15
	DATA ACQUISITION EQUIPMENT	16
5	CHECKOUT AND WHIRL TESTS	19
	DISCUSSION OF HOVER TEST DATA	20
6	WIND TUNNEL TEST	29
	TEST PROGRAM	29
	DISCUSSION OF WIND TUNNEL TEST DATA	34
7	THEORY	95
	MATHEMATICAL MODEL	95
	EQUATIONS OF MOTION	96
	SOLUTION OF EQUATIONS OF MOTION	98
	COMPARISON OF THEORETICAL AND EXPERIMENTAL RESULTS	105
8	CONCLUDING REMARKS	115
9	REFERENCES	117

APPENDIX

A	ANALYSIS OF FREQUENCY RESPONSE DATA	A-1
B	A DISCUSSION OF THE ROTOR 'RESIDUE' FREQUENCY RESPONSE	B-1
C	EXPERIMENTAL ROTOR TRANSFER FUNCTIONS	Vol 2

TABLE OF CONTENTS (CONT'D)

Section		Page
D	EXPERIMENTAL TRANSFER FUNCTIONS FROM WHICH TOTAL PITCH LOOP AND TOTAL ROLL LOOP STABILITIES WERE DETERMINED	Vol 2
E	EXPERIMENTAL CLOSED LOOP STEADY STATE AND FREQUENCY RESPONSE DATA	Vol 2
F	OPEN LOOP STEADY STATE ROTOR RESPONSE DATA	Vol 2

LIST OF FIGURES

Figure	Title	Page
1	Lockheed/AMRDL High Advance Ratio Phase 2 Rotor Model Operational Characteristics	3
2	Schematic Diagram of Phase 2 Model	12
3	θ_s - Actuator Transfer Function	21
4	θ_c - Actuator Transfer Function	22
5	Rotor Longitudinal Frequency Response to Longitudinal Cyclic Pitch, μ = 0.0, 850 rpm (P = 1.30)	25
6	Rotor Lateral Frequency Response to Longitudinal Cyclic Pitch, μ = 0.0, 850 rpm (P = 1.30)	26
7	Rotor Longitudinal Frequency Response to Longitudinal Cyclic Pitch, μ = 0.0, 550 rpm (P = 1.56)	27
8	Rotor Lateral Frequency Response to Longitudinal Cyclic Pitch, μ = 0.0, 550 rpm (P = 1.56)	28
9	Block Diagram of Phase 2 Rotor Model	31
10	Block Diagram of Total Pitch Loop (Δ = 0 deg)	32
11	Block Diagram of Total Roll Loop (Δ = 0 deg)	33
12	Rotor Longitudinal Frequency Response to Collective Pitch, μ = .40, 800 rpm (P = 1.33)	38
13	Rotor Lateral Frequency Response to Collective Pitch, μ = .40, 800 rpm (P = 1.33)	39
14	Rotor Longitudinal Frequency Response to Longitudinal Cyclic Pitch, μ = .29, 800 rpm (P = 1.33)	42
15	Rotor Lateral Frequency Response to Longitudinal Cyclic Pitch, μ = .29, 800 rpm (P = 1.33)	43
16	Rotor Longitudinal Frequency Response to Longitudinal Cyclic Pitch, μ = .66, 800 rpm (P = 1.33)	44
17	Rotor Lateral Frequency Response to Longitudinal Cyclic Pitch, μ = .66, 800 rpm (P = 1.33)	45
18	Rotor Longitudinal Frequency Response to Lateral Cyclic Pitch, μ = .40, 800 rpm (P = 1.33)	47
19	Rotor Lateral Frequency Response to Lateral Cyclic Pitch, μ = .40, 800 rpm (P = 1.33)	48

LIST OF FIGURES (Continued)

Figure	Title	Page
20	Rotor Longitudinal Frequency Response to Collective Pitch, μ = .58, 550 rpm (P = 1.56)	49
21	Rotor Lateral Frequency Response to Collective Pitch, μ = .58, 550 rpm (P = 1.56)	50
22	Rotor Longitudinal Frequency Response to Longitudinal Cyclic Pitch, μ = .58, 550 rpm (P = 1.56)	51
23	Rotor Lateral Frequency Response to Longitudinal Cyclic Pitch, μ = .58, 550 rpm (P = 1.56)	52
24	Rotor Longitudinal Frequency Response to Lateral Cyclic Pitch, μ = .58, 550 rpm (P = 1.56)	53
25	Rotor Lateral Frequency Response to Lateral Cyclic Pitch, μ = .58, 550 rpm (P = 1.56)	54
26	Rotor Longitudinal Frequency Response to Longitudinal Cyclic Pitch, μ = 1.44, 300 rpm (P = 2.32)	56
27	Rotor Lateral Frequency Response to Longitudinal Cyclic Pitch, μ = 1.44, 300 rpm (P = 2.32)	57
28	Primary Pitch Loop Stability Margins from Rotor Transfer Functions (Illustrated)	59
29	Primary Pitch Loop Stability Margins, 800 rpm (P = 1.33)	61
30	Primary Roll Loop Stability Margins, 800 rpm (P = 1.33)	62
31	Longitudinal Transfer Functions ($a_1/\bar{\theta}_s$, $\delta_s/\bar{\theta}_s$), Pitch Loop Open, Roll Loop Closed, μ = .66, 800 rpm (P = 1.33), A = .50, L = 0, Δ = 0 deg	64
32	Total Pitch Loop Stability Margins, 800 rpm (P = 1.33), Δ = 0 deg	66
33	Total Roll Loop Stability Margins, 800 rpm (P = 1.33), Δ = 0 deg	67
34	Rotor Longitudinal Frequency Response to Lateral Cyclic Pitch, Pitch Loop Closed, Roll Loop Open μ = 0.66, 800 rpm (P = 1.33), A = 0.5, L = 0, Δ = 0 deg	68
35	Rotor Lateral Frequency Response to Lateral Cyclic Pitch, Pitch Loop Closed, Roll Loop Open μ = 0.66, 800 rpm (P = 1.33), A = 0.5, L = 0, Δ = 0 deg	69
36	Closed Loop Rotor Longitudinal Frequency Response to θ_o, μ = .54, 800 rpm (P = 1.33), A = 0.50, L = 0, Δ = 0 deg	71
37	Closed Loop Rotor Lateral Frequency Response to θ_o, μ = .54, 800 rpm (P = 1.33), A = 0.50, L = 0, Δ = 0 deg	72

LIST OF FIGURES (Continued)

Figure	Title	Page
38	Rotor Longitudinal Frequency Response to Collective Pitch, μ = 0.54, 800 rpm (P = 1.33)	73
39	Closed Loop Rotor Longitudinal Frequency Response to θ_{long}, μ = .54, 800 rpm (P = 1.33), A = 0.50, L = 0, Δ = 0 deg	74
40	Closed Loop Rotor Lateral Frequency Response to θ_{long}, μ = .54, 800 rpm (P = 1.33), A = 0.50, L = 0, Δ = 0 deg	75
41	Closed Loop Steady-State Rotor Response to an α-Disturbance, μ = .29, 800 rpm (P = 1.33), A/L = 2.5	79
42	Summary of Optimized Phase Angle Δ, 800 rpm (P = 1.33)	81
43	Closed Loop Steady-State Rotor Response to an Angle of Attack Excitation	82
44	Closed Loop Steady-State Rotor Response to a Collective Pitch Excitation	84
45	Closed Loop Steady-State Rotor Response to a Longitudinal Control Input (θ_{long}), μ = 0.29, 800 rpm (P = 1.33), A/L = 5.0, Δ = 42 deg	85
46	Summary of Optimized Phase Angle Γ, 800 rpm (P = 1.33)	86
47	Closed Loop Steady-State Rotor Response Derivatives with Respect to θ_o and α, 800 rpm (P = 1.33), A/L = 5.0, Δ = 10 deg	87
48	Closed Loop Steady-State Rotor Response Derivatives with Respect to θ_{long} and θ_{lat}, 800 rpm (P = 1.33), Δ = 10 deg, Γ = 12 deg	88
49	Open Loop Rotor Response Derivatives with Respect to θ_o and α, 1200 rpm (P = 1.17), γ = 5.0	90
50	Open Loop Rotor Response Derivatives with Respect to θ_s and θ_c, 1200 rpm (P = 1.17), γ = 5.0	91
51	Open Loop Steady-State Rotor Lift Derivatives with Respect to θ_o, α and θ_s, 1200 rpm (P = 1.17), γ = 5.0	92
52	Comparison of Theoretical and Experimental Rotor Transfer Functions, Longitudinal Frequency Response to θ_o, μ = .40, 800 rpm (P = 1.33), γ = 5.0	106
53	Comparison of Theoretical and Experimental Rotor Transfer Functions, Lateral Frequency Response to θ_o, μ = .40, 800 rpm (P = 1.33), γ = 5.0	107

LIST OF FIGURES (Continued)

Figure	Title	Page
54	Comparison of Theoretical and Experimental Rotor Transfer Functions, Longitudinal Frequency Response to θ_c, μ = .40, 800 rpm (P = 1.33), γ = 5.0	108
55	Comparison of Theoretical and Experimental Rotor Transfer Functions, Lateral Frequency Response to θ_c, μ = .40, 800 rpm (P = 1.33), γ = 5.0	109
56	Comparison of Theoretical and Experimental Rotor Transfer Functions, Longitudinal Frequency Response to θ_s, μ = .79, 550 rpm (P = 1.56), γ = 5.0	111
57	Comparison of Theoretical and Experimental Rotor Transfer Functions, Lateral Frequency Response to θ_s, μ = .79, 550 rpm (P = 1.56), γ = 5.0	112
58	Comparison of Theoretical and Experimental Rotor Transfer Functions, Longitudinal Frequency Response to θ_c, μ = .78, 300 rpm (P = 2.32), γ = 5.0	113
59	Comparison of Theoretical and Experimental Rotor Transfer Functions, Lateral Frequency Response to θ_c, μ = .78, 300 rpm (P = 2.32), γ = 5.0	114
60	Harmonic Analysis Error Generated by Incoreect Frequency Selection	A-3
61	Magnitudes of the Fourier Transforms of Blade Flapping Moment and Blade Feathering Angle, θ_s - Excitation, 800 rpm (P = 1.33), μ = 0.66, Excitation Frequency = 25 rad/sec	B-3
62	Magnitudes of the Fourier Transforms of the Rotor Pitching and Rolling Moments, θ_s - Excitation, 800 rpm (P = 1.33), μ = 0.66, Excitation Frequency = 25 rad/sec	B-4
63	Magnitudes of the Fourier Transforms of Blade Flapping Moment and Blade Feathering Angle, θ_s - Excitation, 800 rpm (P = 1.33), μ = 0.66, Excitation Frequency = 125 rad/sec	B-7
64	Magnitudes of the Fourier Transforms of the Rotor Pitching and Rolling Moments, θ_s - Excitation, 800 rpm (P = 1.33), μ = 0.66, Excitation Frequency = 125 rad/sec	B-8

LIST OF TABLES

Table	Title	Page
I	LOCKHEED/AMRDL PHASE 2 HIGH ADVANCE RATIO ROTOR MODEL CHARACTERISTICS	13
II	SUMMARY OF INSTRUMENTATION AND DATA ACQUISITION	17
III	HIGH ADVANCE RATIO RESEARCH PROGRAM PHASE 2 WIND TUNNEL TEST CONDITIONS	35
IV	ROTOR STIFFNESS VS ROTOR SPEED	40
V	STEADY STATE CLOSED LOOP ROTOR RESPONSE CHARACTERISTICS	77
VI	OPEN LOOP ROTOR STEADY STATE RESPONSE DERIVATIVES ADJUSTED TO THE CENTER OF ROTATION	93
VII	VALUES OF FOURIER COEFFICIENTS FOR PERIODIC FUNCTIONS	104

SECTION 1

INTRODUCTION

The Lockheed/U.S. Army Air Mobility Research and Development Laboratory (AMRDL) High Advance Ratio Research Program is currently being conducted in three phases. Phase 1, "Research Program to Determine Rotor Response Characteristics at High Advance Ratios" was completed in February, 1971 and is discussed in Reference 1. During that program, a 7 1/2 ft diameter, 4-bladed direct swashplate control rotor model with Lock numbers 3 and 5 and interchangeable root flexures was fabricated and tested in the AMRDL 7 x 10 ft wind tunnel at Moffett Field, California. Experimental stability and steady state response characteristics were determined over a wide range of advance ratios for an envelope of rotors described by Lock number and flapping frequency. The test data were excellent and facilitated a critical evaluation of a relatively simple theoretical approach to the prediction of hingeless rotor dynamic response.

Phase 2 of the high advance ratio research, "Theoretical and Experimental Investigation of Rotors with Hub Moment Feedback Controls" has recently been completed and is discussed in detail in this report. The program had two principal objectives. The first, as the title indicates, was to determine the dynamic characteristics of hingeless rotors with hub moment feedback controls by both theory and experiment. The theoretical model consisted of the Phase 1 flapping equations of motion coupled with an appropriate mathematical description of the control system. Similarily, the experimental model was obtained by equipping the tested Phase 1 rotor with an electrical hub moment feedback control system. The selected control system can be described most accurately as a steady-state gust alleviation device. It was not chosen for the test because it was considered an optimum system but rather because its simplicity best served the objectives of the program. It was composed of two

uncoupled first order lag filters with variable gains and time constants. The feedback signals were the rotor pitching and rolling moments in stationary coordinates.

The second objective of the program was to obtain experimental rotor transfer functions. These data would greatly enhance the hingeless rotor data bank initiated by the Phase 1 test results. They would also provide sufficient information with which to evaluate control system configurations other than the type (first order lag) selected for the Phase 2 studies.

The third phase of the program will expand the hingeless rotor experimental data bank even more. Rotor frequency response to shaft pitching and rolling will be measured over a range of advance ratios for several rotor configurations (γ, P). In addition, the existing μ-P envelope for which data have been acquired will be expanded by testing a softer set of flapping flexures. The Phase 3 activity was begun in October, 1971 and the wind tunnel entry is currently scheduled for March, 1972.

As a prelude to later discussions, the operational characteristics of the Phase 2 rotor model are qualitatively illustrated in Figure 1. A photograph of an oscillograph record of various rotor and control system measurements is shown. The time history begins with the rotor in an open loop mode, rotating at 800 rpm at zero forward velocity. The tunnel speed is increased to approximately 100 knots (μ=0.54) over the next 90 seconds. Because of nominal collective pitch and angle-of-attack angles and local airflow characteristics the increase in μ generates a rotor response which is reflected by increased blade flapping moments and rotor pitching and rolling moments. Additionally, the rotor is seen to respond to unsteady tunnel airflow with low frequency/random oscillations. During the next 45 seconds of the time history, the system is converted from an open loop to a closed loop mode. This is accomplished by closing first the pitch loop and then the roll loop. For safety's sake the loop closures are made with the control filter gains set at zero. Once a loop is closed the gain is slowly increased to its prescribed value. The action of the feedback control system is reflected by responses of the feedback signals δ_s and δ_c which in turns generate cyclic pitch θ_s and θ_c. With

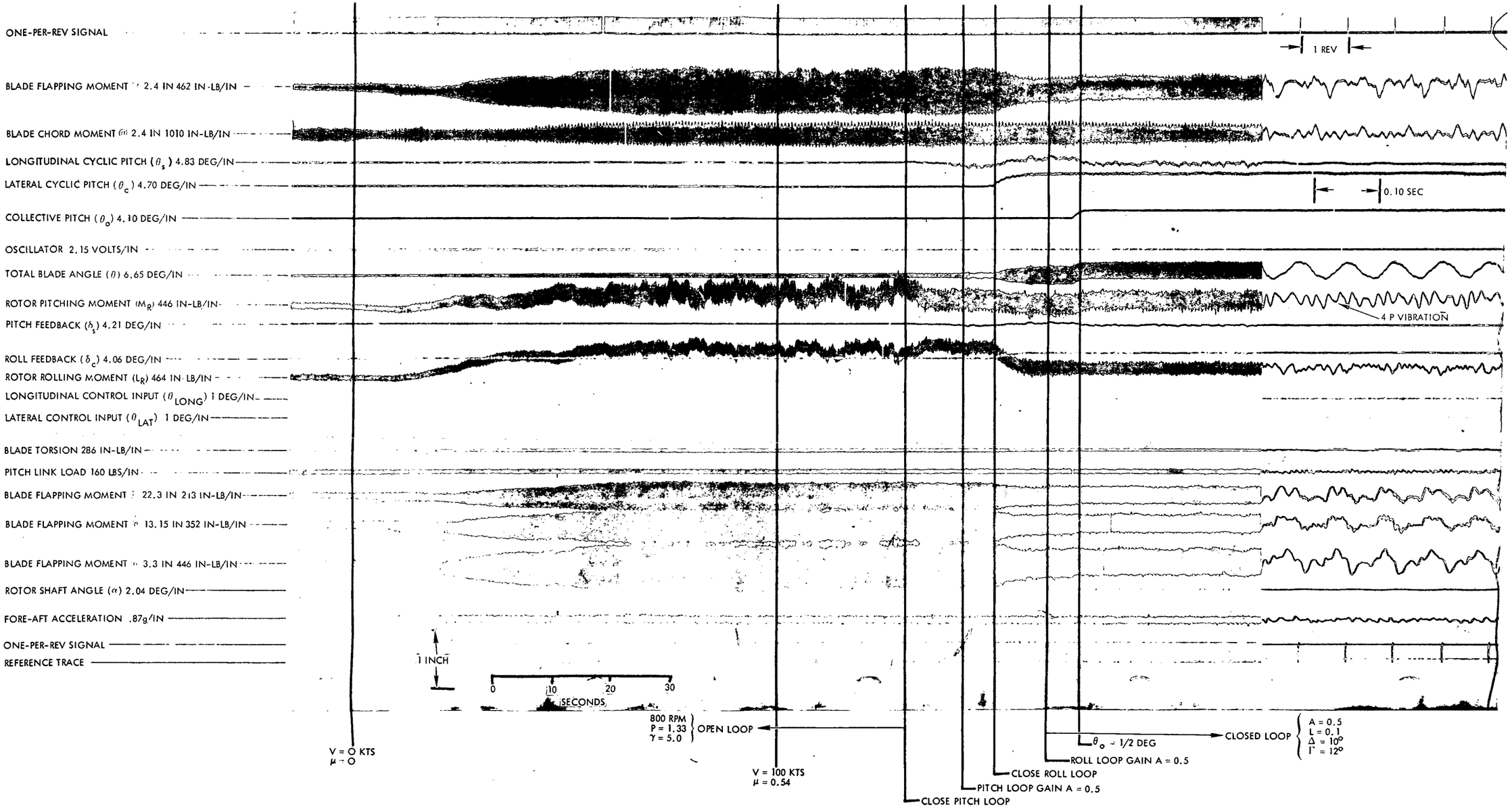

Figure 1. Lockheed/AMRDL High Advance Ratio Phase 2 Rotor Model Operational Characteristics

Page Intentionally Left Blank

the automatic control system fully operational the rotor moment responses are reduced to nearly zero. Further it is clear from the figure that the rotor oscillatory response to the tunnel turbulance is also alleviated.

When a collective pitch increment of 1/2 deg is applied to rotor, the excitation is treated as an external disturbance by the control system and automatically compensated for. The expanded time scale at the end of the record reveals two things: normal 4-per-rev vibration in the rotor moments and a small 1-per-rev flapping response. As will be discussed later, if $L \neq 0$, the automatic feedback control system can not provide complete alleviation of 1P flapping.

Page Intentionally Left Blank

SECTION 2

SYMBOLS

a	lift curve slope
a_o	rotor coning angle, deg
a_1	longitudinal rotor tilt, deg
b_1	lateral rotor tilt, deg
a_2, b_2	second harmonic blade flapping, deg
c	blade chord, ft
c_2	pitch loop disable switch (0 = loop open, 1 = loop closed)
c'_2	roll loop disable switch (0 = loop open, 1 = loop closed)
c_m	pitching moment coefficient $$c_m = \frac{M_R}{\pi R^3 \rho (\Omega R)^2}$$
c_l	rolling moment coefficient $$c_l = \frac{L_R}{\pi R^3 \rho (\Omega R)^2}$$
db	decibels = 20 LOG_{10} (amplitude ratio)
i	index referring to blades 1, 2, 3 and 4
j	$j = \sqrt{-1}$
$m_\alpha(\psi)$	nondimensional excitation of blade flapping by a rotor angle of attack change
$m_{\theta_o}(\psi)$	nondimensional excitation of blade flapping by collective pitch
s	Laplace operator
A	feedback control system gain parameter
$C(\psi)$	nondimensional aerodynamic damping of blade flapping

$C_{T/\sigma}$	blade loading coefficient $\frac{C_T}{\sigma} = \frac{\text{rotor lift}}{\pi R^2 \rho \sigma (\Omega R)^2}$
$K(\psi)$	nondimensional aerodynamic spring rate of blade flapping
K_β	rotor blade flapping stiffness, in.-lb/deg
K_θ	rotor stiffness, $K_\theta = 2K_\beta$, in.-lb/deg
L	feedback control system lag parameter
L_R (r in.)	rotor rolling moment at blade station r, roll right positive, in.-lb
M_R (r in.)	rotor pitching moment at blade station r, pitch up positive, in.-lb
M_{β_i}(r in.)	rotating blade flapping moment at blade station r, i = 1, 2, 3, 4, in.-lb
P	nondimensional blade flapping frequency
R	rotor blade radius, ft
α	rotor shaft angle of attack, deg
β_i	blade flapping angles i = 1, 2, 3, 4, deg
γ	Lock number
δ_s	pitch feedback control signal, deg
δ_c	roll feedback control signal, deg
ζ	actuator damping ratio
θ	blade feathering angle, deg

$$\theta = \theta_o + \theta_s \sin\psi + \theta_c \cos\psi$$

θ_c	lateral cyclic pitch, deg
$\bar{\theta}_c$	oscillator input to the θ_c - actuator, volts
θ_s	longitudinal cyclic pitch, deg
$\bar{\theta}_s$	oscillator input to the θ_s - actuator, volts
θ_o	collective pitch, deg
θ_{lat}	lateral control input, deg
θ_{long}	longitudinal control input, deg

μ	advance ratio
σ	rotor solidity
ψ	rotor azimuth angle, deg
ω	excitation frequency, rad/sec
ω_n	actuator natural frequency, rad/sec
Γ	feedback system cyclic control phase angle, deg
Δ	feedback control system phase angle, deg
Ω	rotor rotational frequency, rad/sec

Page Intentionally Left Blank

SECTION 3

MODEL DESCRIPTION

The Lockheed/AMRDL Phase 2 High Advance Ratio Rotor Model is composed of Phase 1 "rotor configuration 1" (soft flexure without tip weight, Lock number = 5.0) coupled with an electrical first order lag hub moment feedback control system. Rotor moments are formed by sensing the four rotating blade flapping moments with strain gages and resolving them into stationary coordinates by means of a sine-cosine potentiometer. These moments in stationary coordinates, scaled by the rotor stiffness $(2K_\beta)$ constitute the feedback signals to the pitch and roll control filters which have variable gains and time constants. The control system outputs in turn drive the cyclic pitch actuators. They can be combined through a phase angle Δ for the purpose of decoupling the rotor pitch and roll responses. Rotor cyclic control is exercised through longitudinal and lateral inputs $(\theta_{long}, \theta_{lat})$ to the two feedback loops. These inputs may also be phased through an angle Γ to decouple the steady rotor response. The conventional rotor cyclic pitch inputs are maintained so that the rotor can be excited when the feedback control system is disengaged. These inputs also represent one-per-rev rotor disturbances when the control system is operational. Conventional collective pitch control is also maintained. During the test the model was always operated in a fixed shaft mode.

A schematic of the system is shown in Figure 2. It is noted that the cyclic pitch actuator gain (K_1) and linkage ratio (K_3) are compensated for by reducing the control filter gain by the factor $\frac{3_1}{K_1 K_3}$. Section 3 of Reference 1 contains a complete description of the model without the feedback control system. As a convenience, the more important characteristics of the Phase 2 model are listed in Table I.

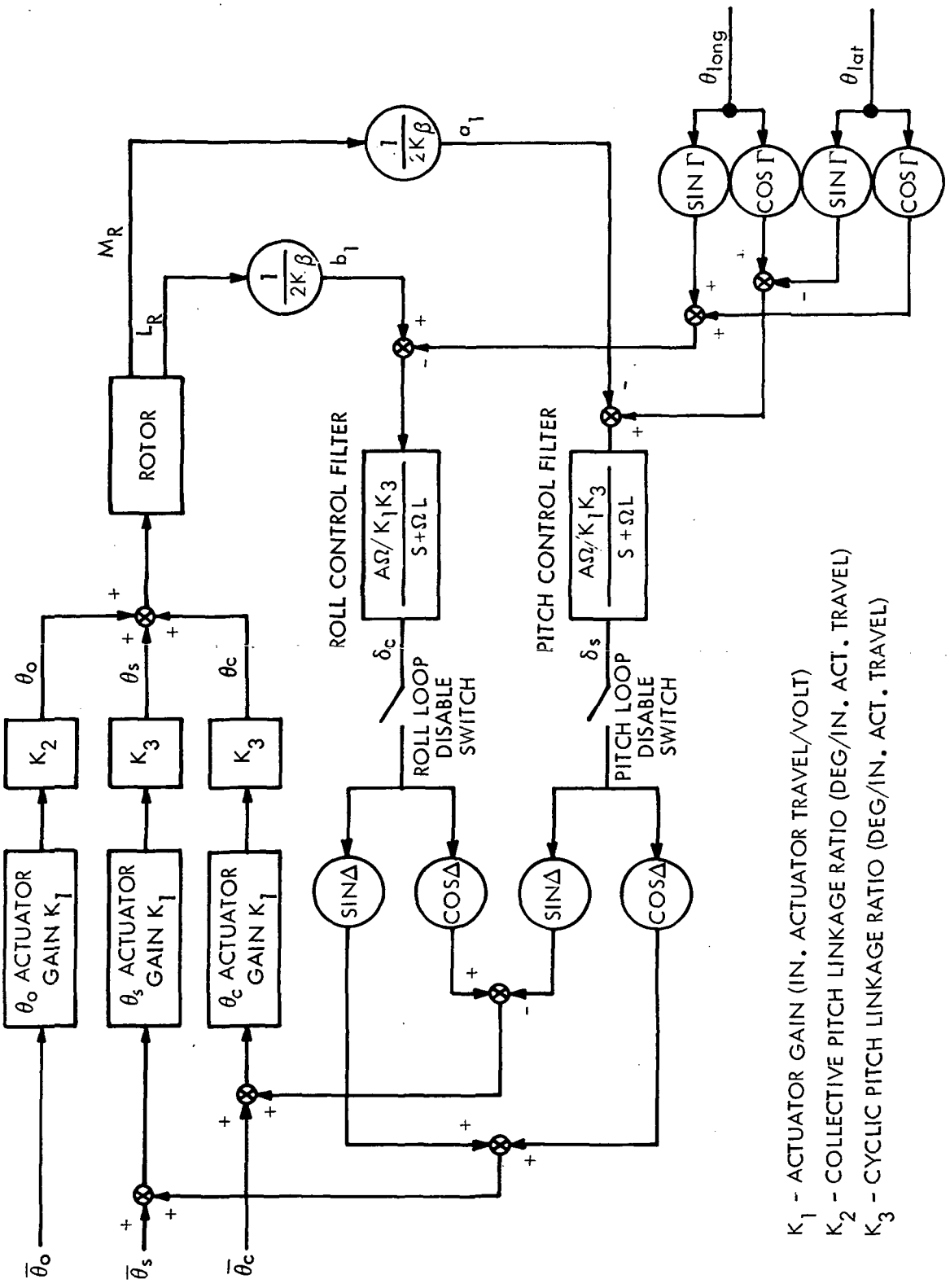

K_1 - ACTUATOR GAIN (IN. ACTUATOR TRAVEL/VOLT)
K_2 - COLLECTIVE PITCH LINKAGE RATIO (DEG/IN. ACT. TRAVEL)
K_3 - CYCLIC PITCH LINKAGE RATIO (DEG/IN. ACT. TRAVEL)

Figure 2. Schematic Diagram of Phase 2 Model

TABLE I

LOCKHEED/AMRDL PHASE 2 HIGH ADVANCE RATIO ROTOR MODEL CHARACTERISTICS

Number of Blades:	4
Radius:	45 in.
Chord:	4.5 in.
Solidity:	0.127
Airfoil Section:	NACA 0012
Lock Number:	5.0 ($a = 2\pi$)
Drive System:	Two 37 horsepower variable frequency induction motors
Rotor Control:	Direct swashplate or Moment feedback
Features of Moment Feedback Control System:	First order lag filter Variable gain Variable time constant Rotor response decoupling possible through phase angles Δ and Γ
Model Type	Fixed shaft

Page Intentionally Left Blank

SECTION 4

DATA ACQUISITION SYSTEM

INSTRUMENTATION

The Phase 2 model instrumentation consisted of the devices provided during the Phase 1 test plus appropriate measurements consistent with the addition of the feedback control system. The additional data were obtained by direct voltage readings and included the output of the control filters (δ_s and δ_c) and the control commands (θ_{long} and θ_{lat}). The mechanical phase angles Δ and Γ were recorded manually. A linear position potentiometer calibrated to indicate the rotor shaft angle-of-attack, was also added.

Because of the importance of the nonrotating rotor moments in the operation of the feedback control system, a review of the method by which they were generated is timely. Each rotor blade was equipped with a strain gage located at 3.3 inches from the center of rotation. The gages measure the flapping moments (M_{β_i}) of the rotating blades. The four signals were individually transferred to the stationary system through the slipring assembly. Each was then stabilized with an amplifier and passed through a multideck sine-cosine potentiometer which was attached to the rotor shaft and which generated the continuous functions sin Ωt and cos Ωt
The eight products

$$\left.\begin{array}{l} M_{\beta_i} \sin \Omega t \\ M_{\beta_i} \cos \Omega t \end{array}\right\} \qquad i = 1, 2, 3, 4$$

were then electrically summed to obtain the stationary moments, i.e.,

$$M_R\ (3.3\ \text{in.}) = (M_{\beta_3} - M_{\beta_1}) \cos\ \Omega t + (M_{\beta_2} - M_{\beta_4}) \sin\ \Omega t$$

$$L_R\ (3.3\ \text{in.}) = (M_{\beta_3} - M_{\beta_1}) \sin\ \Omega t + (M_{\beta_4} - M_{\beta_2}) \cos\ \Omega t$$

DATA ACQUISITION EQUIPMENT

The data acquisition equipment was the same as that used during the Phase 1 test:

- AMRDL DATEX System
- Honeywell Medium Band Analog Tape Recorder
- Honeywell Visicorder

A brief description of each device is presented in Section 4 of Reference 1. In addition, a transfer function analyzer was used to facilitate the acquisition of on-line frequency response data. The primary use of the analyzer was to obtain the open loop transfer functions required to determine closed loop stability margins.

All of the data recorded during the test are summarized in Table II. Listed also are the instrumentation and recording equipment used to acquire each datum.

TABLE II

SUMMARY OF INSTRUMENTATION AND DATA ACQUISITION

DATUM	INSTRUMENTATION	DATA ACQUISITION EQUIPMENT
Flap Bending Moment at Sta 22.3	Flap Bending Strain Gage at Sta 22.3	V
Flap Bending Moment at Sta 13.15	Flap Bending Strain Gage at Sta 13.15	V
Flap Bending Moment at Sta 3.3	Flap Bending Strain Gage at Sta 3.3	V, T
Flap Bending Moment at Sta 2.4	Flap Bending Strain Gage at Sta 2.4	V
Rotor Pitching and Rolling Moments at Sta 3.3	4-Flap Bending Strain Gages at Sta 3.3	V, T, D
Chord Bending Moment at Sta 13.15	Chord Bending Strain Gage at Sta 13.15	*
Chord Bending Moment at Sta 2.4	Chord Bending Strain Gage at Sta 2.4	V, T
Blade Torsion Moment at Sta 9.28	Torsion Gage at Sta 9.28	V
Pitch Link Tension/Compression Load	Pitch Link Tension/Compression Strain Gage	V
Instantaneous Pitch Angle of Blade No. 1	Blade Feathering Position Potentiometer (Pot.)	V, T
Body Moments and Forces	Body Mounted Strain Gage Balance	D (LIFT ON T)
Applied Longitudinal Cyclic Pitch (θ_s)	Longitudinal Cyclic Pitch Actuator Position Pot.	V, T, D
Applied Lateral Cyclic Pitch (θ_c)	Lateral Cyclic Pitch Actuator Position Pot.	V, T, D
Applied Collective Pitch (θ_o)	Collective Pitch Actuator Position Pot.	V, T, D
Rotor Shaft Angle (α)	Rotor Shaft Angle Actuator Position Pot.	V, D
Longitudinal Control Input (θ_{long})	Longitudinal Control Input Pot.	V, D
Lateral Control Input (θ_{lat})	Lateral Control Input Pot.	V, D
Pitch Feedback Control Signal (δ_s)	Direct - Voltage Measurement	V, T, D
Roll Feedback Control Signal (δ_c)	Direct - Voltage Measurement	V, T, D
Fore - aft Model Acceleration	Accelerometer	V
Oscillator Output	Direct - Voltage Measurement	V, T
Rotor Rotational Speed	One-Per-Rev Magnetic Pickup	V, T, D
Body Moments and Forces	Wind Tunnel Balance	D
Tunnel Dynamic Pressure	Wind Tunnel Pitot Static Probe	D
Tunnel Temperature	Wind Tunnel Temperature Probe	D

V = Visicorder, T = Analog Tape, D = Datex

* Datum not recorded because slip rings required for rotor moment feedback.

SECTION 5

CHECKOUT AND WHIRL TESTS

The checkout and whirl test of the model was conducted at Lockheed's Rye Canyon facility. As is normally the case, the primary objective of the activity was to insure that the model was totally operational prior to its shipment to Moffett Field. Since whirl tests were not planned at Ames, the acquisition of hover data was also a primary concern.

During the functional checkout of the model, particular attention was paid to the portions of the model which represented changes from the Phase 1 configuration. The most important modification was the addition of the feedback control system. Since this was electrical, verification of its proper implementation was easily accomplished by monitoring the voltage levels at appropriate locations in the circuitry. Both static and dynamic checks were made with gain and phase relationships indicative of correct operation.

Since the cyclic pitch actuators were important components of the system, it was important that their dynamic characteristics be suitable for the anticipated test program. This involved two things. First, the bandwidths of the actuators' transfer functions had to be maximized to insure enough actuator arm travel (and therefore blade angle) at high frequencies so that rotor transfer functions could be accurately determined. If the bandwidths were narrow, large phase shifts would be introduced by the actuators during closed loop operation which would compromise the stability of the system. Through the use of a constant current servo valve driver, a very acceptable actuator bandwidth of approximately 160 rad/sec was realized. Second, the frequency responses of the actuators had to be approximately the same to insure symmetry of the pitch and roll feedback control loops. The transfer functions were matched by adjusting the actuator feedback gains. The degree to which the

matching was successful is indicated by the measured actuator transfer functions plotted in Figures 3 and 4. The dynamic characteristics of the two actuators are nearly identical except for the gains at high frequencies. Since the discrepancy occurs at frequencies which are outside the range of effectiveness of the control system, it is acceptable. The dimensions of the transfer functions are:

$$\frac{\text{IN. ACTUATOR TRAVEL}}{\text{VOLT}} \times \frac{\text{DEG BLADE ANGLE}}{\text{IN. ACTUATOR TRAVEL}} = \frac{\text{DEG}}{\text{VOLT}}$$

The steady state gain therefore is made up of the normal actuator gain plus the mechanical advantage of the swashplate linkage to the blade.

Other ground test activities included rotor track and balance, instrumentation calibration check, and activation of a remote rotor angle-of-attack mechanism. With the system fully operational, whirl tests were begun.

DISCUSSION OF HOVER TEST DATA

Besides the obvious purpose of acquiring data, hover tests served as the ultimate check of the functional suitability of the model and data acquisition system and as a training course in the operation of the system. A very complete whirl test program was conducted which included both open loop and closed loop experiments. The same types of tests were subsequently conducted in the wind tunnel and are reviewed thoroughly in the discussion of that data (Section 6). Therefore to avoid repetition only those portions of the hover tests which compliment the ensuing wind tunnel test will be discussed.

The most important whirl test data acquired were open loop rotor transfer functions. They were generated by driving the θ_s-actuator with a sine wave function generator at a series of discrete frequencies. For all the data which will be presented, the magnitude of the excitation was nominally 3 deg and a collective pitch of ~ 4 deg was maintained to stabilize the effects of downwash. The measured pitching and rolling moments are related to the output of the actuator (i.e., the longitudinal cyclic pitch (θ_s) applied to the rotor) in terms of amplitude ratio and phase shift. The

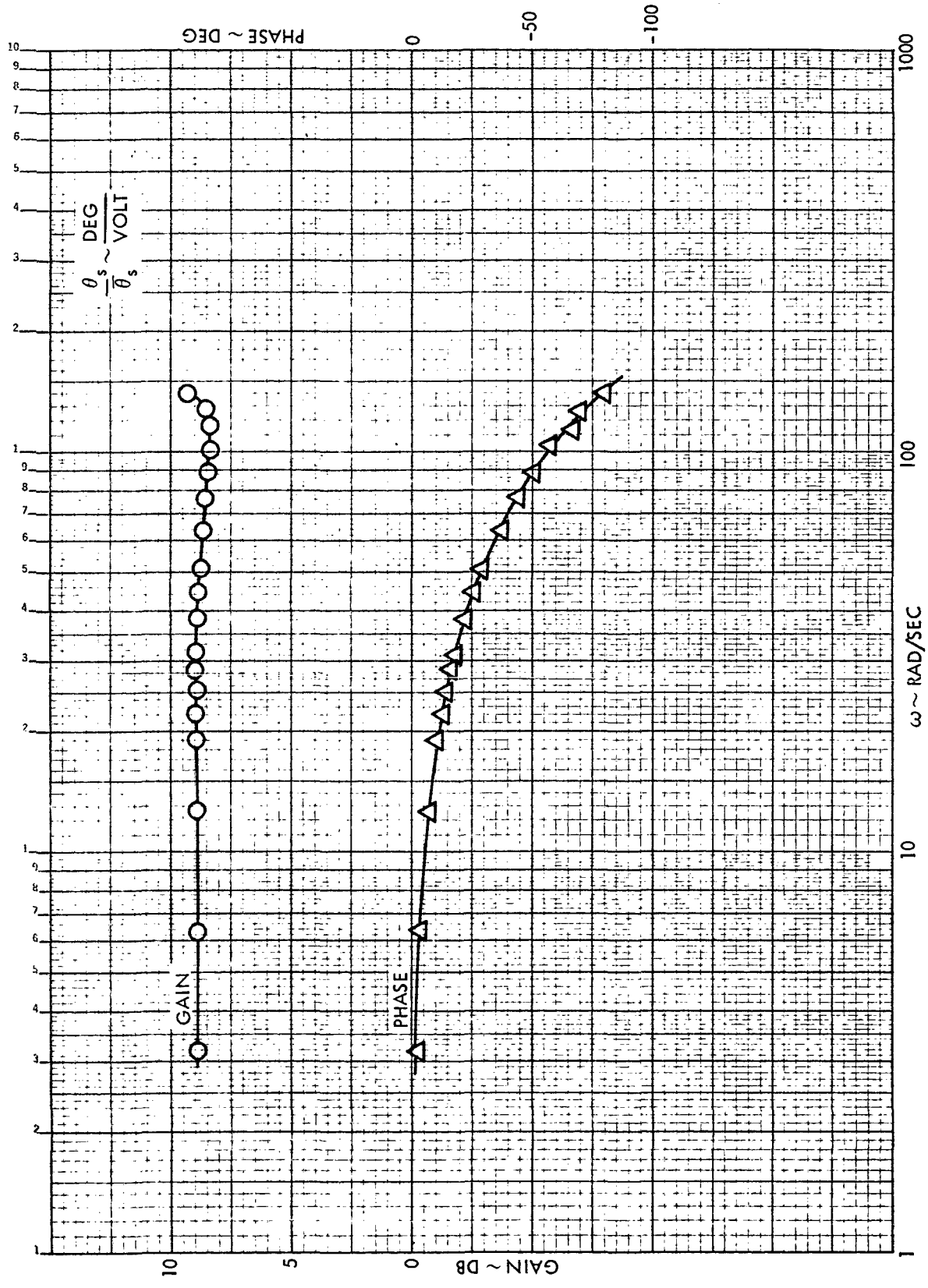

Figure 3. θ_s - Actuator Transfer Function

LOCKHEED
CALIFORNIA COMPANY

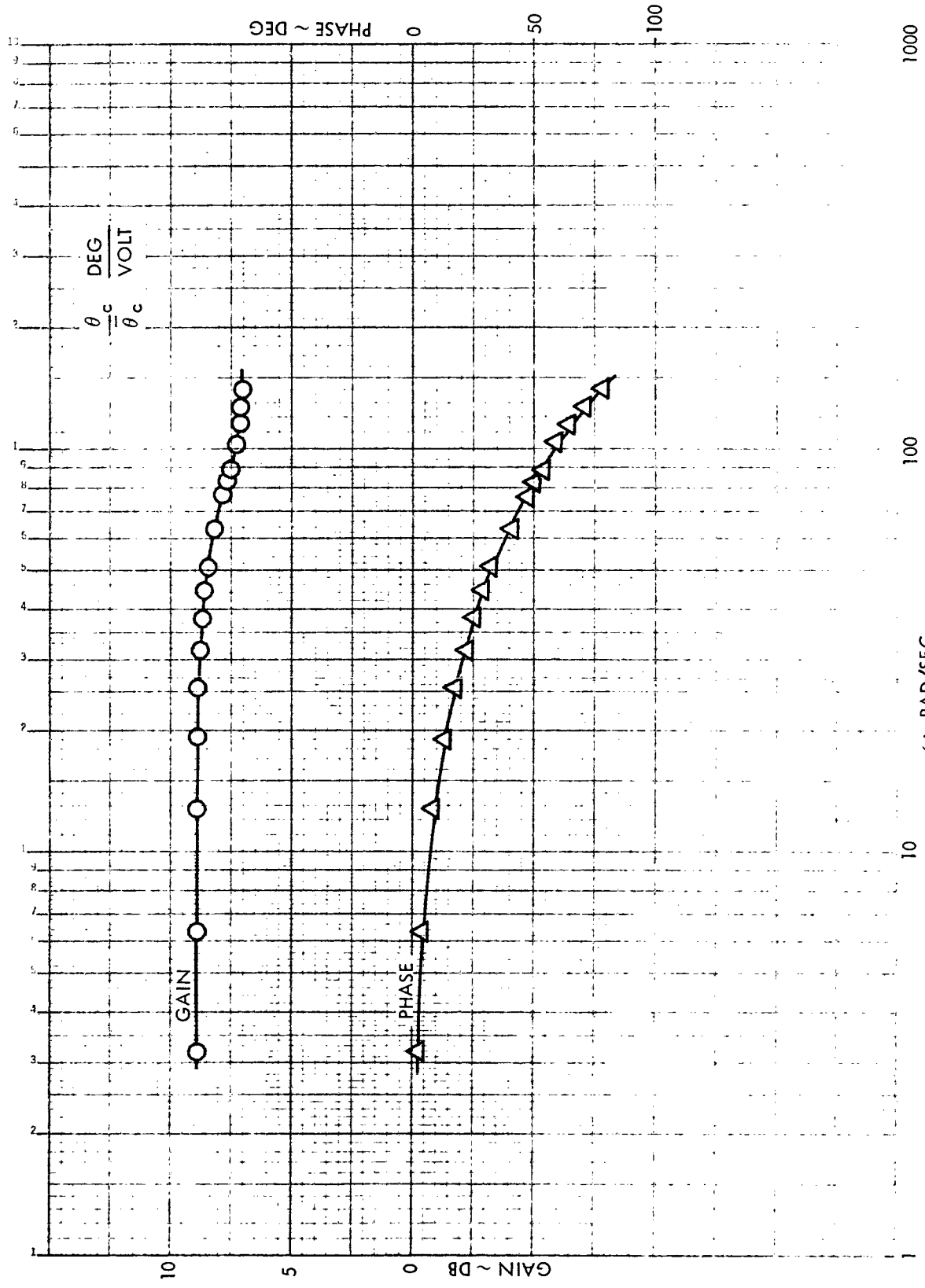

Figure 4. θ_c - Actuator Transfer Function

amplitude ratio is expressed in decibels and the phase shift in degrees calculated in the range +180 → -180 deg. The rotor frequency response at 850 rpm is plotted in Figures 5 and 6. The moments have been nondimensionalized by the rotor stiffness, K_θ, (see Table IV) resulting in longitudinal frequency response, a_1/θ_s and the lateral response, b_1/θ_s, both with the dimensions deg/deg. An explanation of the nature of the curves is contained in the discussion of the wind tunnel test data in Section 6.

The first frequency sweep revealed what was to become the one difficulty experienced during the program which was not totally resolved. The problem was the vibration of the entire model when the frequency of the driving function was near one of the natural frequencies of the support stand. As indicated on the curves, the frequency range where data may be affected was from 6 - 12 Hz. Accelerometer signals indicate that two support stand modes were excited within that range. The vibration was improved considerably during the wind tunnel test through the use of a viscous damper. The location and effect of this modification is discussed in Section 6. It is noted that the stand vibration seems to affect the rotor pitching response more than the roll response. Figures 7 and 8 indicate that the effects are diminished at lower rotational speeds.

Rotor transfer functions were also determined at a rotor speed of 550 rpm. The longitudinal and lateral frequency responses to θ_s are plotted in Figures 7 and 8. The characteristics of the curves are similar to those for 850 rpm. A wider nondimensional frequency range was achieved because of the lower Ω.

Several other open loop frequency response tests were conducted which lead to the following conclusions concerning the rotor transfer functions in hover.

1. The rotor frequency responses to longitudinal cyclic pitch and lateral cyclic pitch are symmetric in hover.

i.e.:

$$\frac{a_1}{\theta_s} = \frac{-b_1}{\theta_c}$$

$$\frac{b_1}{\theta_s} = \frac{a_1}{\theta_c}$$

2. The magnitude of the rotor frequency response is linear. Tests conducted with a θ_s magnitude of 4° produced the same transfer functions as similar tests with a 2° magnitude.

3. The linearity of the transfer functions is dependent upon having a nominal steady collective pitch setting sufficient to stabilize the uniform induced velocity field.

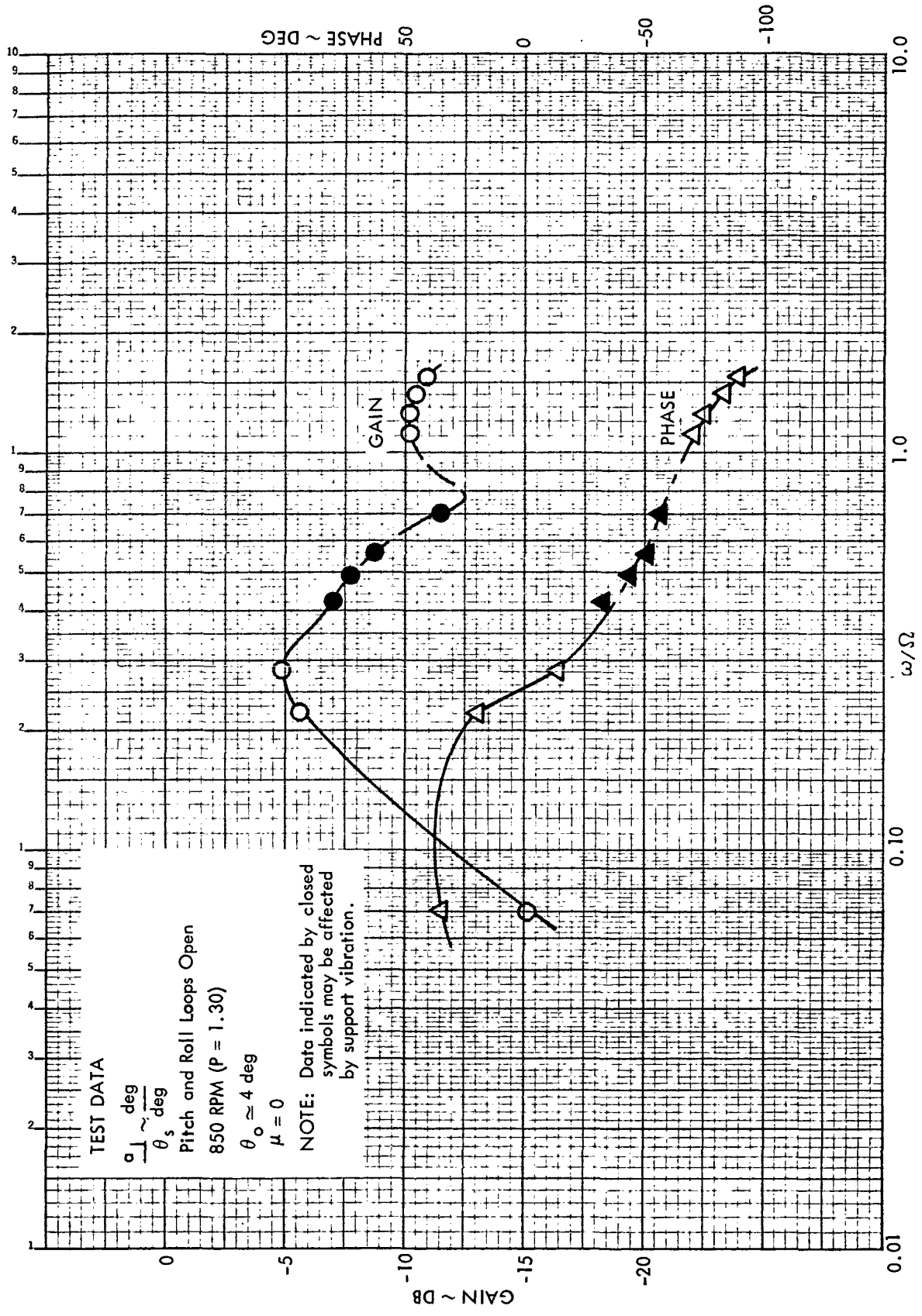

Figure 5. Rotor Longitudinal Frequency Response to Longitudinal Cyclic Pitch, μ = 0.0, 850 rpm (P = 1.30)

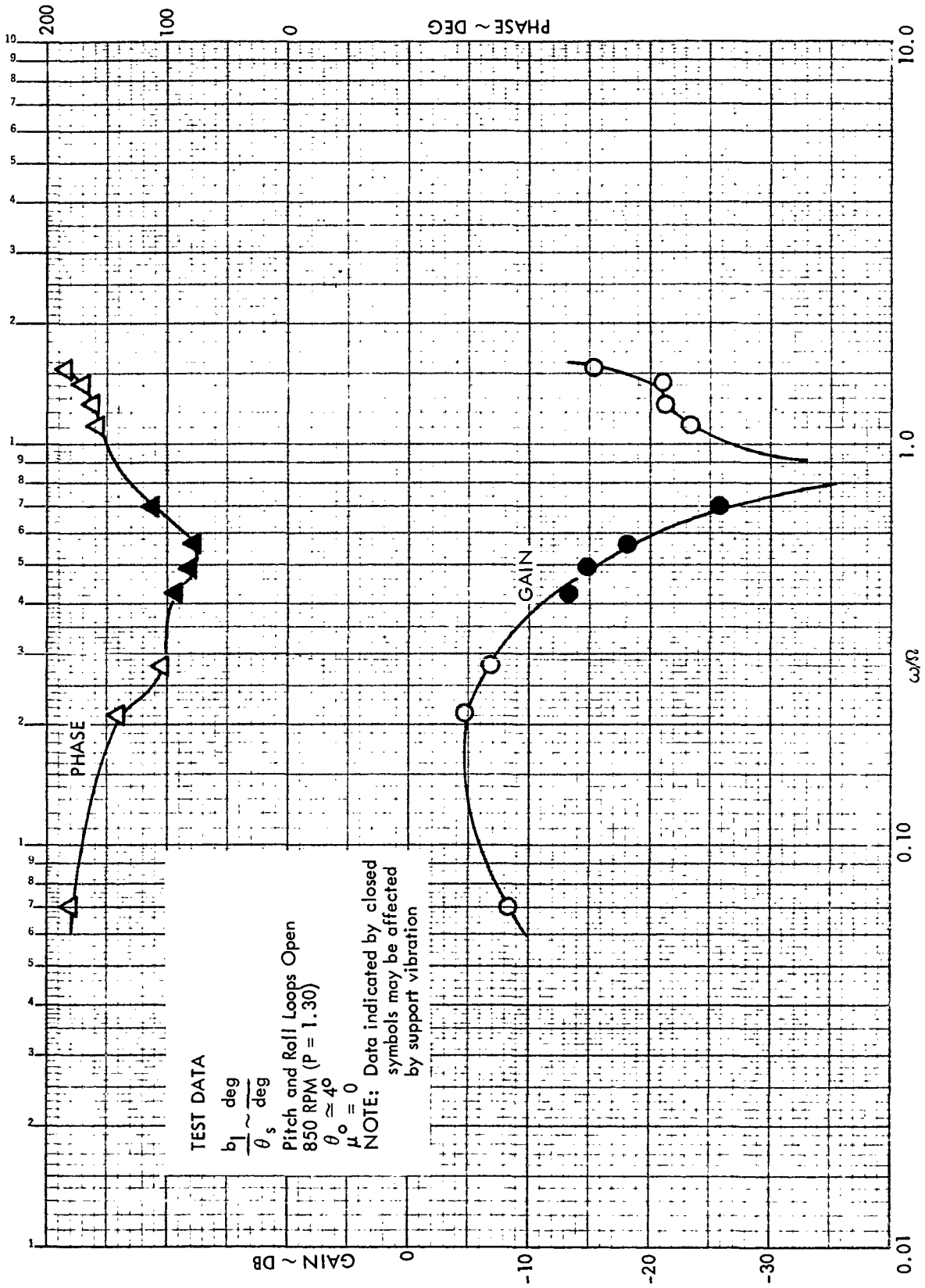

Figure 6. Rotor Lateral Frequency Response to Longitudinal Cyclic Pitch
μ = 0.0, 850 rpm (P = 1.30)

LOCKHEED
CALIFORNIA COMPANY

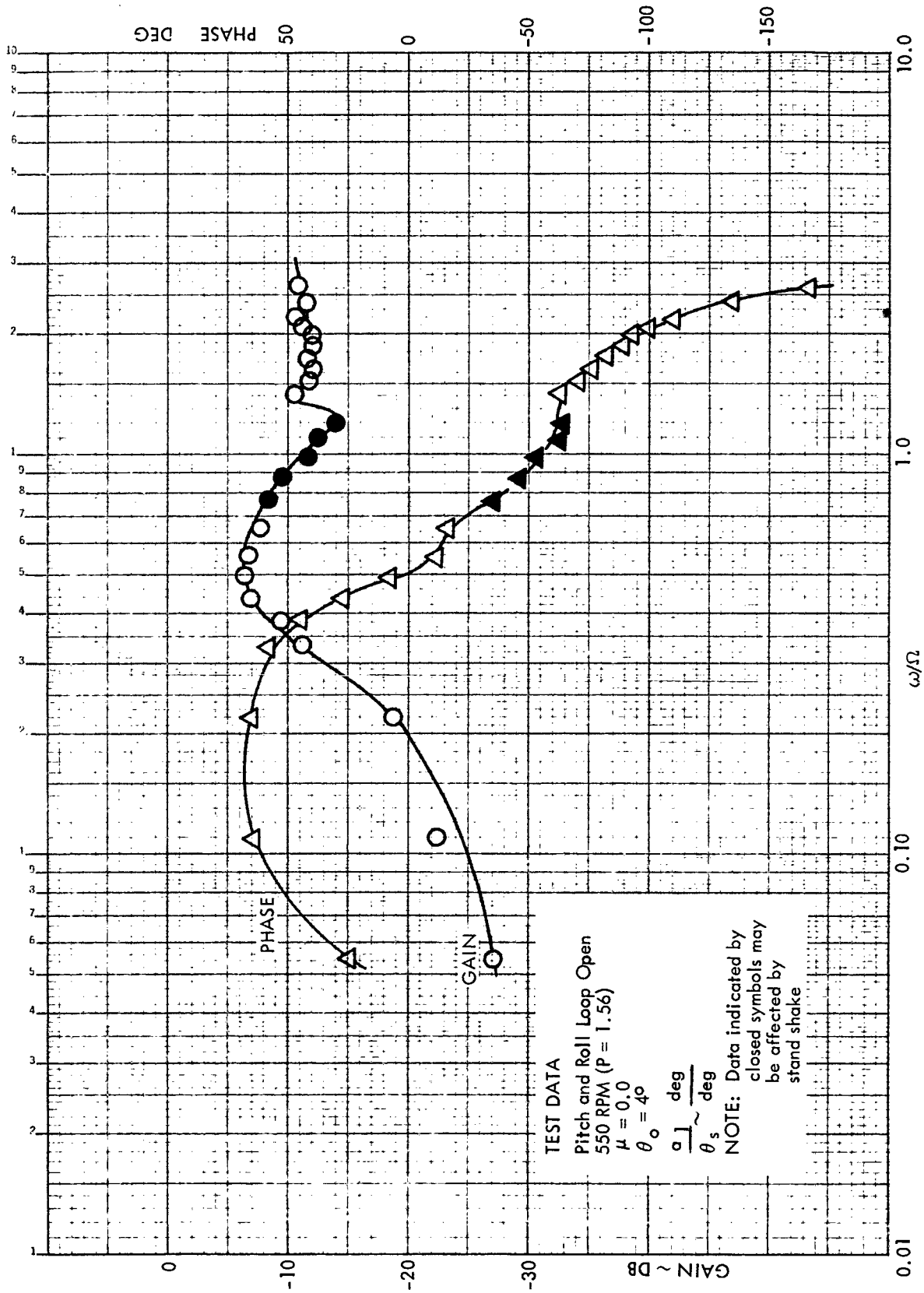

Figure 7. Rotor Longitudinal Frequency Response to Longitudinal Cyclic Pitch, $\mu = 0.0$, 550 rpm ($P = 1.56$)

LOCKHEED CALIFORNIA COMPANY

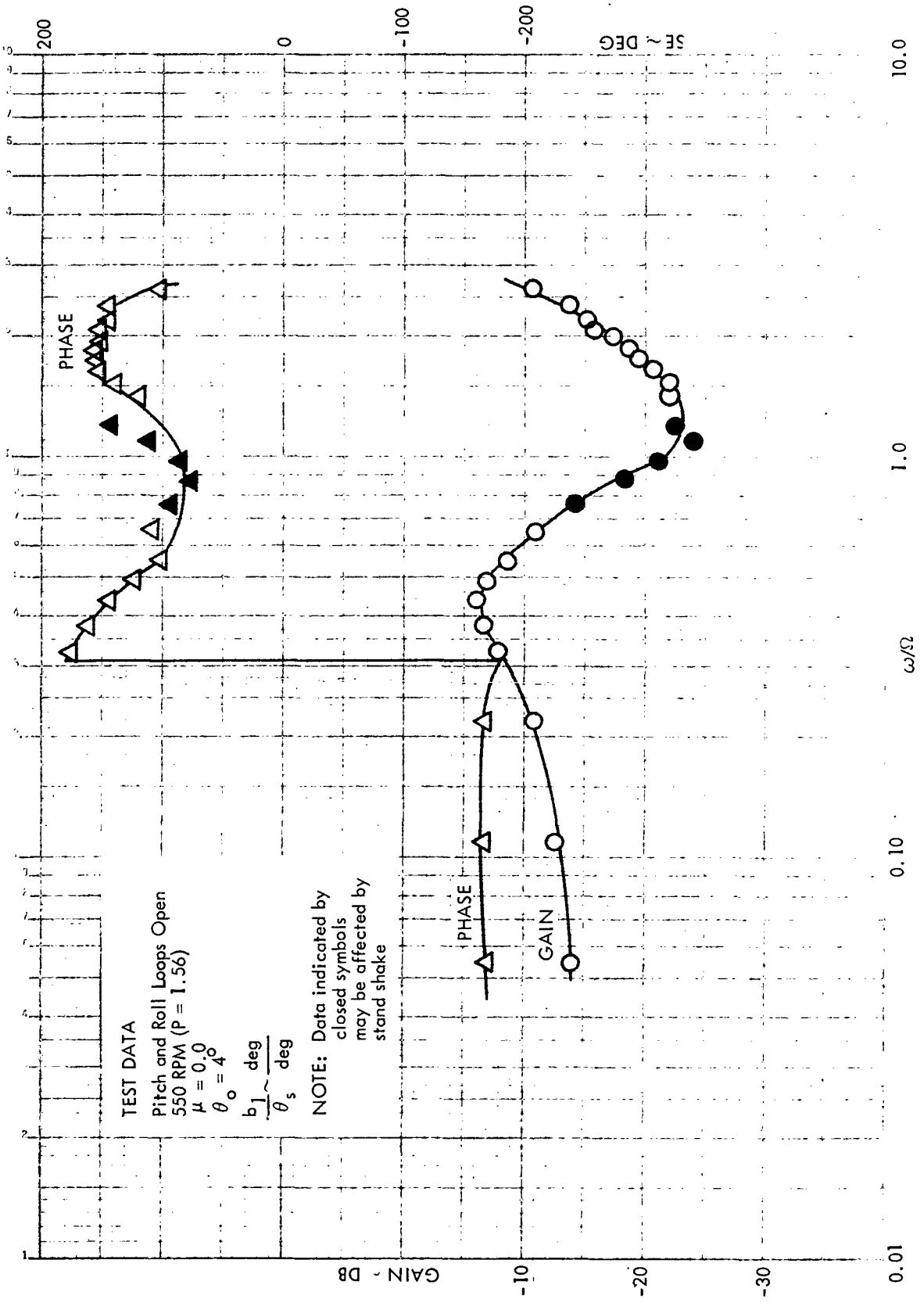

Figure 8. Rotor Lateral Frequency Response to Longitudinal Cyclic Pitch, $\mu = 0.0$, 550 rpm ($P = 1.56$)

SECTION 6

WIND TUNNEL TEST

The wind tunnel test was conducted in the AMRDL 7 x 10 foot wind tunnel at Moffett Field, California from April 30 to May 27, 1971. The model was installed in the tunnel exactly as it was during the Phase 1 test. Pages 33 - 36 of Reference 1 present the more important features of the test facility as well as a verbal and photographic description of the model installation.

TEST PROGRAM

The tests conducted can be categorized as either steady state or frequency response. During the steady state tests nonoscillatory control inputs or external excitations were applied to the rotor system. Frequency response tests were characterized by periodic oscillating control or external inputs.

The configurations tested can be broadly described as either open loop or closed loop. The term closed loop is self descriptive indicating simply that both pitch and roll control loops are engaged. Open loop, however, may denote any one of three loop closure configurations as follows:

- both pitch and roll loops open
- pitch loop open, roll loop closed
- roll loop open, pitch loop closed

The schedule of tests was arranged to fulfill the objectives of the program with minimum risk to the model. Essentially, this means that closed loop stability margins were determined from open loop frequency response data before any loop was closed. Since the system under consideration is a multiple loop network, a definite sequence of loop closures was required to predict the closed loop stability completely.

The first series of tests conducted were open loop frequency response with both control loops open. These tests served a two-fold purpose. First, they directly fulfilled one of the two primary objectives of the program, to obtain experimental rotor transfer functions. Second, they provided data from which the closed loop stabilities of the primary pitch and roll loops could be determined. The primary pitch and roll loops are defined graphically in Figure 9. The block diagram is an expansion of the schematic diagram shown in Figure 2 with the rotor represented by its pitching and rolling moment transfer functions with respect to collective and cyclic pitches. The primary pitch loop is composed of only those transfer functions which are excited by, and which directly contribute to, the longitudinal response of the system. The primary roll loop is similarily described in the terms of the lateral response.

The next series of tests were performed to determine the stabilities of the total pitch and total roll loops. The total pitch loop is formed by closing the roll loop and consists of all those transfer functions which contribute either directly or indirectly to the longitudinal response of the rotor. The total roll loop may be similarily described in terms of lateral rotor response. Figures 10 and 11 are respectively block diagram representations of the total pitch loop and the total roll loop with the phase angle $\Delta = 0$. As indicated, the tests required the closing of either the primary roll loop (for total pitch loop tests) or the primary pitch loop (for total roll loop tests). These loop closures were made with complete confidence since the degree of stability of the primary loops were already known experimentally. All primary and total loop stability margins were determined for several control system gains and time constants.

Once the stabilities of the total pitch loop and total roll loop were known, the closed loop stability of the total system was also known. Therefore, the next series of tests, closed loop steady state response and frequency response, were conducted with the certainty that an instability would not be encountered. The closed loop testing satisfied the other stated objective of the program, to determine the dynamic characteristics of hingeless rotors with moment feedback controls.

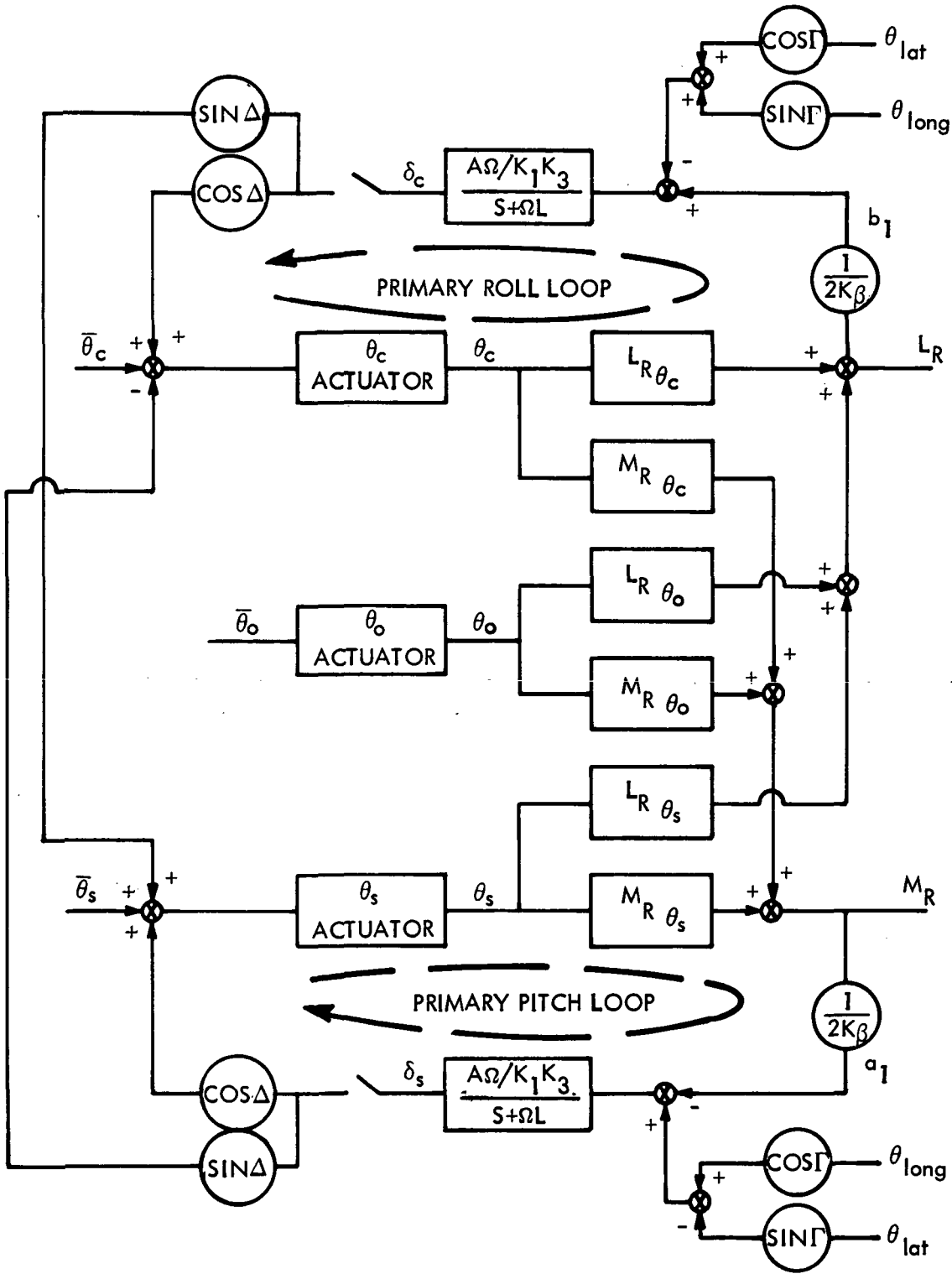

Figure 9. Block Diagram of Phase 2 Rotor Model

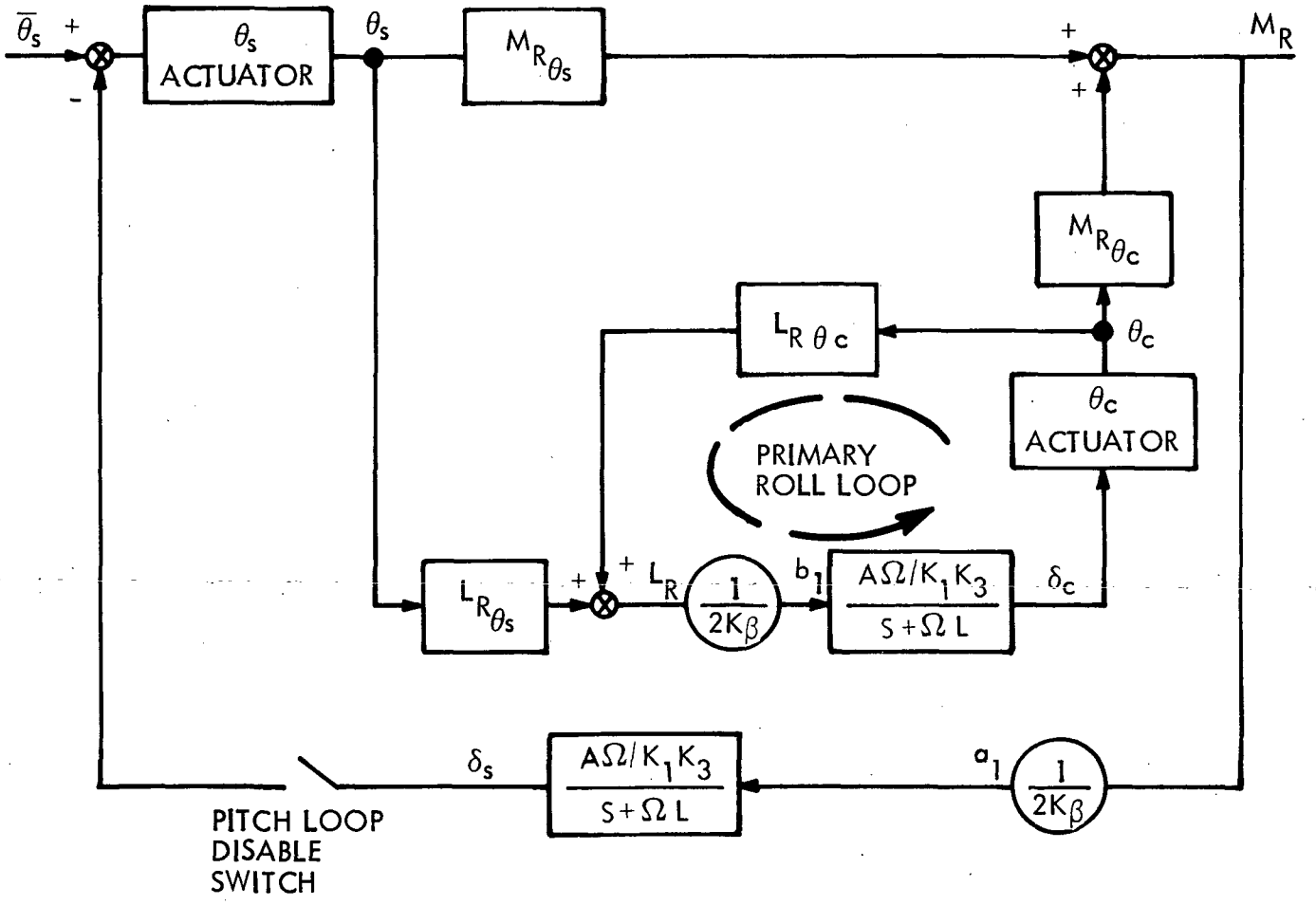

Figure 10. Block Diagram of Total Pitch Loop (Δ = 0 deg)

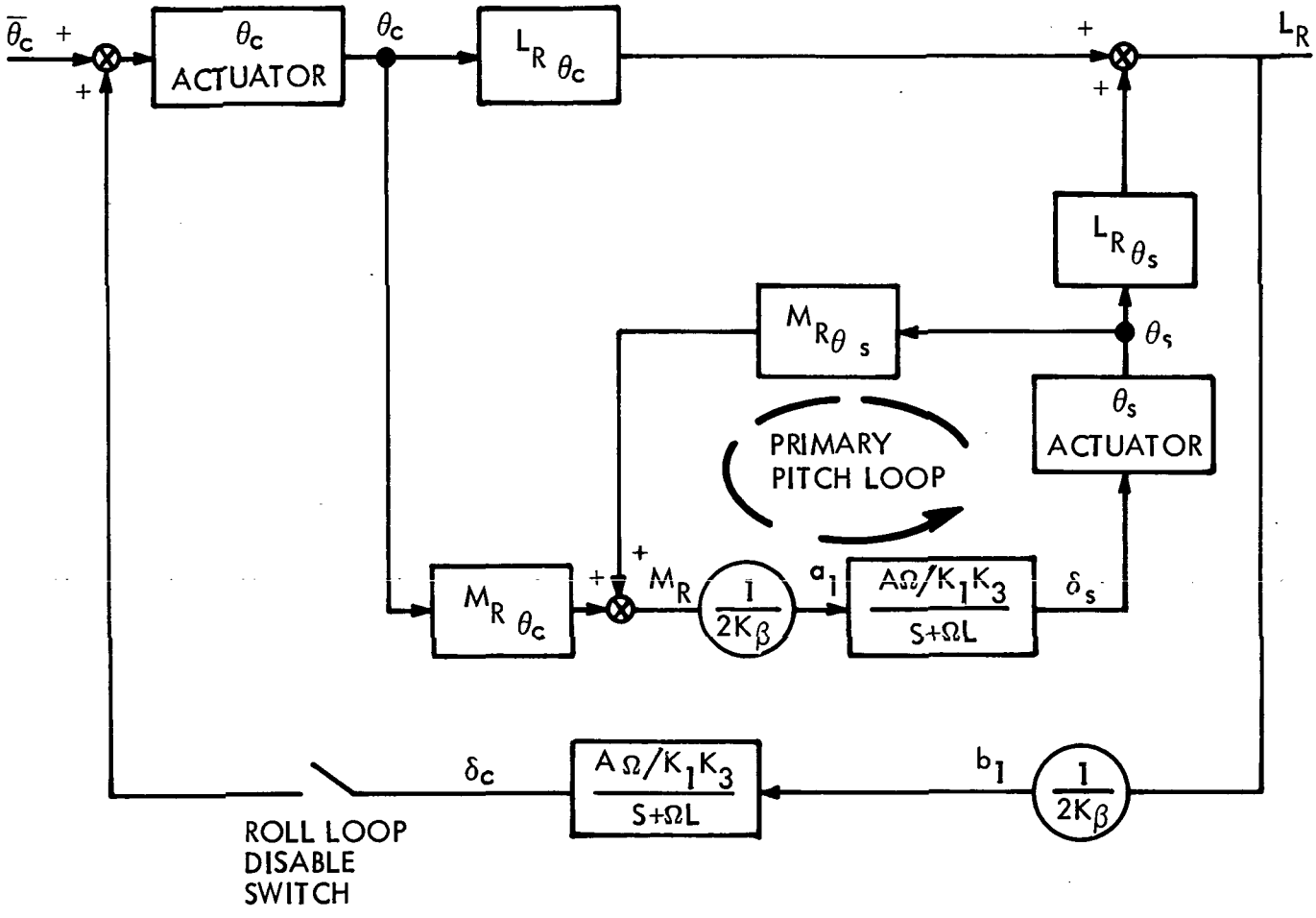

Figure 11. Block Diagram of Total Roll Loop (Δ = 0 deg)

A limited number of open loop steady state rotor response tests were also conducted. They were similar to the Phase 1 tests except a higher rotor rotational speed was considered. The purpose of this activity was to obtain rotor response derivatives at lower nondimensional flapping frequencies than those tested during Phase 1. A rotor rpm of 1200 was tested which corresponds to a flapping frequency of 1.17 Ω .

A summary of the types of tests conducted is as follows:

1. Open loop frequency response (pitch and roll loops open).
2. Open loop frequency response (pitch loop open, roll loop closed).
3. Open loop frequency response (roll loop open, pitch loop closed).
4. Closed loop steady state response.
5. Closed loop frequency response.
6. Open loop steady state response (pitch and roll loops open).

In order to maintain consistency between the Phase 1 and Phase 2 data banks, identical operation conditions $(V,\Omega R)$ were examined during both tests. One exception is noted: For convenience, open loop steady state rotor response derivatives at 1200 RPM in hover were approximated by a test in the tunnel at a $\mu = 0.07$.

A summary of the Phase 2 test program is contained in Table III. Included in the compendium are the test conditions $(V,\Omega R)$, the rotor definitions (γ, P), the control system transfer function parameters, the excitations, and the data acquired from each series of tests.

DISCUSSION OF WIND TUNNEL TEST DATA

A rather large quantity of data was accumulated during the test which can be attributed to the lack of serious problems during the experiment. It is probable that the success is largely due to the fact that it was the second

TABLE III. HIGH ADVANCE RATIO RESEARCH PROGRAM PHASE 2 WIND TUNNEL TEST CONDITIONS

TYPE OF TEST	RPM	V KNOTS	μ	P	γ	EXCITATIONS	EXCITATION FREQUENCIES	DATA ACQUIRED
Open Loop Freq. Response, Pitch and Roll Loops Open	800	50 75 100 120	0.29 0.40 0.54 0.66	1.33	5	$\bar{\theta}_o$, $\bar{\theta}_s$, $\bar{\theta}_c$	0 → 24 CPS	Rotor Transfer Functions *Primary Pitch Loop Stability *Primary Roll Loop Stability Actuator Transfer Functions
Open Loop Freq. Response, Pitch and Roll Loops Open	550 300	50 75 100 120 50 75 100	0.43 0.58 0.79 0.96 0.78 1.07 1.44	1.56 2.32	5	$\bar{\theta}_o$, $\bar{\theta}_s$, $\bar{\theta}_c$	0 → 24 CPS	Rotor Transfer Functions
Open Loop Freq. Response; Pitch Loop Open Roll Loop Closed or Roll Loop Open Pitch Loop Closed	800	50 75 100 120	0.29 0.40 0.54 0.66	1.33	5	$\bar{\theta}_s$, $\bar{\theta}_c$	0 → 12 CPS	*Total Pitch Loop Stability *Total Roll Loop Stability
Closed Loop Steady State Response	800 300	50 75 100 120 50 75 100	0.29 0.40 0.54 0.66 0.78 1.07 1.44	1.33 2.32	5	θ_o, α, θ_{long}, θ_{lat}	0	Closed Loop Steady State Response Characteristics
Closed Loop Freq. Response	800	50 100	0.29 0.54	1.33	5	θ_o, $\bar{\theta}_s$, θ_{long}, θ_{lat}	0 → 24 CPS	Closed Loop Frequency Response
Open Loop Steady State Response, Pitch and Roll Loops Open	1200	20 50 75 100 120	0.07 0.19 0.27 0.36 0.44	1.17	5	θ_o, θ_s, θ_c, α	0	Rotor Steady State Response Characteristics

*Primary Loop and Total Loop Stabilities were determined for the following combinations of A and L with Δ = 0 deg (A = 0.5, L = 0.1), (A = 0.5, L = 0.05), (A = 0.2, L = 0), (A = 0.5, L = 0)

tunnel entry for the model. Most problems which might have resulted in lengthy delays were anticipated. For example, the strain gages on the flexures which make up the moment resolution circuit failed midway through the test. This same difficulty occurred during the Phase 1 test and prompted the fabrication and instrumentation of a spare set of flexures. Consequently, when the difficulty appeared, the flexures were immediately replaced with a minimum loss of time.

All of the test data are documented in appendices in Volume 2. Sufficient representative curves are discussed in the report so that the salient aspects of the data are clearly understood. Wherever possible, the test data are condensed in summary curves.

Open Loop Rotor Transfer Functions

Experimental rotor transfer functions were determined from data obtained during open loop frequency response tests where both pitch and roll control loops were open. The tests were conducted as follows. At a fixed rotor rotational speed and tunnel velocity the residual rotor moments due to the nominal collective pitch (0.5 → 1.0 deg) and effective angle-of-attack created by local flow characteristics were manually trimmed by application of appropriate cyclic pitch. The rotor was then excited by either collective pitch (θ_o), longitudinal cyclic pitch (θ_s) or lateral cyclic pitch (θ_c) at a prescribed magnitude and frequency. In general the magnitudes of the excitations were in the range of 1 to 4 degree. The excitation was applied by driving (electrically) the selected actuator with a sine wave function generator. The rotor pitching and rolling moments obtained from the moment resolution circuit were measured and related to the output of the actuator to form the transfer functions. The transfer functions are classical and linear, i.e., they express the moment response of the rotor at the exciting frequency to the excitation in terms of amplitude ratio and phase shift. The amplitude ratio (in.-lb/deg) is expressed in decibels (db), i.e.

$$DB = 20 \ LOG_{10} \ (AMPLITUDE \ RATIO)$$

and the phase shift in degrees. As mentioned before the phase is calculated in the range +180 degree to -180°. In general, the range of frequencies considered during the test was 0.5 → 24 H_z with the upper limit dictated by structural considerations.

As indicated, the transfer functions presented in this report are linear. In the present context linear refers to frequency as well as magnitude. That is, a transfer function is termed linear if it is calculated from the response at the excitation frequency only. Because rotors encounter periodic (on ψ) aerodynamic spring and damping coefficients and forcing functions, they can also respond at frequencies which are combinations of the sum and difference of the driving frequency (ω) and the rotational frequency (Ω), (i.e. $n\Omega \pm \omega$, $n = 1, 2, 3, \ldots$). This response is called a residue. A discussion of the rotor 'residue' frequency response including examples from test data is contained in Appendix B. It is shown that the 'residue' frequency response of the rotor does not affect the linear transfer functions.

The frequency response data presented in this report were obtained from a Fourier analysis of digitized analog singals recorded on the Honeywell FM tape recorder. During the reduction of the digital data several interesting problems were encountered. Since the experience may aid others involved in similar activities, the techniques and the problems are documented in Appendix A.

The problem of model vibration and its effect upon the hover data was discussed in Section 5. It was indicated that the addition of a viscous damper to the model prior to the wind tunnel test reduced the vibration. The damper was installed so that it damped the angular motion of the model about the pitch pivot. The net effect was to reduce the number of natural support modes which were excited from two to one and thereby limit the affected frequency range. The maximum vibration occurred at ~ 8 Hz with the effects detectable from ~ 6 to ~ 10 Hz. As was the case with the hover results, the pitching moment data are affected more than the rolling moment data, and the influence of the vibration decreases with rotor speed.

The rotor frequency response to collective pitch (θ_o) is shown in Figures 12 and 13. Longitudinal response (a_1) is presented in Figure 12 and lateral response (b_1) in Figure 13. The measured rotor moments have been nondimensionalized by the rotor stiffness (K_θ) to obtain the angular responses (a_1 and b_1), i.e.:

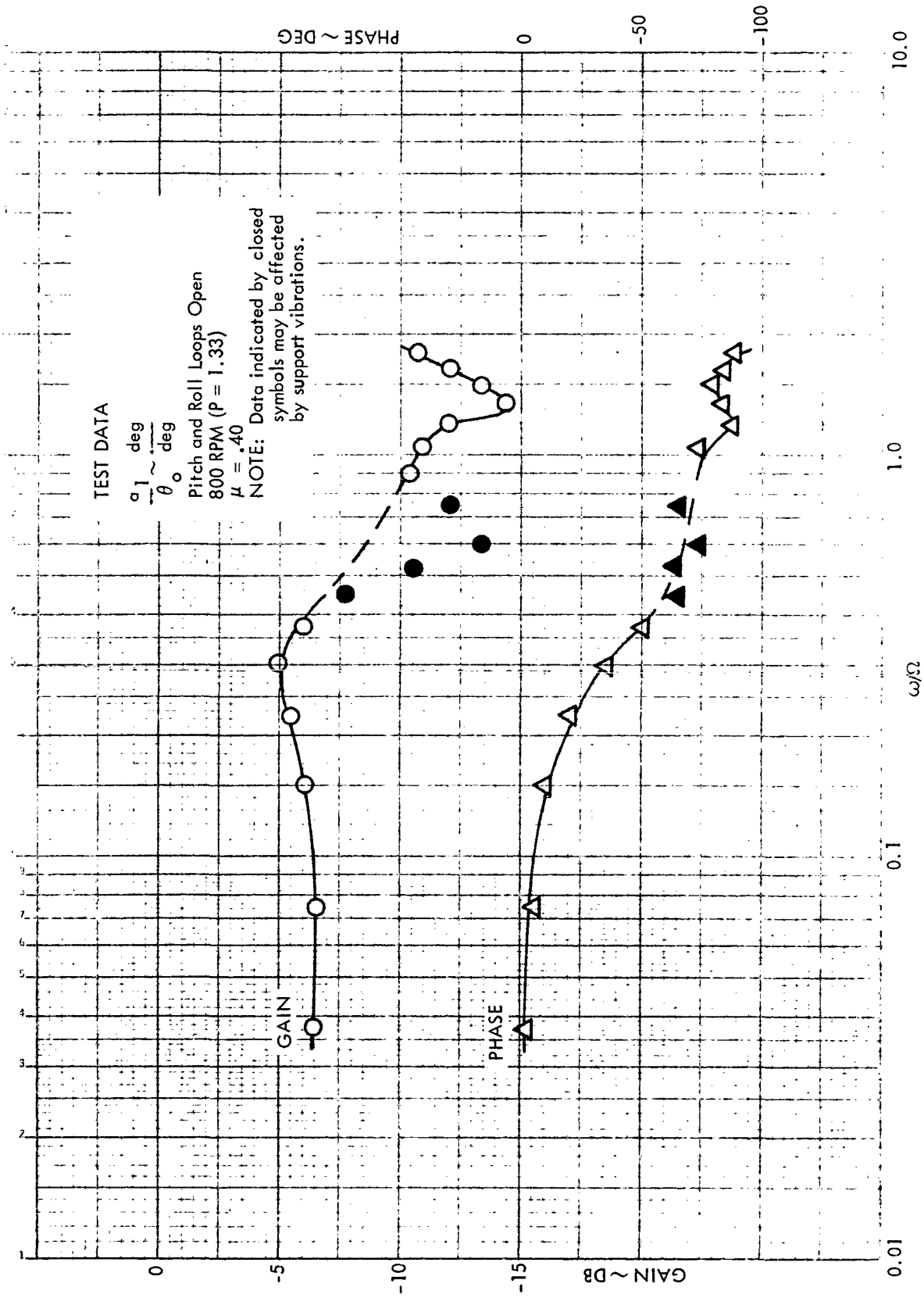

Figure 12. Rotor Longitudinal Frequency Response to Collective Pitch, μ = .40, 800 rpm (P = 1.33)

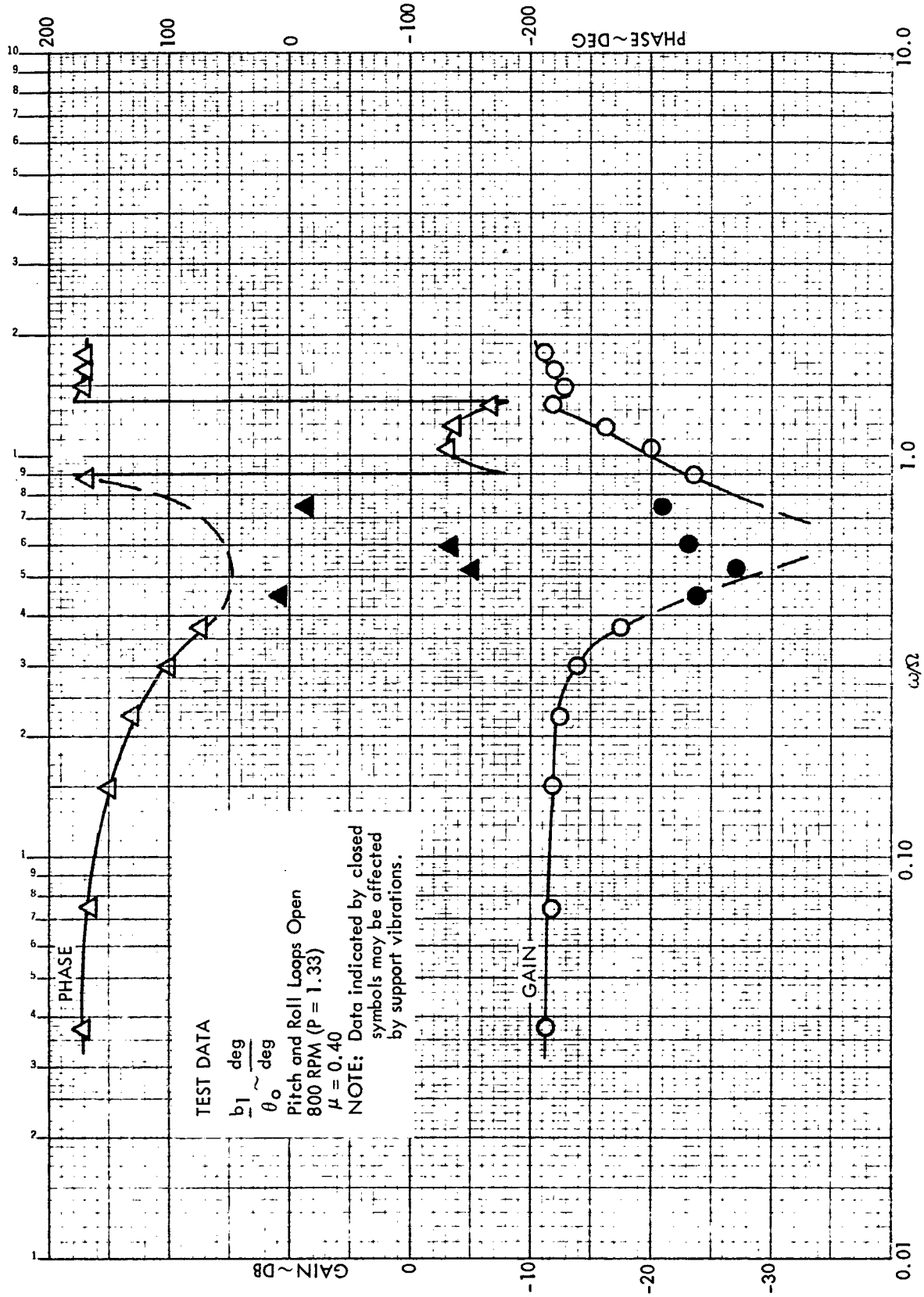

Figure 13. Rotor Lateral Frequency Response to Collective Pitch, μ = .40, 800 rpm (P = 1.33)

LOCKHEED CALIFORNIA COMPANY

$$a_1 = \frac{M_R \text{ (3.3 in)}}{K_\theta \text{ (3.3 in)}}$$

$$b_1 = \frac{L_R \text{ (3.3 in)}}{K_\theta \text{ (3.3 in)}}$$

An explanation of the rotor stiffness can be found on Pages 80 - 84 of Reference 1. For the current investigations the K_θ (3.3 in) values used for each rotor speed are listed in Table IV. The value at 850 rpm is applicable for the hover data.

TABLE IV

ROTOR STIFFNESS VS ROTOR SPEED

RPM	K_θ (3.3 in)
300	309
550	327
800	348
850	353
1200	385

The transfer functions shown in Figures 12 and 13 are typical of the rotor collective pitch frequency response at a rotational speed of 800 rpm (83.78 rad/sec). The gain and phase relationships of the responses are plotted over the nondimensional frequency range $0.0375\ \Omega \rightarrow 1.8\ \Omega$ at an advance ratio of $\mu = 0.40$. $\omega/\Omega = 1.8$ corresponds to a driving frequency of 24 Hz. The rotor pitching response is seen to peak at a driving frequency ratio of approximately 0.3. Since ω is defined in stationary coordinates, a value of $0.3\ \Omega$, when viewed in rotating coordinates, appears as a frequency of $1.3\ \Omega$. At a rotor speed of 800 rpm the rotor first flap bending mode natural frequency expressed in rotating coordinates is $1.33\ \Omega$. With this in mind, it is clear that the peaking is simply the resonant response of the rotor at its first flap bending natural frequency. Since the blade flapping motion is aerodynamically damped, it is expected that the peak response would occur at a frequency which is slightly less than its undamped natural flapping frequency. The lack of a similar increase in the rotor lateral response at $\omega/\Omega = 0.3$ is indicative of a changing rotor phase angle of response with excitation frequency.

The frequency response data also show an increase in the rotor response as the excitation frequency approaches $\omega/\Omega = 2.0$. While frequency ratios greater than 1.8 (at 800 rpm) were not tested, it is expected that the rotor response would have peaked at $\omega/\Omega \simeq 2.3$. This frequency would have generated an excitation of the rotor in rotating coordinates at 1.3Ω creating a resonance condition similar to that experienced at $\omega/\Omega \simeq 0.3$.

As previously indicated, data which are suspected of being contaminated by support stand vibrations are closed for the purposes of identification. It is noted that, the fairing of the curves through the frequency range where the data are not totally credible is somewhat arbitrary, being guided only by similar theoretical results.

The experimental rotor frequency response to longitudinal cyclic pitch (θ_s) is illustrated for two advance ratios ($\mu = 0.29$, and $\mu = 0.66$) in Figures 14 to 17. Again, the rotational speed is 800 rpm and the rotor response is described by both pitch and roll transfer functions. An immediate observation (irrespective of advance ratio) is that the rotor response to θ_s is similar to that obtained for the collective pitch excitation. The peaking of the response when the flapping frequency is in resonance with the driving frequency is present and the shapes of the gain and phase curves are similar. In fact, even the effect that the stand shake has on the response is the same.

Two sets of frequency response curves (Figures 14, 15 and Figures 16, 17) are shown to illustrate the effects of advance ratio. The anticipated increase in the magnitude of the response derivatives with μ is clearly seen by comparing the gain curves. The amount of peaking of the response (steady state gain versus maximum gain) is indicative of the damping of the rotor flapping motion. A decrease in damping is manifested by increased peaking. The magnitude of the lateral response of the rotor is flat out to $\omega/\Omega \simeq 0.3$ for both advance ratios. Therefore the peaking of the total rotor response is closely approximated by the peaking of the pitching motions (Figures 14

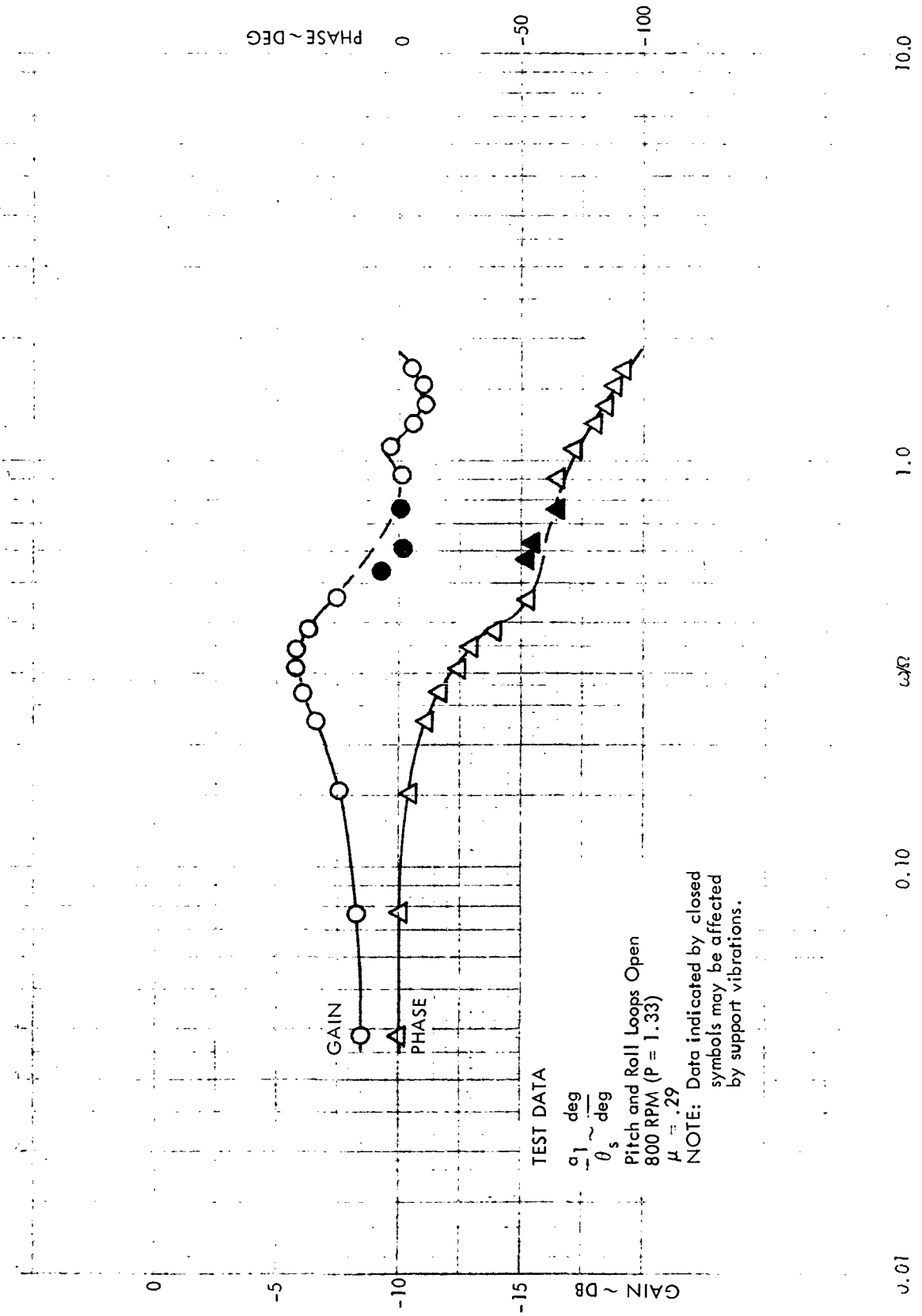

Figure 14. Rotor Longitudinal Frequency Response to Longitudinal Cyclic Pitch, μ = .29, 800 rpm (P = 1.33)

LOCKHEED CALIFORNIA COMPANY

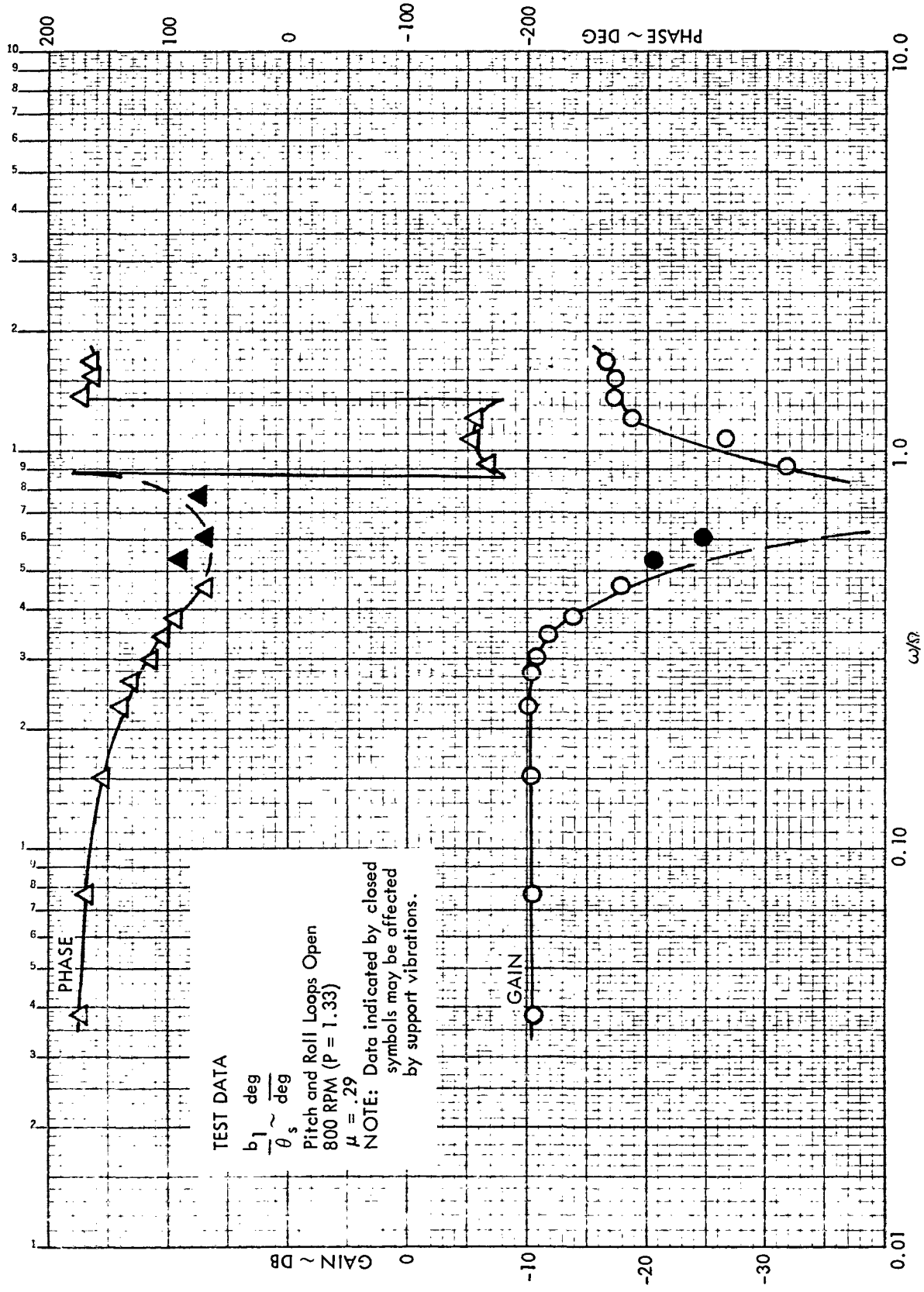

Figure 15. Rotor Lateral Frequency Response to Longitudinal Cyclic Pitch, $\mu = .29$, 800 rpm (P = 1.33)

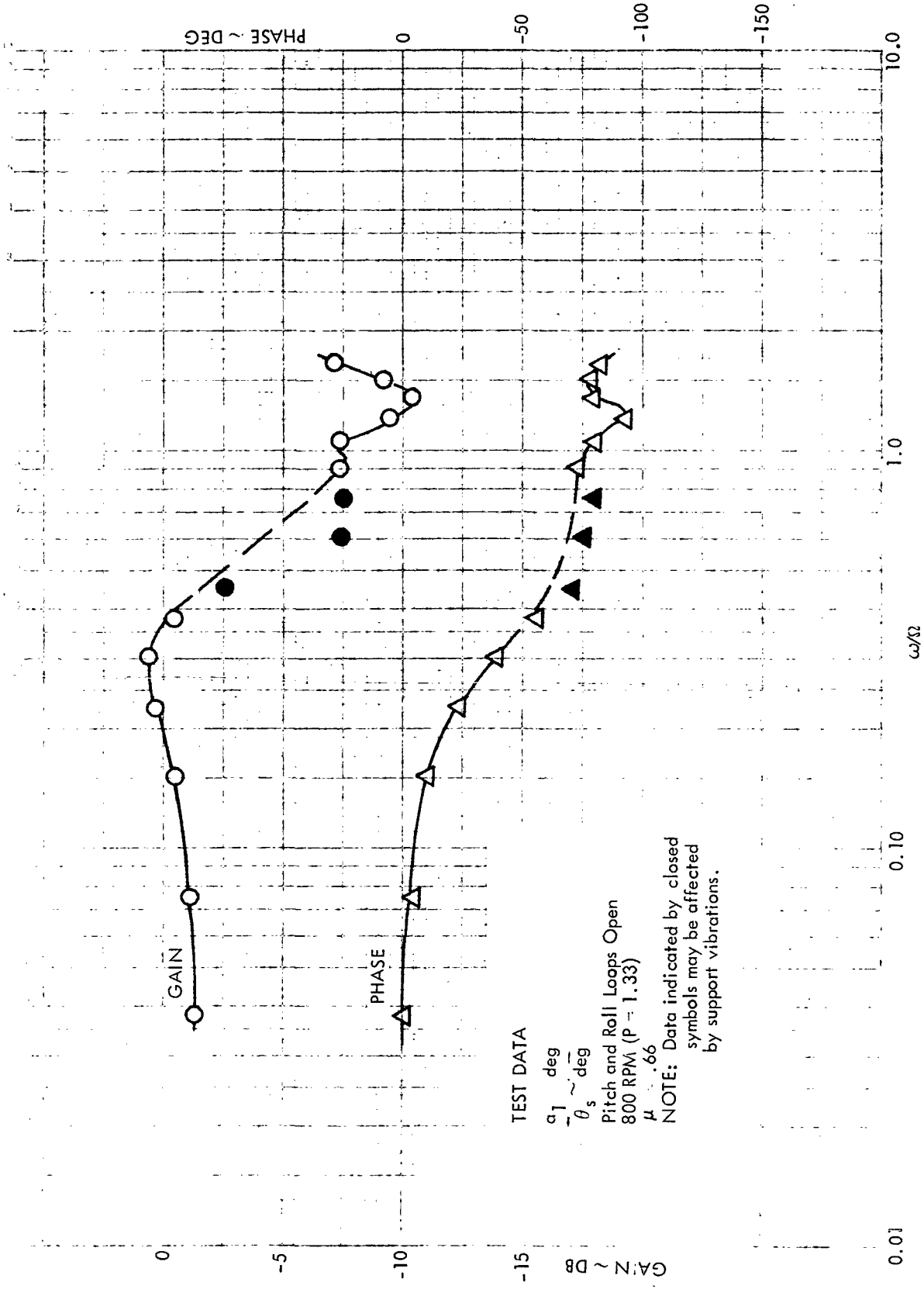

Figure 16. Rotor Longitudinal Frequency Response to Longitudinal Cyclic Pitch, μ = .66, 800 rpm (P = 1.33)

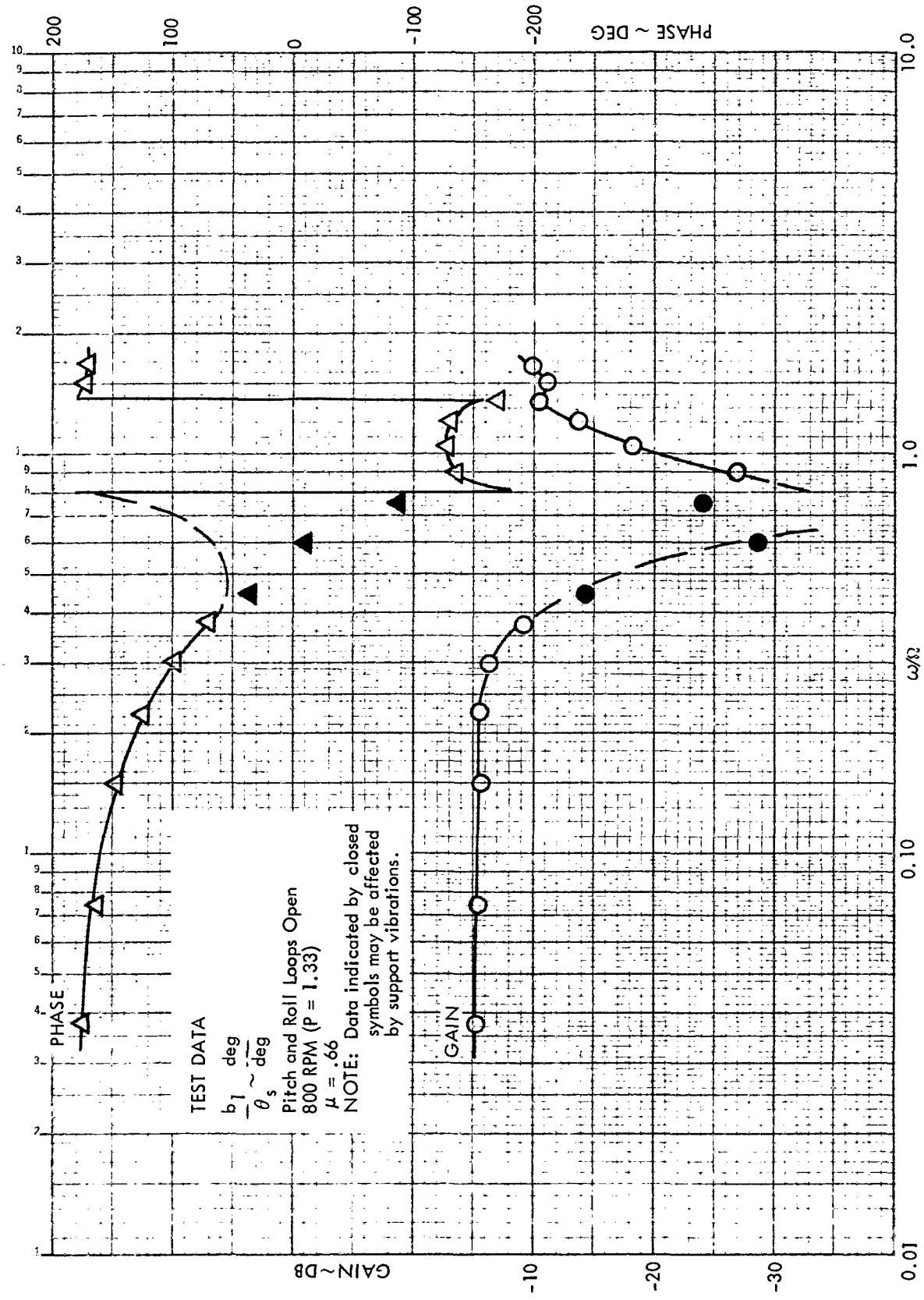

Figure 17. Rotor Lateral Frequency Response to Longitudinal Cyclic Pitch, μ = .66, 800 rpm (P = 1.33)

and 16). For $\mu = 0.29$ the increase in response is about 2.7 db and at $\mu = 0.66 \sim 2$ db. The implication is that the damping of the rotor flapping motion increases with advance ratio. If the frequencies at which the maximum rotor response occurs for the two advance ratios are now compared, it is seen that the frequency decreases with advance ratio. This is in line with the increased damping since the frequency corresponds to the damped natural frequency of the flapping motion. Increased damping is expected to reduce the frequency. The increase in damping and decrease in natural frequency of the flapping motion with increasing advance ratio are in agreement with previous theoretical stability investigations reported on Pages 102 - 103 of Reference 1.

An example of the rotor frequency response to lateral cyclic pitch (θ_c) at 800 rpm is shown in Figures 18 and 19. The characteristics noted in the collective pitch and longitudinal cyclic pitch frequency response curves are also seen in the θ_c curves. In addition, a distinct increase in the rotor pitch response occurs at $\omega/\Omega \simeq 1.10$. It will be seen later that this characteristic is not predicted by the simple rigid blade flapping theory. It is suggested (without theoretical substantiation) that this peaking may be caused by the response of the rotor in the second flap bending mode. At 800 rpm the natural frequency of the mode is $\sim 4.15\ \Omega$ (Page 21 of Reference 1). It is noted that similar (though smaller) peaks are detectable at the same frequency in the longitudinal frequency responses with respect to both θ_o and θ_s (Figures 12 and 14).

As discussed earlier, the model support was not excited significantly during these tests and, therefore, had little effect upon the measured rotor response.

Typical rotor transfer functions obtained at a rotational speed of 550 rpm are illustrated by Figures 20 to 25. The longitudinal and lateral rotor frequency responses to the three excitations (θ_o, θ_s, θ_c) are plotted over the nondimensional frequency range $0.055 \rightarrow 2.4$ at an advance ratio of $\mu = 0.58$. The characteristics of the curves are approximately the same as those obtained at 800 rpm. There are two notable differences however. First, and most important,

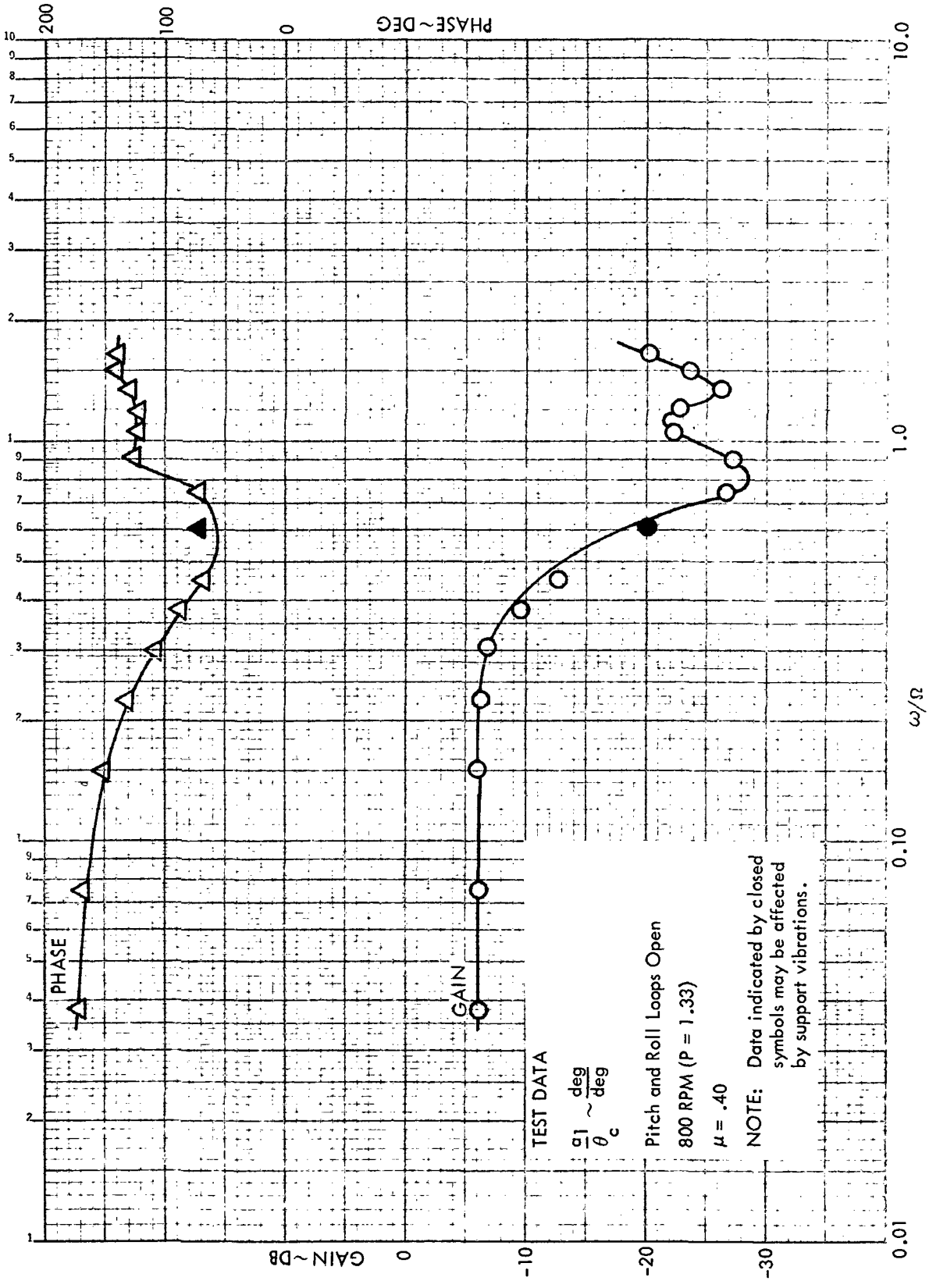

Figure 18. Rotor Longitudinal Frequency Response to Lateral Cyclic Pitch, μ = .40, 800 rpm (P = 1.33)

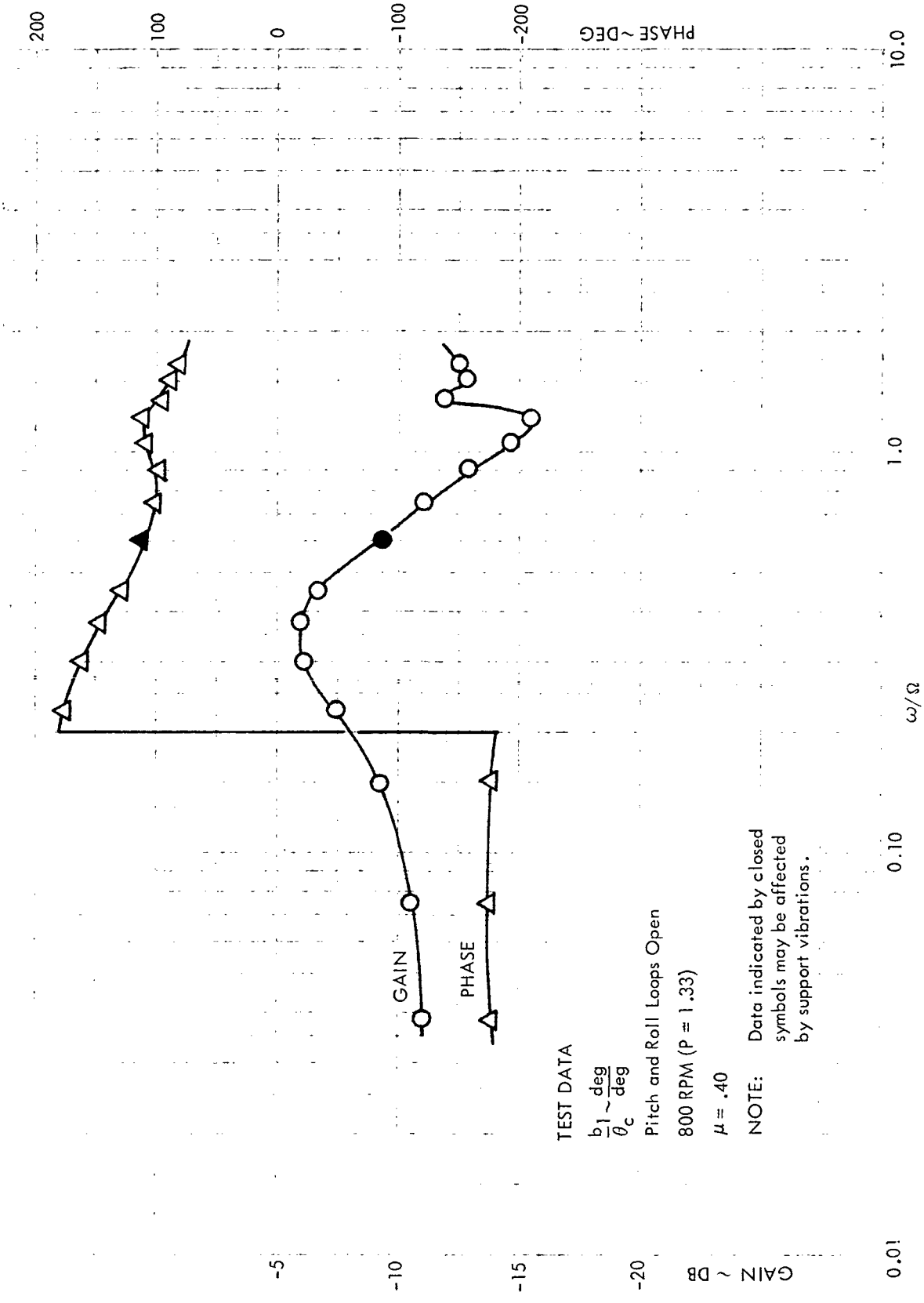

Figure 19. Rotor Lateral Frequency Response to Lateral Cyclic Pitch, μ = .40, 800 rpm (P = 1.33)

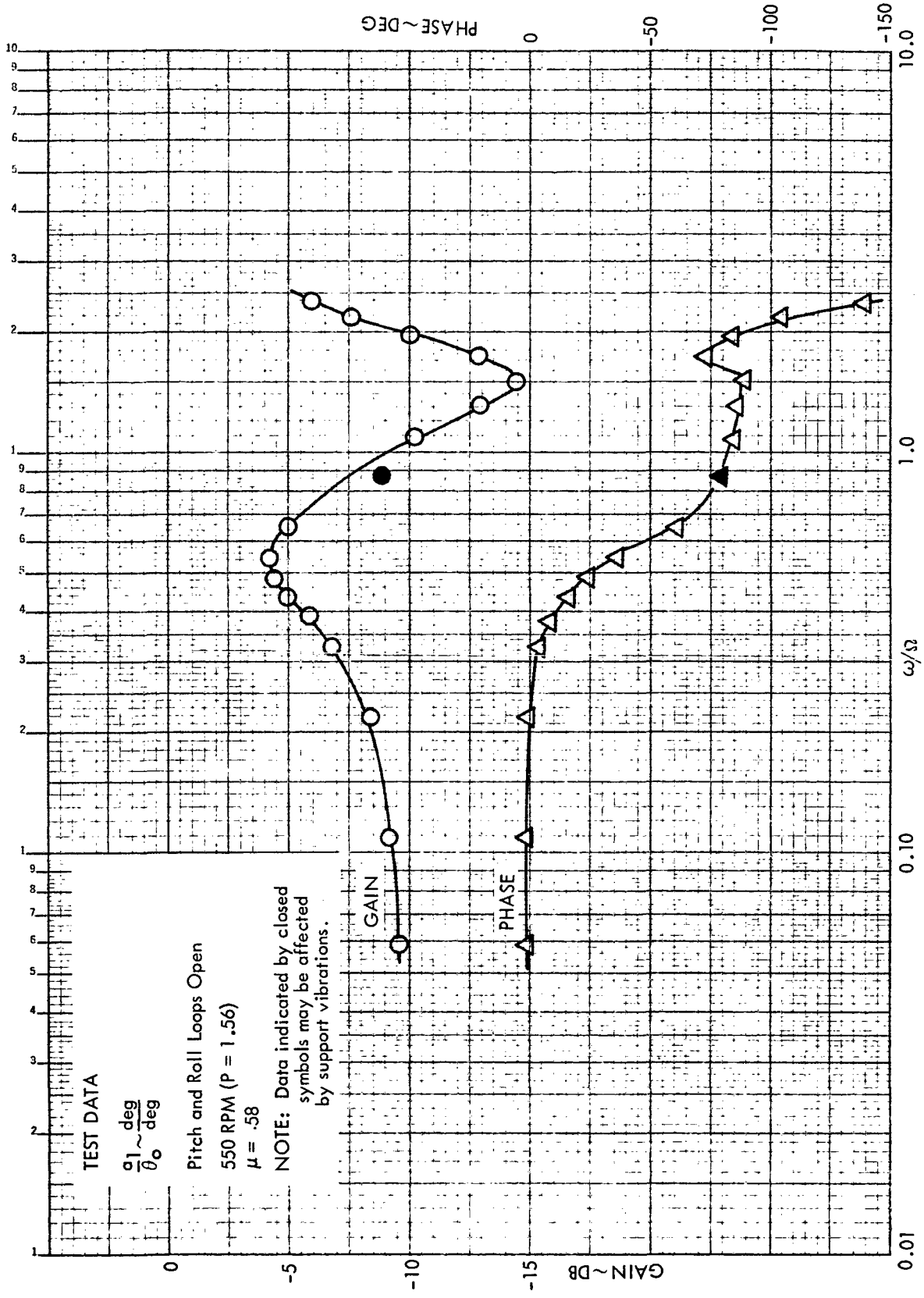

Figure 20. Rotor Longitudinal Frequency Response to Collective Pitch, μ = .58, 550 rpm (P = 1.56)

LOCKHEED CALIFORNIA COMPANY

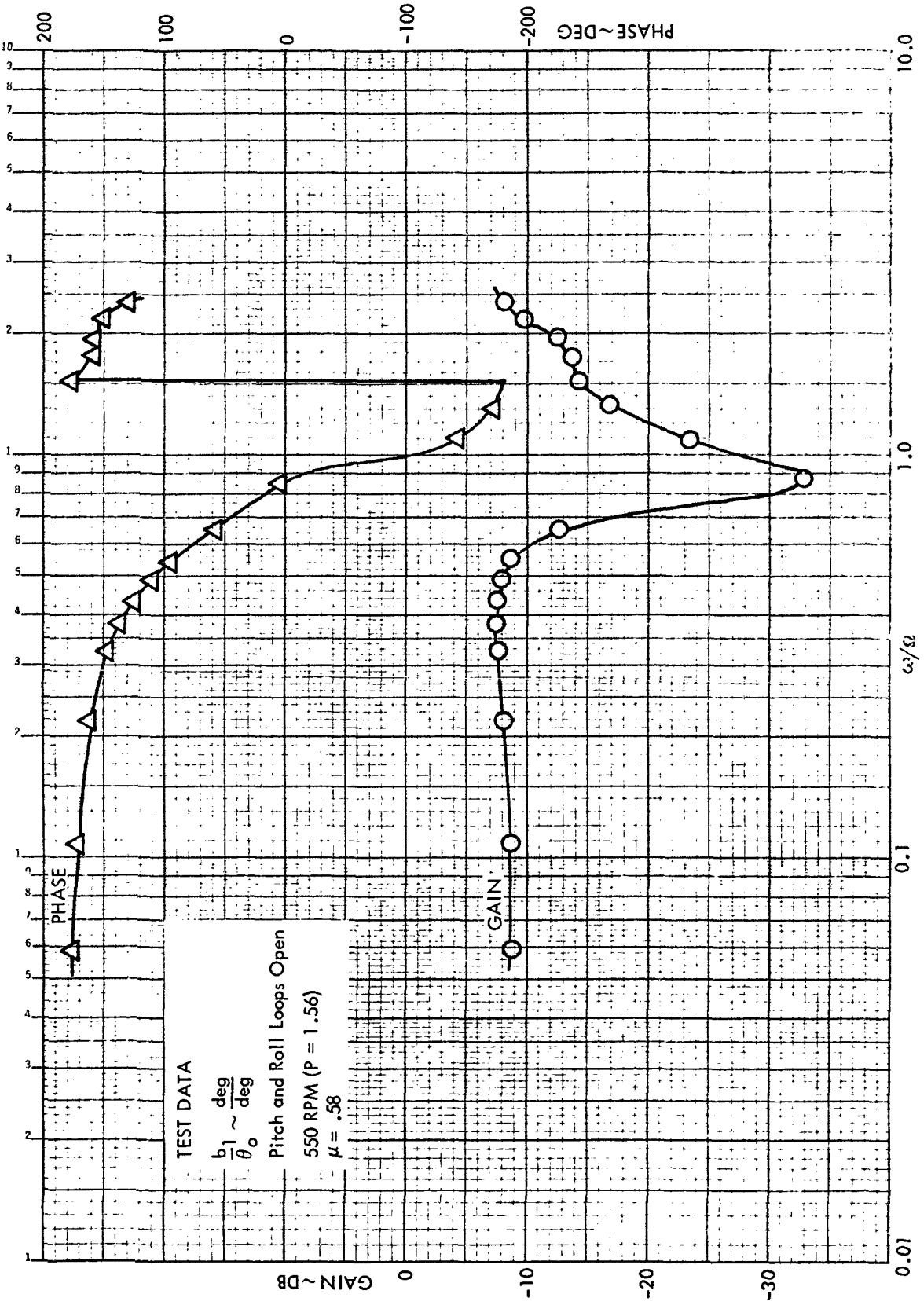

Figure 21. Rotor Lateral Frequency Response to Collective Pitch, μ = .58, 550 rpm (P = 1.56)

LOCKHEED CALIFORNIA COMPANY

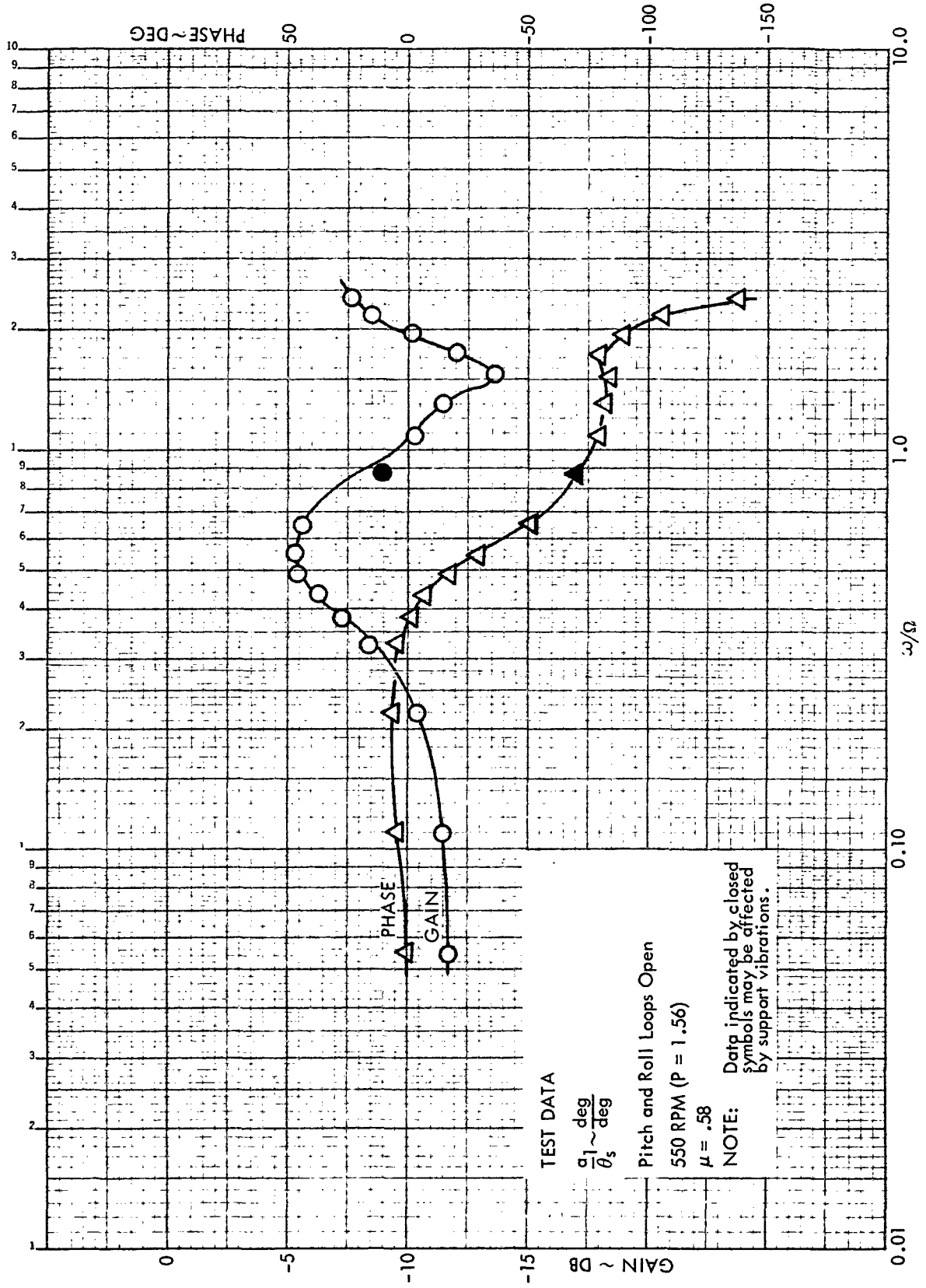

Figure 22. Rotor Longitudinal Frequency Response to Longitudinal Cyclic Pitch, μ = .58, 550 rpm (P = 1.56)

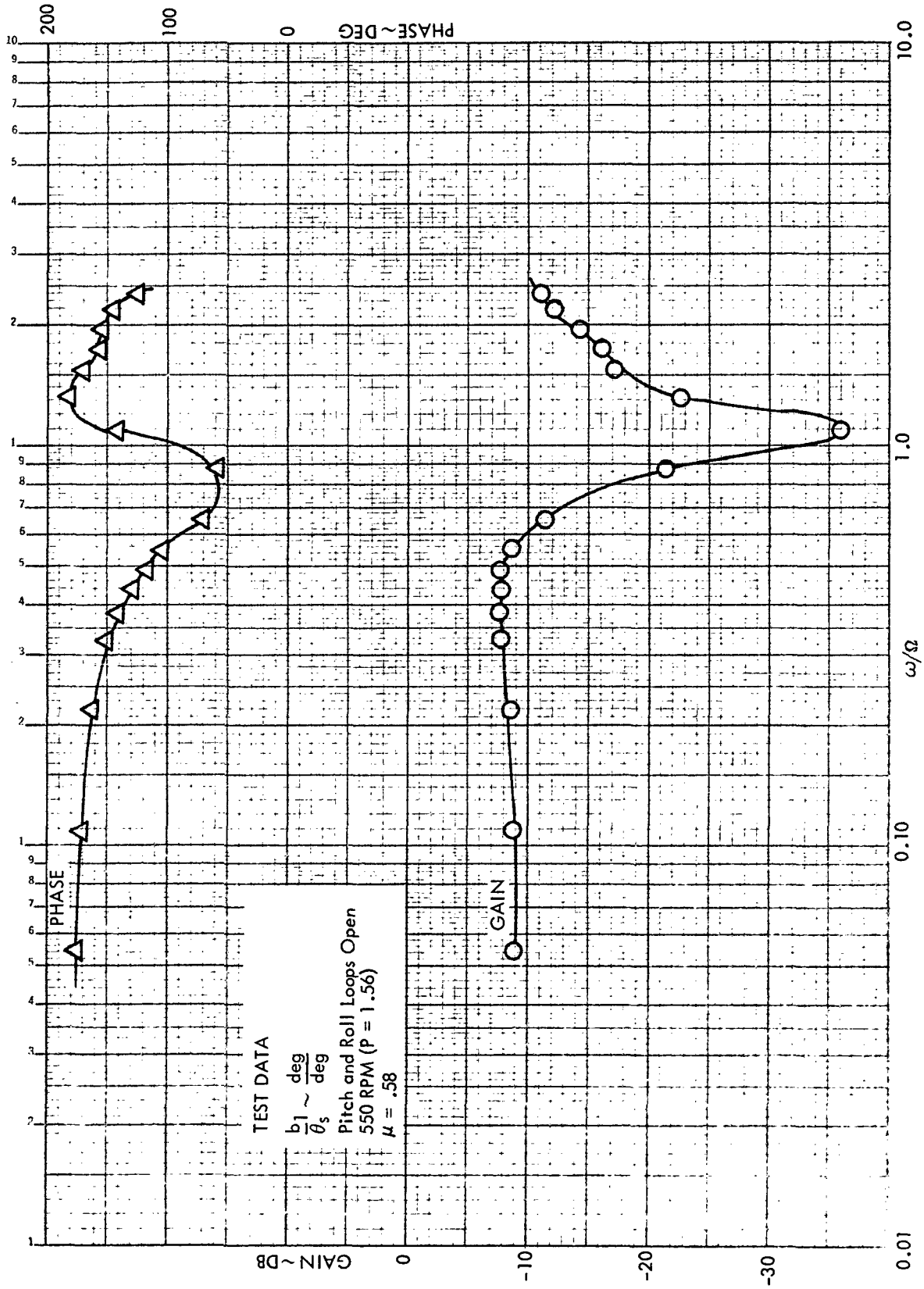

Figure 23. Rotor Lateral Frequency Response to Longitudinal Cyclic Pitch, μ = .58, 550 rpm (P = 1.56)

LOCKHEED CALIFORNIA COMPANY

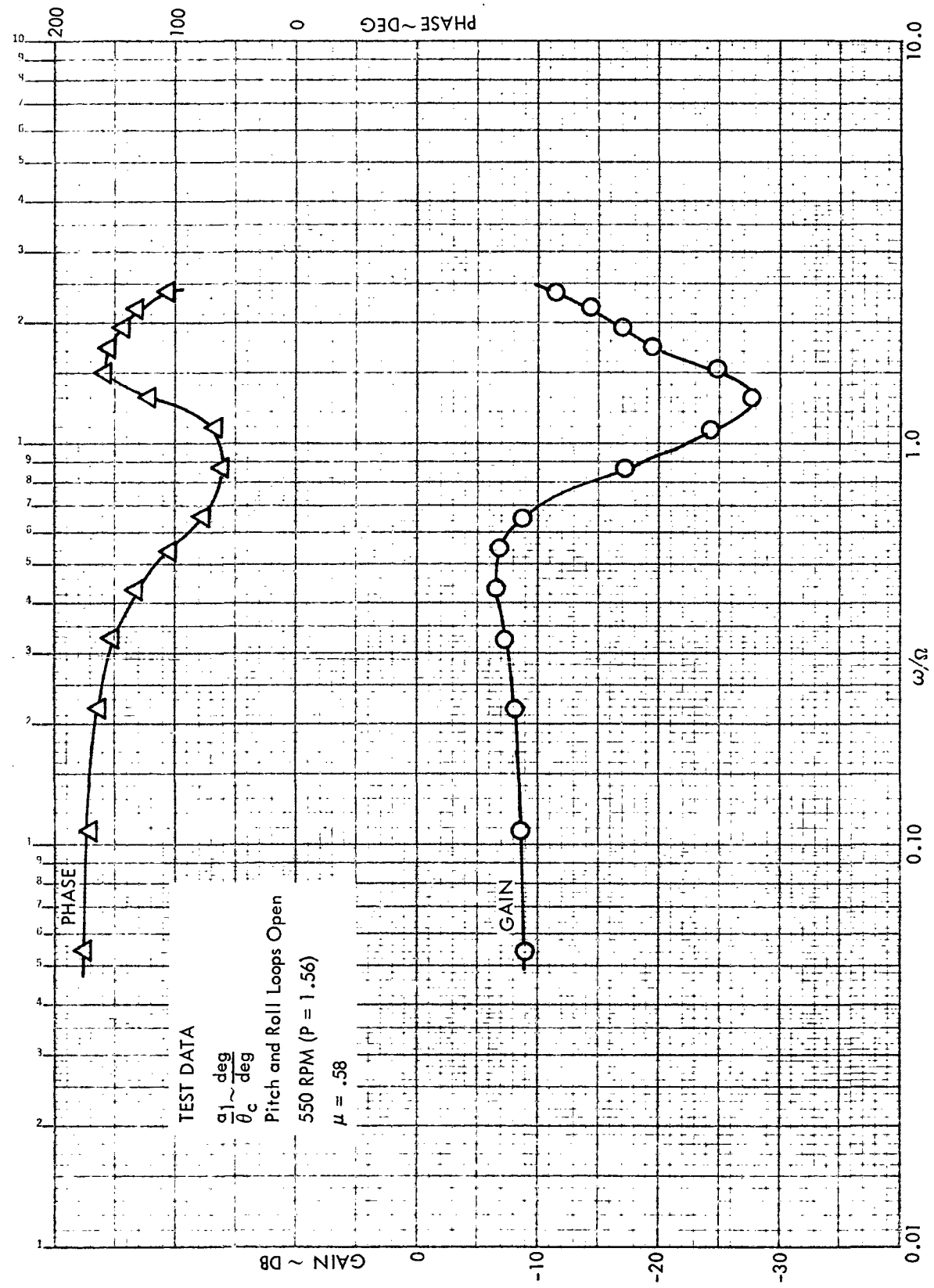

Figure 24. Rotor Longitudinal Frequency Response to Lateral Cyclic Pitch, μ = .58, 550 rpm (P = 1.56)

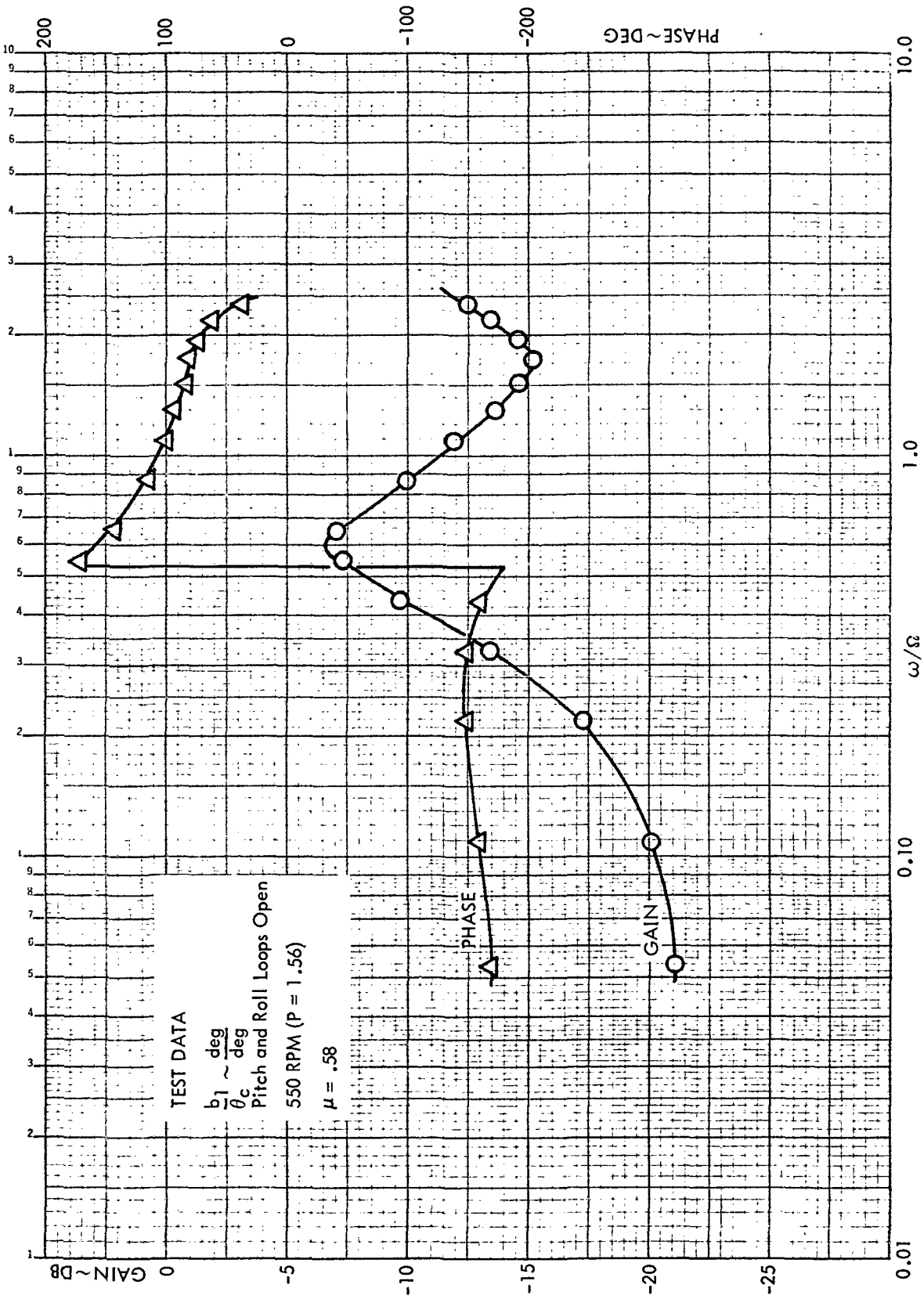

Figure 25. Rotor Lateral Frequency Response to Lateral Cyclic Pitch, μ = .58, 550 rpm (P = 1.56)

LOCKHEED
CALIFORNIA COMPANY

an increase in rotor response comparable to that observed at a frequency ratio of $\sim$ 1.1 at 800 rpm is not detectable. The absence of this characteristic tacitly lends credence to the supposition that it is caused by the involvement of the second flap bending mode in the response. At 550 rpm the natural frequency of the second flap mode is approximately $5.5\,\Omega$ (Page 21 of Reference 1) and the possibility of exciting it is remote. Second, there is the apparent minimized effect of the stand shake on the response. The effect is only detectable in the rotor pitching response at a frequency of 8 Hz ($\omega/\Omega = 0.87$).

Typical rotor transfer functions at 300 rpm are illustrated in Figures 26 and 27. A longitudinal cyclic pitch excitation is considered and the advance ratio is 1.44. The two prominent peaks in the gain curve represent the response of the rotor at its first flap bending natural frequency. It is noted that the combination of flapping frequency and rotor speed at 300 rpm is such that the rotor experiences the resonance condition twice (i.e., when $\frac{\omega}{\Omega} \cong$ P-1 and $\frac{\omega}{\Omega} \cong$ P + 1). As indicated in prior discussions, the effect of the stand shake on the rotor response is not detectable.

All of the rotor transfer functions which were obtained during the test are documented in Appendix C. In addition to plotted data the appendix contains a tabulation of the measured moment derivatives transfered to the center of rotation. They are listed in coefficient from versus the excitation frequency and test conditions.

Primary Pitch and Roll Loop Stabilities

During the open loop frequency response tests (pitch and roll loops open) conducted to obtain rotor transfer functions, sufficient data were also acquired to permit the determination of the primary pitch and roll loop stability margins. For example, the primary pitch loop stability for $\Delta = 0$ is directly obtainable from the transfer function $\delta_s/\bar{\theta}_s$. $\delta_s/\bar{\theta}_s$ is formed by multiplying the measured transfer function M_R/θ_s by the measured actuator transfer

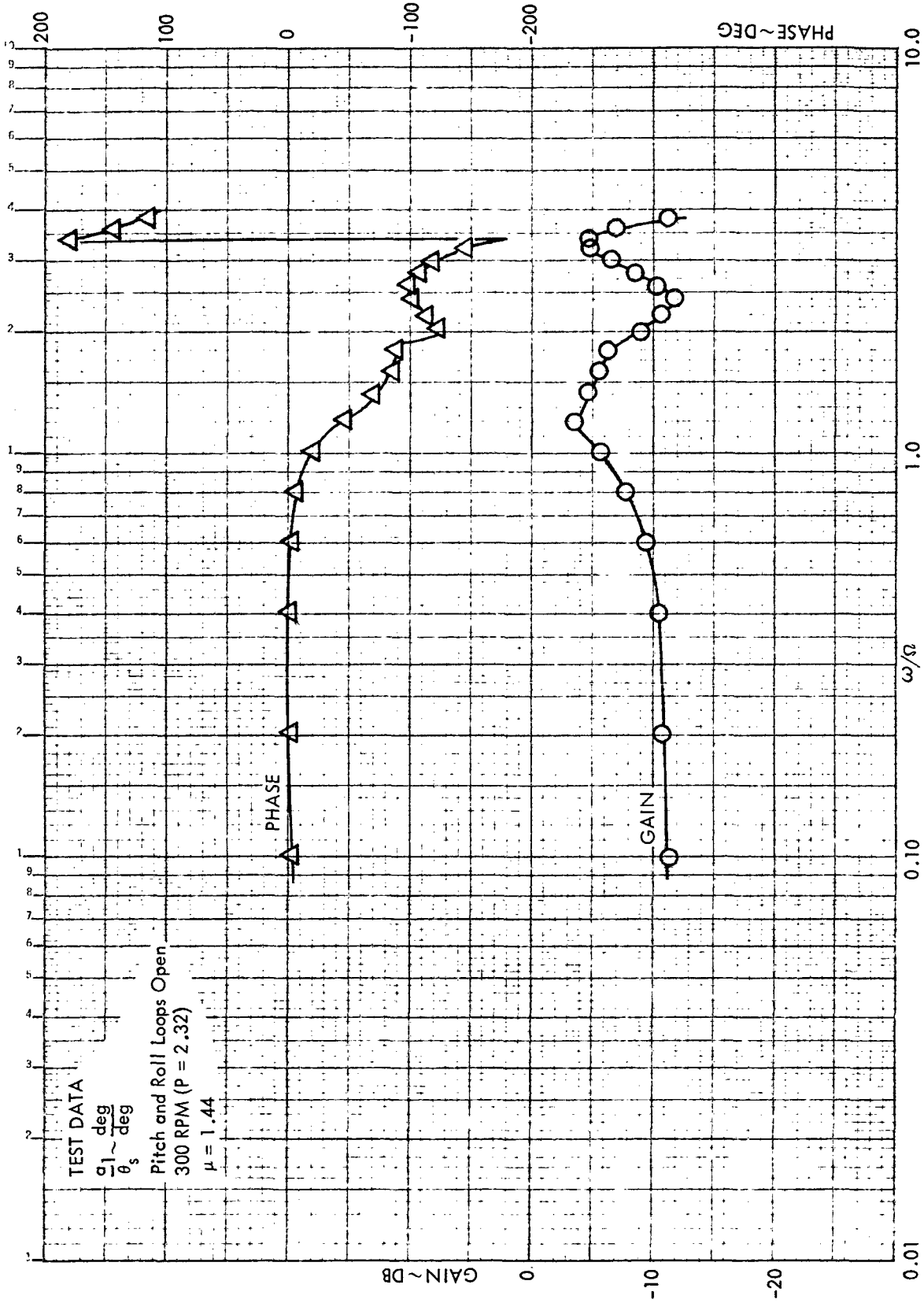

Figure 26. Rotor Longitudinal Frequency Response to Longitudinal Cyclic Pitch, $\mu = 1.44$, 300 rpm (P = 2.32)

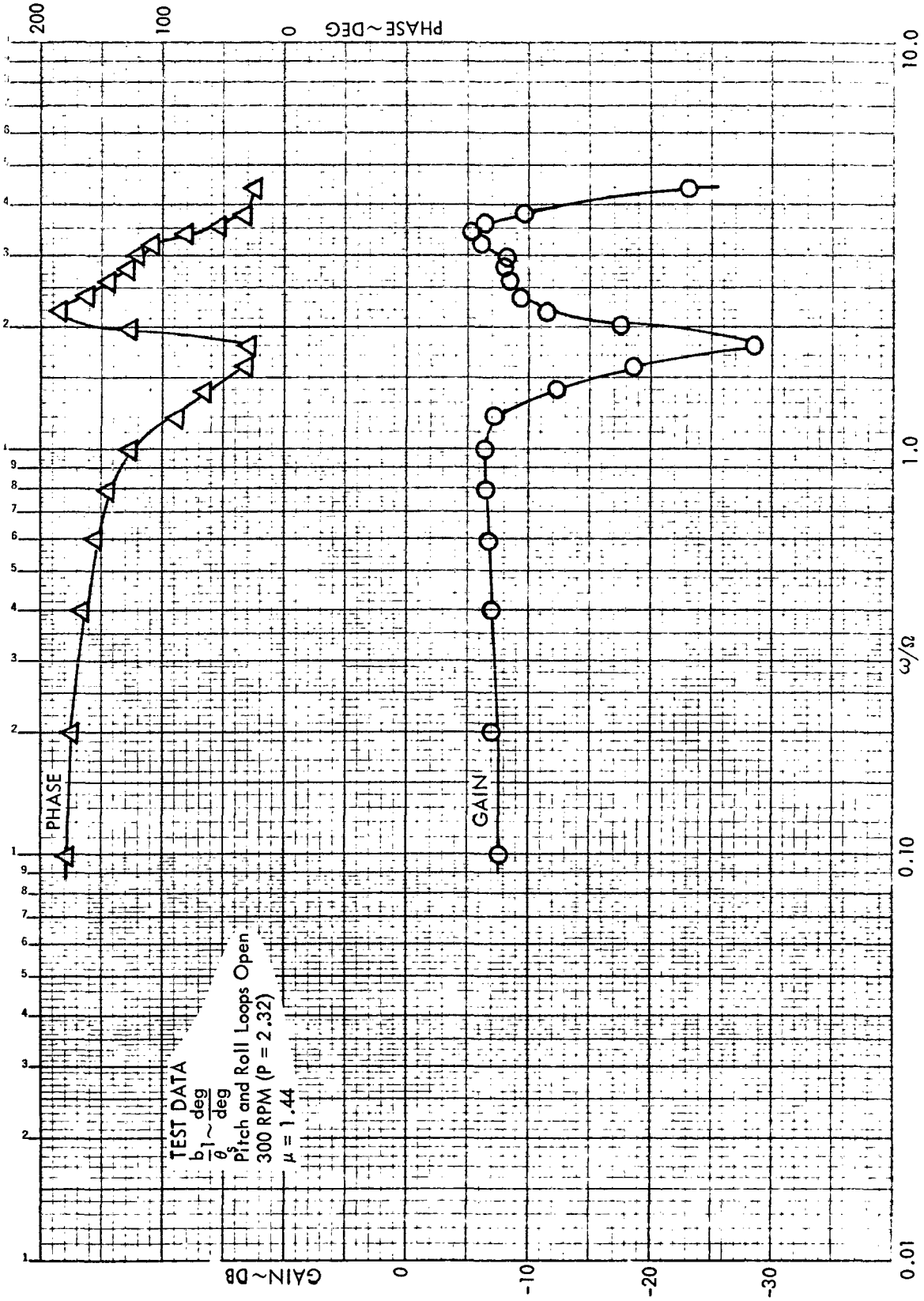

Figure 27. Rotor Lateral Frequency Response to Longitudinal Cyclic Pitch, $\mu = 1.44$, 300 rpm (P = 2.32)

function $\theta_s/\bar{\theta}_s$, the scaling pot

$$\frac{a_1}{M_R} = \frac{1}{2K_\beta}$$

and the control system transfer function

$$\frac{\delta_s}{a_1} = \frac{A\,\Omega/K_1K_3}{S + \Omega\,L}$$

i.e.

$$-\frac{\delta_s}{\bar{\theta}_s} = \left(\frac{\theta_s}{\bar{\theta}_s}\right)\left(\frac{M_R}{\theta_s}\right)\left(\frac{a_1}{M_R}\right)\left(\frac{\delta_s}{a_1}\right)$$

Since the transfer functions a_1/M_R and δ_s/a_1 are well defined, the formation of $\delta_s/\bar{\theta}_s$ was accomplished analytically. It could have been determined completely experimentally since the proper instrumentation was available. This would, however, have required a repetition of tests for each combination of control system parameters (A and L) and was obviously not considered a prudent alternative.

An example of the procedure used to determine primary pitch loop stability is illustrated in Figure 28. The development of $\delta_s/\bar{\theta}_s$ begins with the rotor transfer function a_1/θ_s (the multiplication

$$\left(\frac{M_R}{\theta_s}\right)\quad\left(\frac{a_1}{M_R}\right)$$

has already been carried out.) The transfer functions $\theta_s/\bar{\theta}_s$ and δ_s/a_1 are added (multiplication is accomplished by addition when gains are expressed in decibels, phases angles are always additive) to obtain $\delta_s/\bar{\theta}_s$. The stability of the loop is then expressed in terms of gain and phase margins. The gain margin is the difference between the gain and 0 db at the frequency where the phase shift is -180°. If the gain is less than zero db, the margin is defined as positive and the system is termed gain stable. Similarly, the

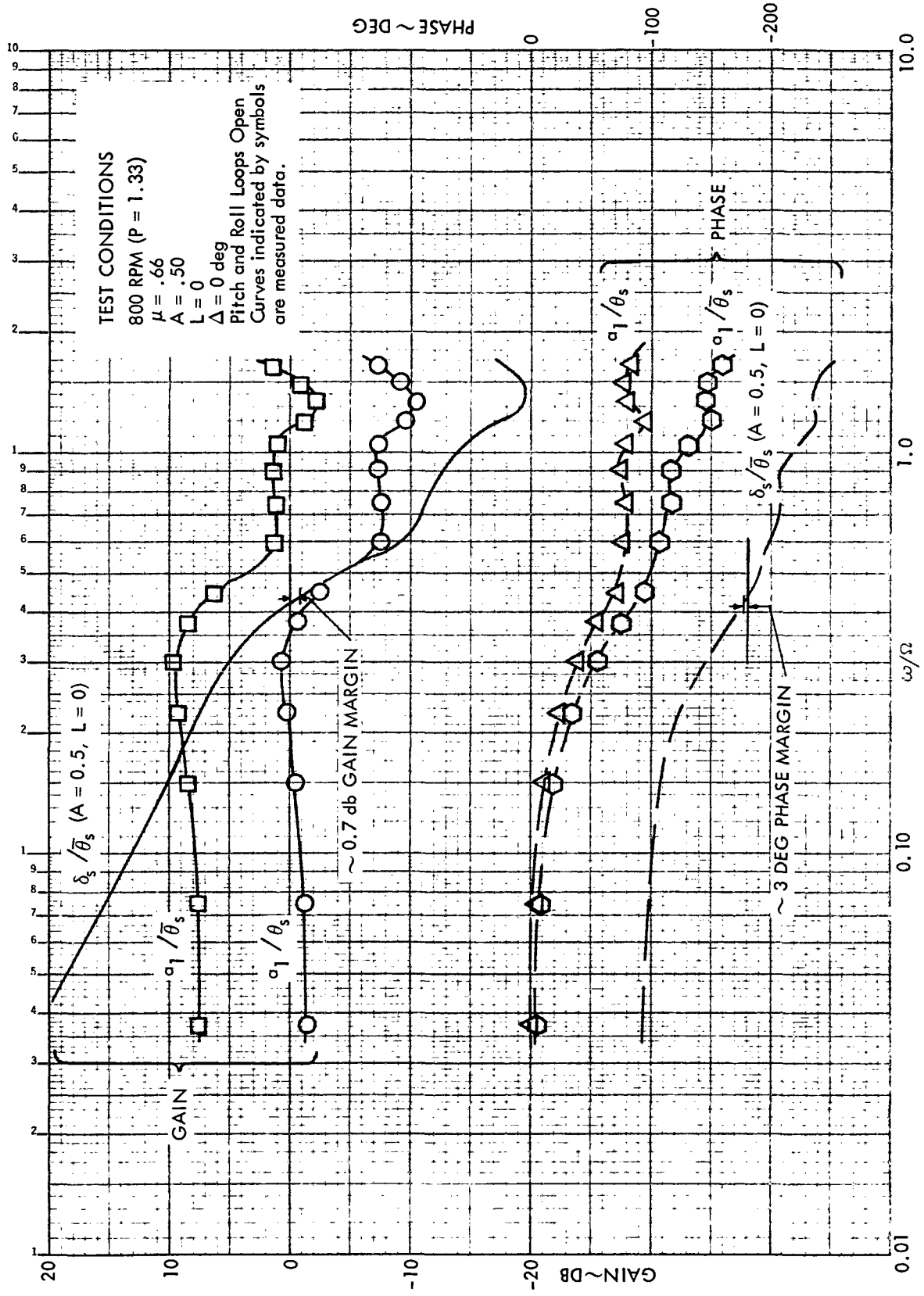

Figure 28. Primary Pitch Loop Stability Margins from Rotor Transfer Functions (Illustrated)

LOCKHEED CALIFORNIA COMPANY

phase margin is measured at the frequency where the gain is 0 db. If the phase is less than -180°, the margin is positive and system is phase stable. For the example shown, the primary pitch loop is almost neutrally stable having only a gain margin of 0.7 db and a 3° phase margin. This condition is the least stable of all those tested.

In Figure 28 you will note that the transfer function $a_1/\bar{\theta}_s$ is identified as measured data. Since $\bar{\theta}_s$ is exactly the sine wave function generator output which was recorded, it was convenient to calculate the transfer function a_1/θ_s directly from the data rather than by adding the effect of the actuator to the rotor transfer function a_1/θ_s. However, for those who would examine different control system configurations, the actuators transfer functions would be required. The functions have been determined from the test data and have been previously presented in Figures 3 and 4. They were generally invariant for the conditions examined during the test.

The results of the primary pitch loop stability analysis at 800 rpm are summarized in Figure 29. Gain and phase margins are plotted versus μ for several control system descriptions. The anticipated decreases in stability with increases in feedback gain, time constant, and advance ratio are noted.

Figure 30 shows the results of the primary roll loop stability analysis at 800 rpm. The combinations of parameters including A, L and μ are the same as those in the previous figure. The effect of the control parameter variations are the same as for the pitch loop stability analysis. There are two main differences in the stability characteristics of the two loops. First, the primary roll loop is generally more stable than the primary pitch loop, particularly at the higher advance ratios. A trend toward comparable stability margins is noted at lower μs. It is clear that at $\mu = 0$, the stabilities of the two primary loops are identical. Second, there is the lack of sensitivity of the roll loop stability to changes in advance ratio.

Total Pitch and Roll Loop Stabilities

Once the stabilities of the primary loops were known, the experimental investigations continued with the determination of the total pitch loop and total roll loop stability margins. It is recalled that the primary roll

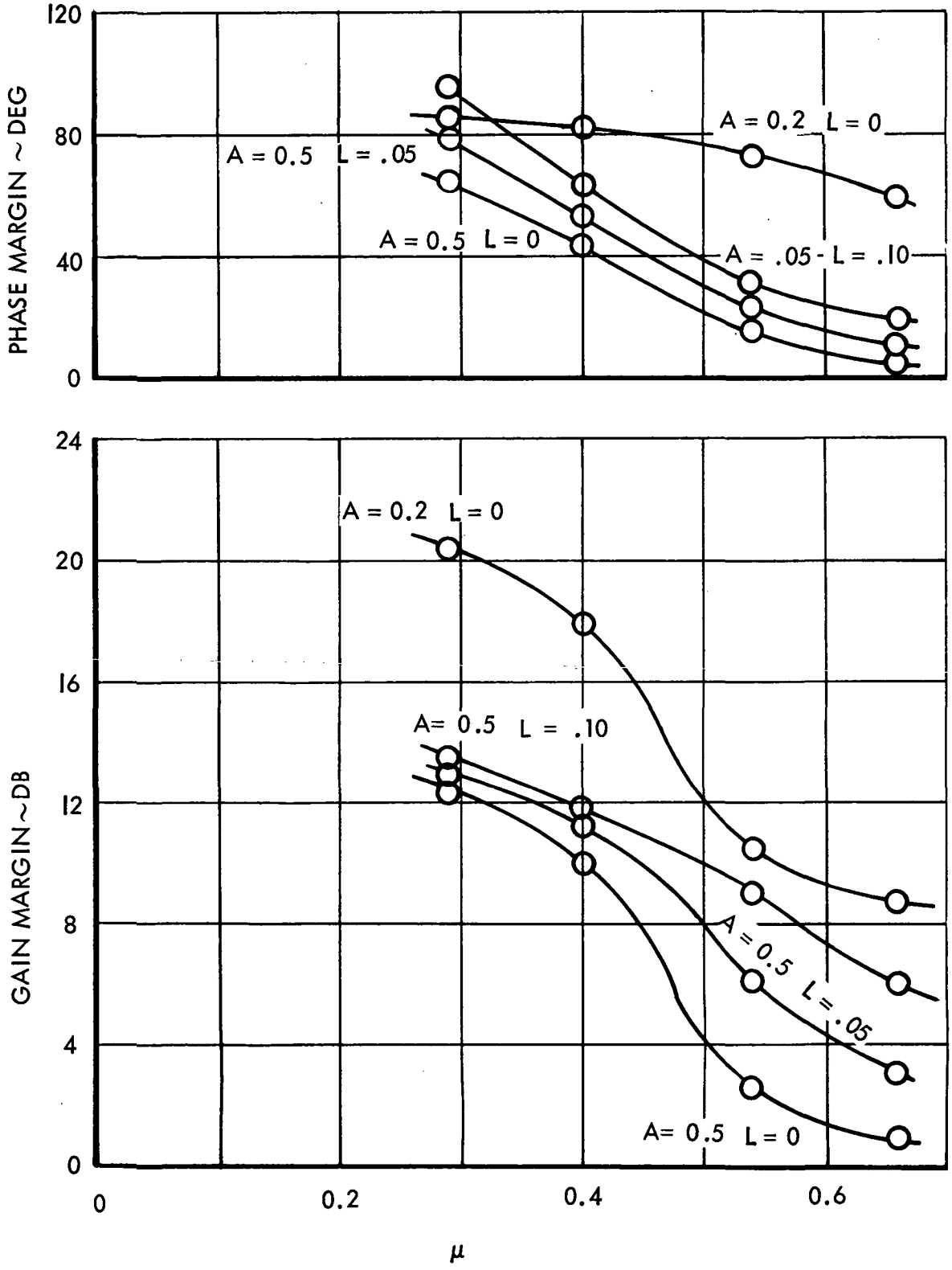

Figure 29. Primary Pitch Loop Stability Margins, 800 rpm (P = 1.33)

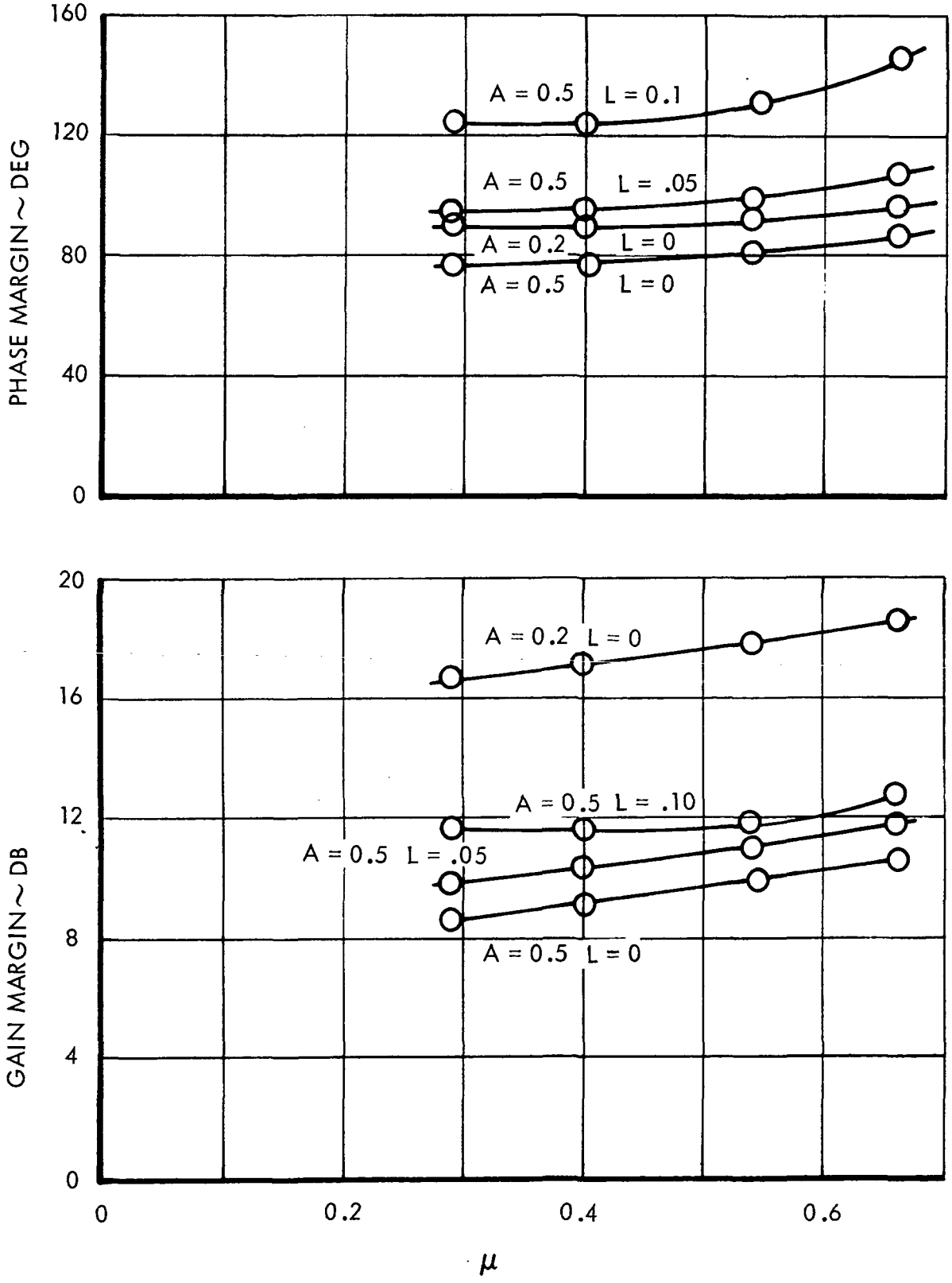

Figure 30. Primary Roll Loop Stability Margins, 800 rpm (P = 1.33)

loop is contained within the total pitch loop and the primary pitch loop within the total roll loop (See Figures 10 and 11). The tests were conducted as follows. To determine total pitch loop stability the system was excited with a $\bar{\theta}_s$ command with the pitch loop open and the roll loop closed in order to generate the frequency response derivative $\delta_s / \bar{\theta}_s$. Stability was then indicated by the gain and phase margins deduced from this transfer function. For total roll loop stability the pitch loop was closed and the roll loop left open. A $\bar{\theta}_c$ excitation was used to generate the transfer function $\delta_c / \bar{\theta}_c$ from which the stability margins were extracted. For all of these tests a symmetric control system was maintained. That is, the parameters A and L were the same for both the pitch loop and the roll loop.

As an example, the data and procedure used to determine total pitch loop stability is presented in Figure 31. The test conditions (V, ΩR) and control system description (A, L) are the same as those of Figure 28 where primary pitch loop stability was examined. Two transfer functions are plotted $a_1 / \bar{\theta}_s$ and $\delta_s / \bar{\theta}_s$. $a_1 / \bar{\theta}_s$ is obtained directly from measured data where $\bar{\theta}_s$ is the oscillator input to the θ_s actuator and

$$a_1 = M_R \text{ (3.3 in.)}/2K_\theta \text{ (3.3 in.)}$$

The $\delta_s / \bar{\theta}_s$ curves are obtained by adding the control system transfer function

$$\frac{\delta_s}{a_1} = \frac{A \Omega / K_1 K_3}{S + \Omega L}$$

to a_1/θ_s. This semi-analytical determination of $\delta_s/\bar{\theta}_s$ was required because with L = 0 the control system was a pure integrator which drifted in the open loop mode. The integrator would drift into saturation sporadically preventing an accutate δ_s measurement. It is noted that such integrator behavior is normal. For cases where $L \neq 0$, the control system is not a pure integrator and the $\delta_s / \bar{\theta}_s$ transfer functions are determined directly from measured data.

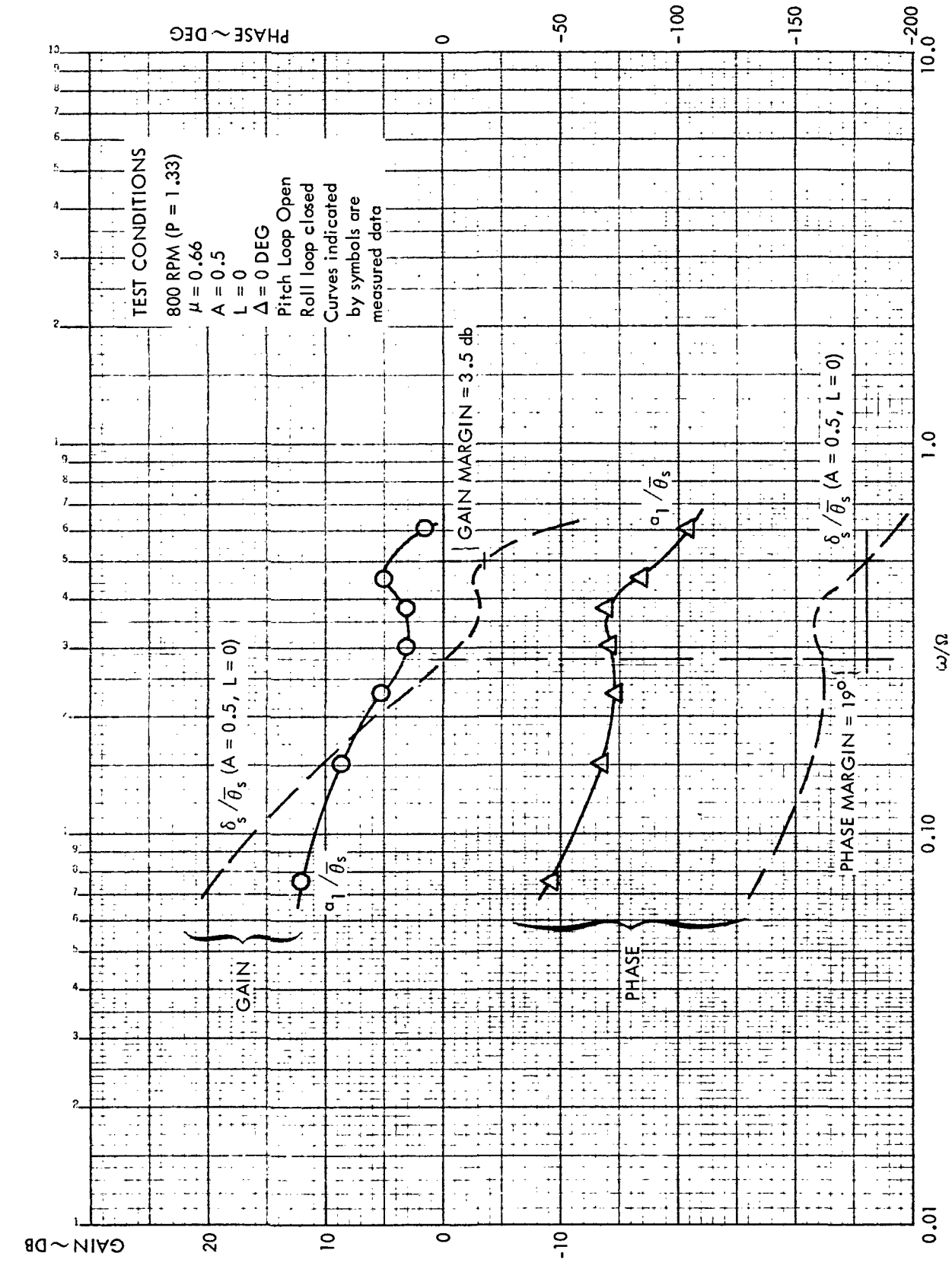

Figure 31. Longitudinal Transfer Functions ($a_1/\bar{\theta}_s$, $\delta_s/\bar{\theta}_s$), Pitch Loop Open, Roll Loop Closed, μ = .66, 800 rpm (P = 1.33), A = .50, L = 0, Δ = 0 deg

For the example shown, the total pitch loop stability margins are 3.5 db and 19 degree. For the same conditions the primary pitch loop margins were only 0.7 db and 3 degree. The implication is that the pitch loop is stabilized by the roll loop. This was generally found to be true at the two higher of the four tested advance ratios. A summary of the total pitch loop stability margins versus μ constitutes Figure 32. The control system configurations (A, L) are the same as those examined during the primary loop stability investigations.

The total roll loop stability was also examined experimentally for two control system parameter combinations, one of which (A = 0.5, L = 0) has been seen to generate the least stable system. Figure 33 is a summary curve showing the results of these investigations. A comparison with the primary roll loop stability margins reveals that the pitch loop generally degrades the stability of the roll loop. The degradation however is mild.

One of the more interesting conditions encountered during the total roll loop stability tests was the case where the primary pitch loop was marginally stable (See Figure 28). The rotor longitudinal and lateral frequency response to a $\bar{\theta}_c$ excitation for this case are plotted in Figures 34 and 35. The pitch loop is excited by a $\bar{\theta}_c$ excitation through the rotor transfer functions $M_{R_{\theta_c}}$ and it in turn contributes to the roll response through the transfer function $L_{R_{\theta_s}}$ (See Figure 11). There is a large increase in rotor pitching response and corresponding rapid shift in phase when the system is excited at the phase margin frequency of the primary pitch loop. The large longitudinal rotor response also generates a similar lateral response. This resonance response of the pitch loop is confined to a small frequency range and has little effect upon the stability of the total roll loop.

From the total loop stability investigations it can be concluded that the overall stability of the closed loop system is approximated by the total pitch loop stability. This is particularly true in those regions where the stability margins are small. All of the experimental transfer functions used to determine

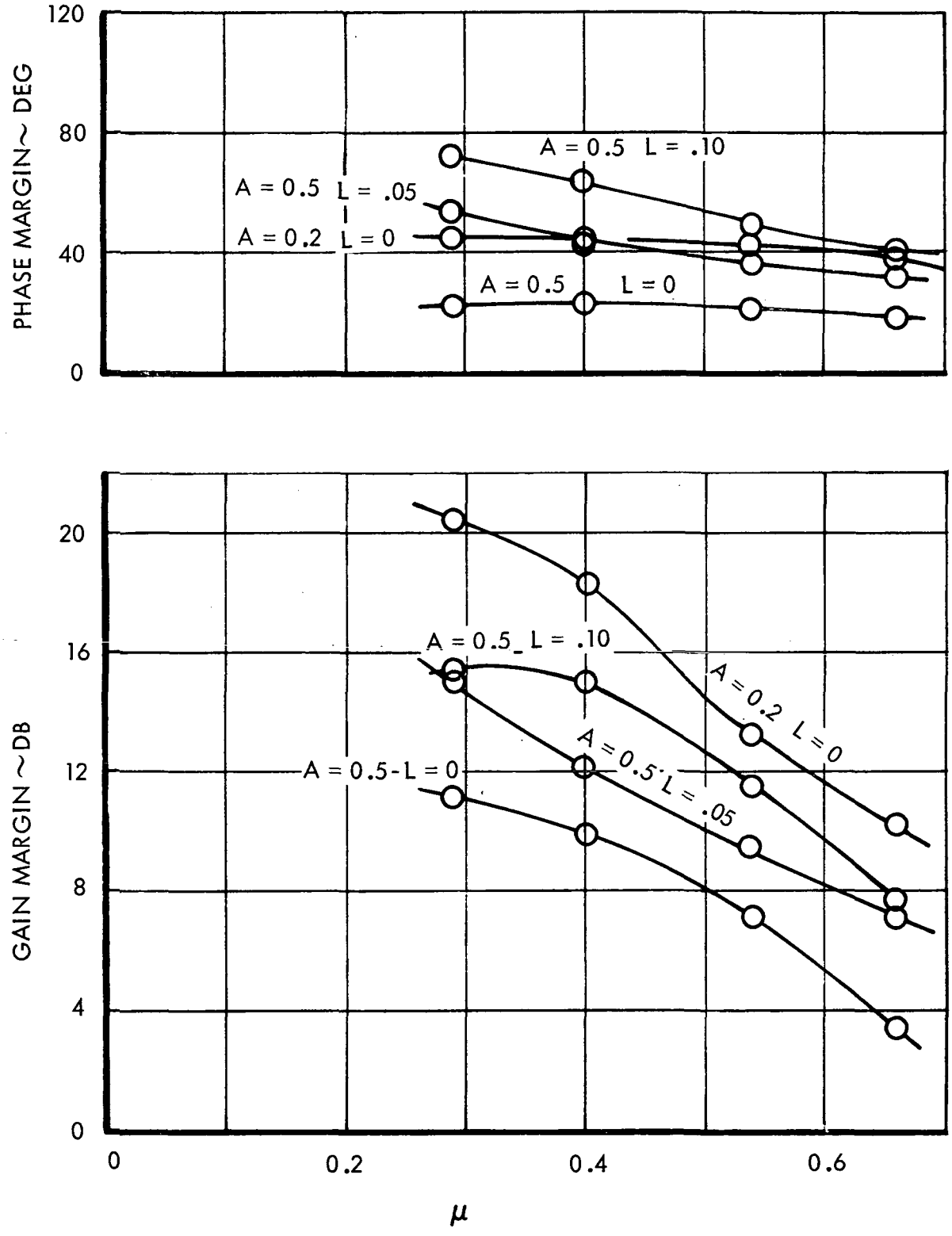

Figure 32. Total Pitch Loop Stability Margins, 800 rpm (P = 1.33), Δ = 0 deg

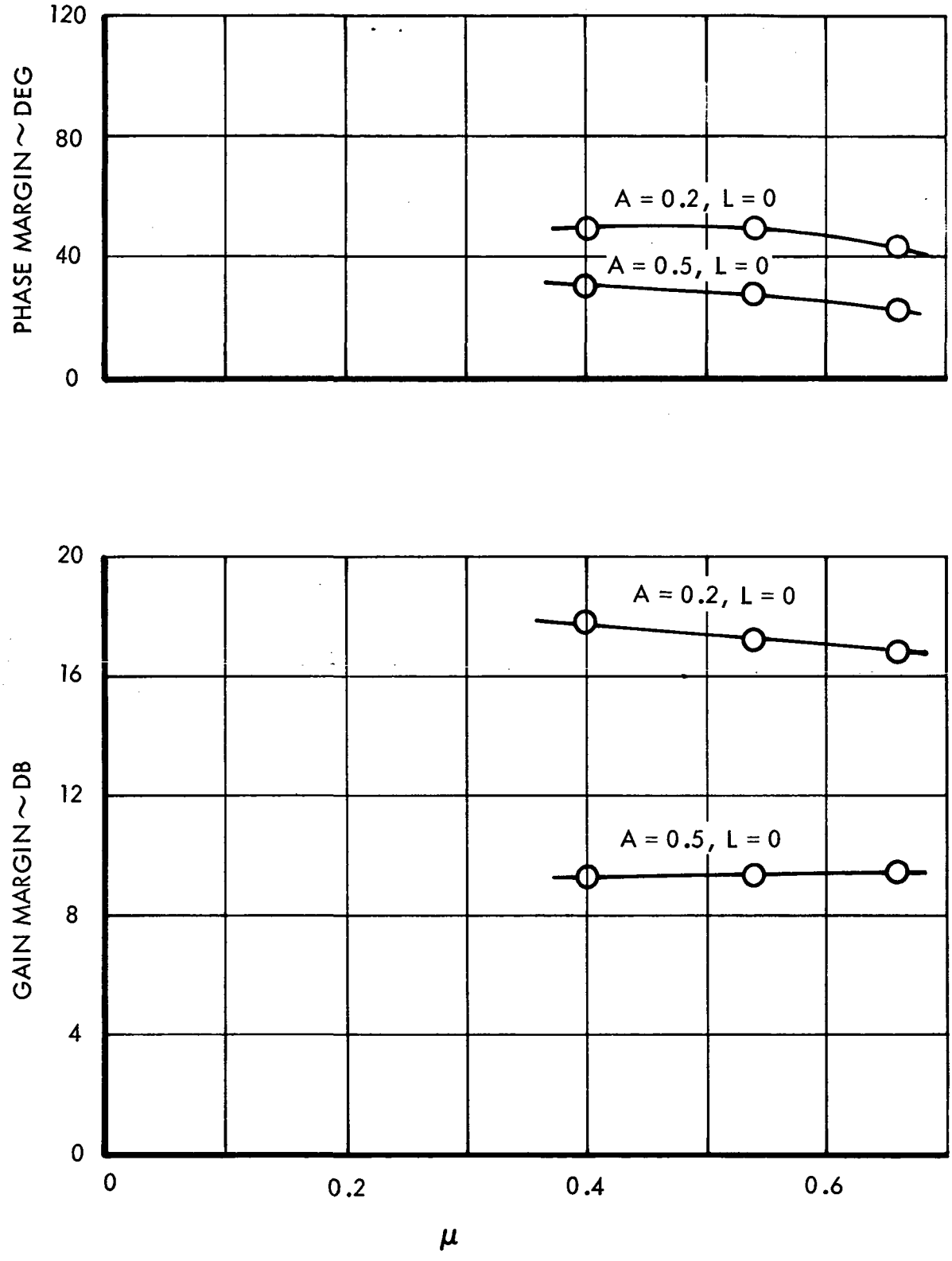

Figure 33. Total Roll Loop Stability Margins, 800 rpm (P = 1.33), Δ = 0 deg

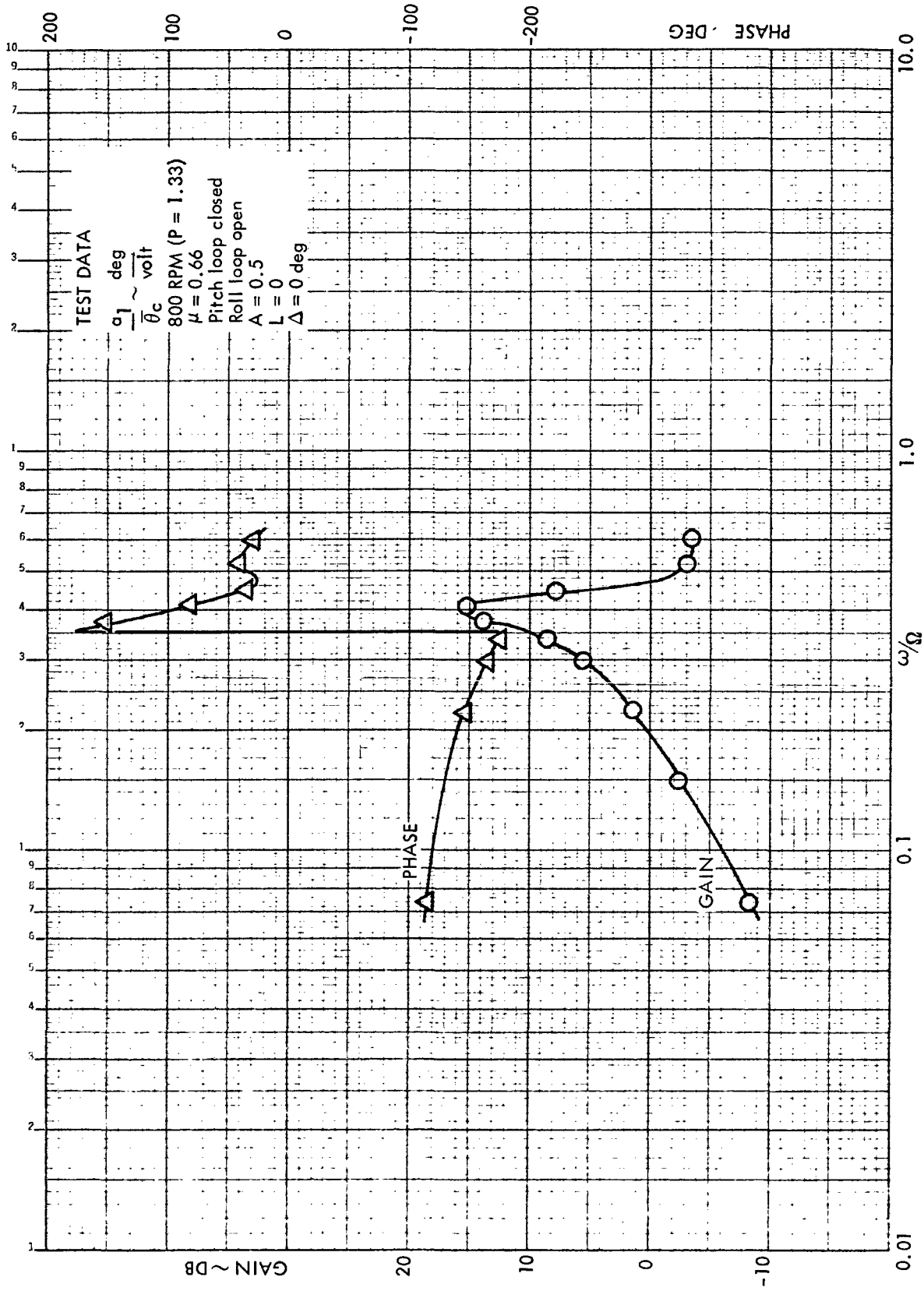

Figure 34. Rotor Longitudinal Frequency Response to Lateral Cyclic Pitch, Pitch Loop Closed, Roll Loop Open μ = 0.66, 800 rpm (P = 1.33), A = 0.5, L = 0, Δ = 0 deg

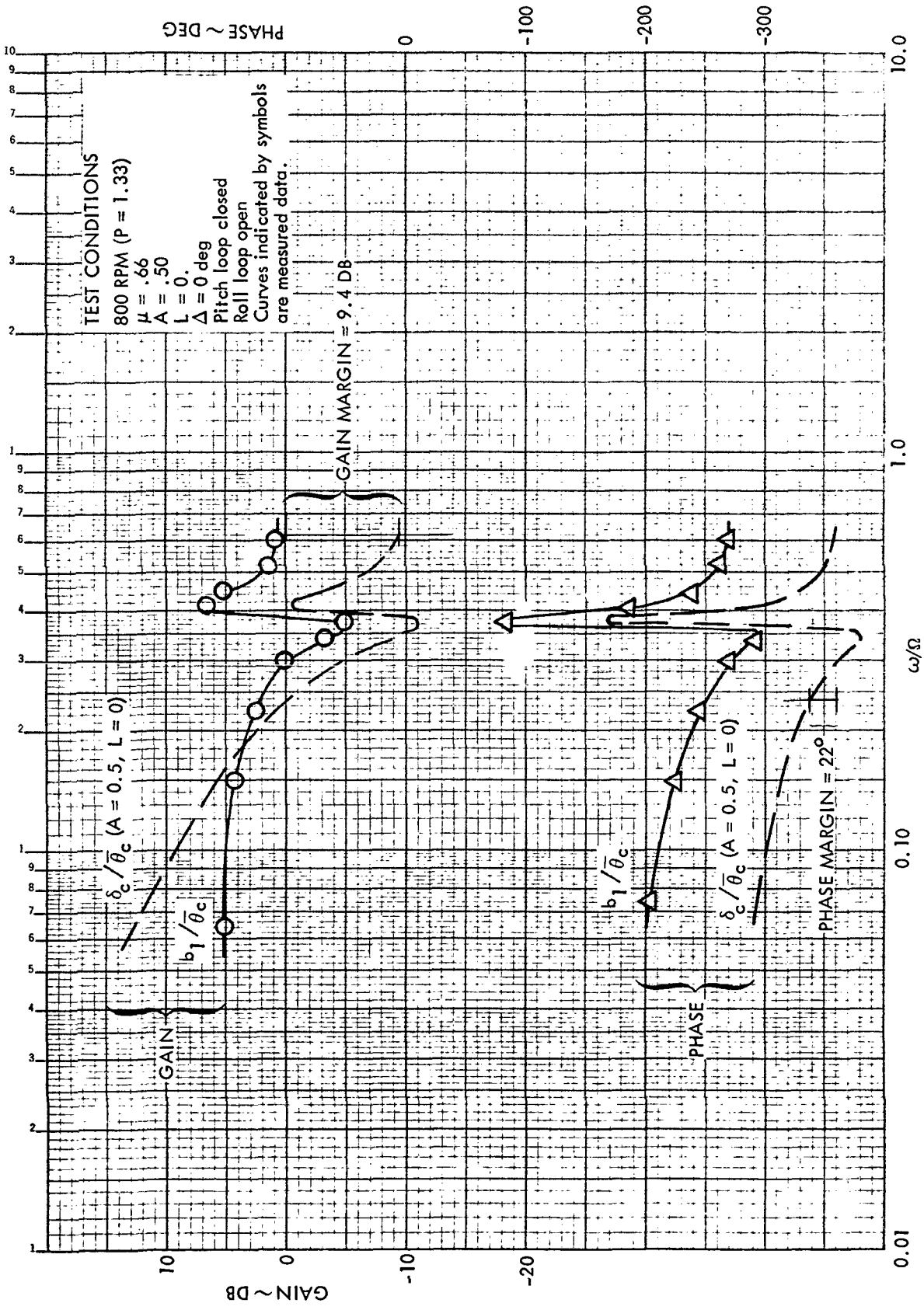

Figure 35. Rotor Lateral Frequency Response to Lateral Cyclic Pitch, Pitch Loop Closed, Roll Loop Open $\mu = 0.66$, 800 rpm (P = 1.33), A = 0.5, L = 0, Δ = 0 deg

the total pitch and roll loop stabilities are presented in graphical form in Appendix D.

Closed Loop Frequency Response

A series of closed loop frequency response tests were conducted in order to define the transient behavior of the system. The excitations included θ_o, $\bar{\theta}_s$, θ_{long} and θ_{lat}. With the feedback control loops operational, θ_{long} constitutes the longitudinal control command, θ_{lat} the lateral command, and the rotor moments generated by θ_o and $\bar{\theta}_s$ are treated as external disturbances.

The closed loop frequency response of the rotor to θ_o is shown in Figures 36 and 37. The data was taken at 800 rpm, $\mu = 0.54$, with the control system parameters set at $A = 0.5$, $L = 0$, and $\Delta = 0$. A measure of the effectiveness of the control system as a gust alleviation device can be obtained by comparing the closed loop response with similar open loop curves. For example, Figure 38 shows the open loop rotor transfer function a_1/θ_o for the same rpm and advance ratio as the closed loop response of Figure 36. The two sets of data clearly demonstrate the capability of the control system in reducing the rotor response to external low frequency disturbances. The control system is also seen to be totally ineffective when high frequency disturbances are considered. This is implied by the similarity of the open and closed loop responses at the high frequency end of the data. For the mid-frequency data the open loop response is less than the closed loop response. This characteristic identifies the need for optimization of the control system with respect to transient response as well as steady state response.

An example of the rotor closed loop frequency response to θ_{long} is shown in Figures 39 and 40. The important characteristics illustrated by the curves include the following. At low frequencies the rotor response to θ_{long} is pure pitch. This is highly desirable and reflects one of the control system design criteria. As the frequency of the control input increases, the response of

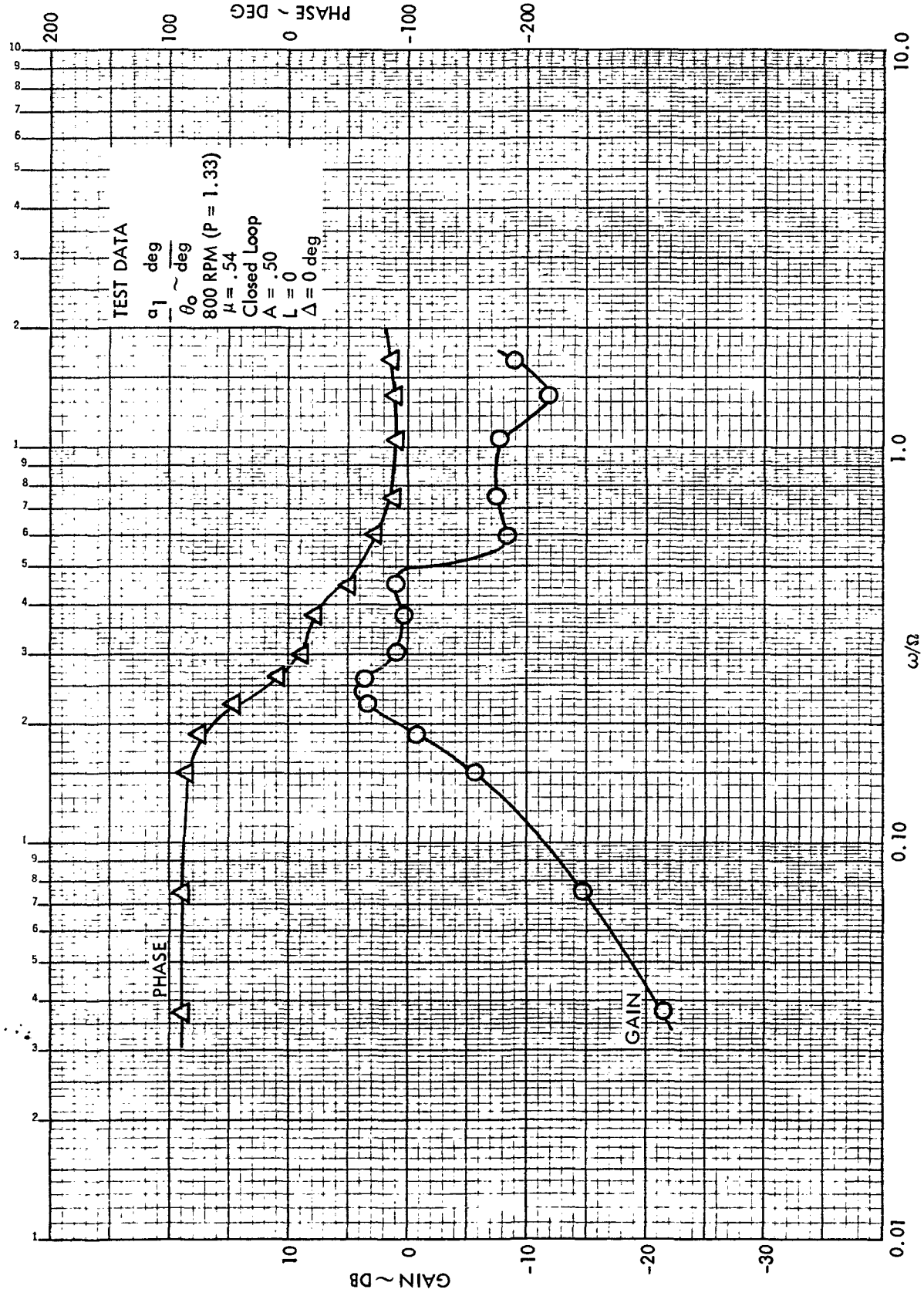

Figure 36. Closed Loop Rotor Longitudinal Frequency Response to θ_o, μ = .54, 800 rpm (P = 1.33), A = 0.50, L = 0, Δ = 0 deg

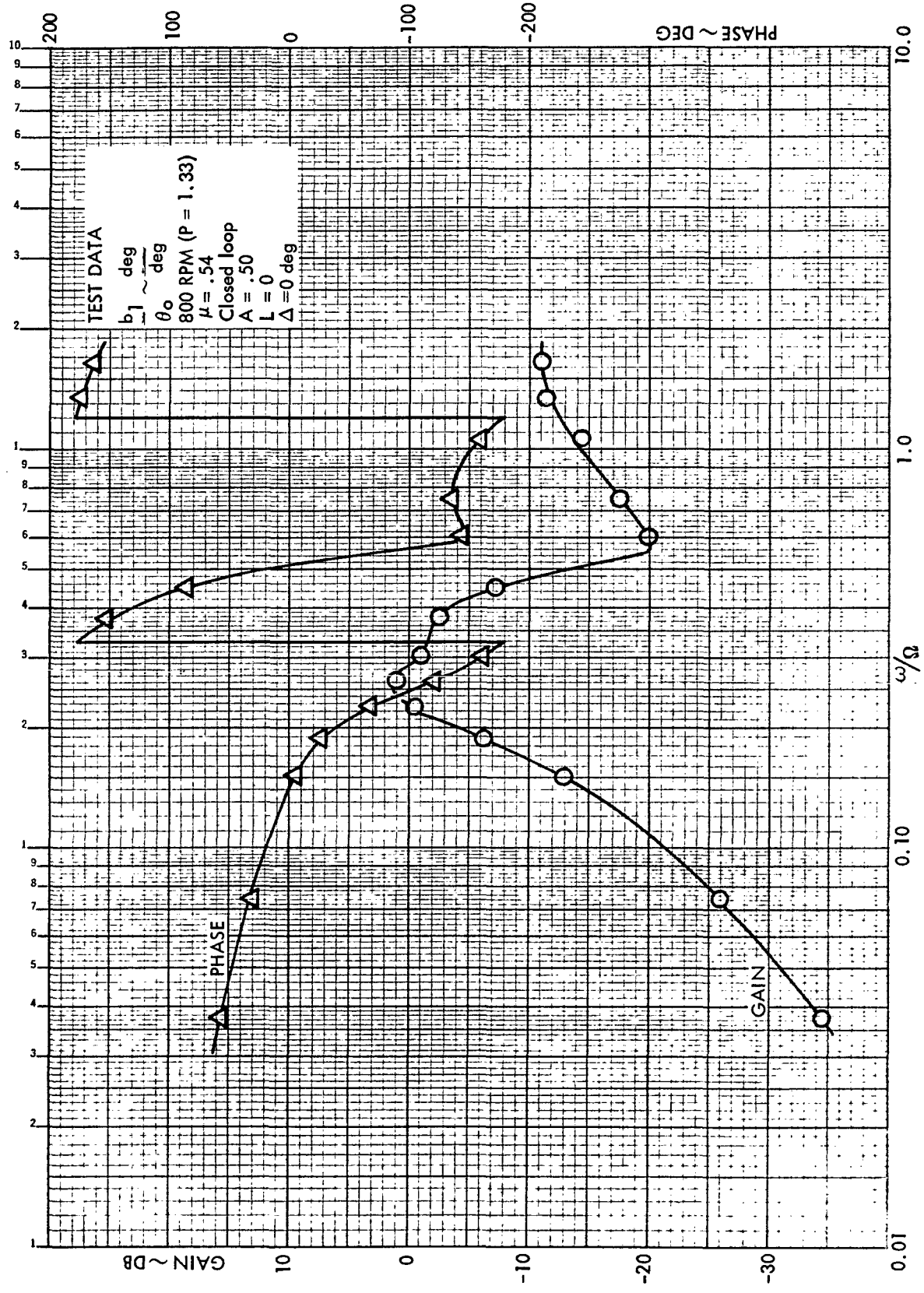

Figure 37. Closed Loop Rotor Lateral Frequency Response to θ_o, μ = .54, 800 rpm (P = 1.33), A = 0.50, L = 0, Δ = 0 deg

LOCKHEED CALIFORNIA COMPANY

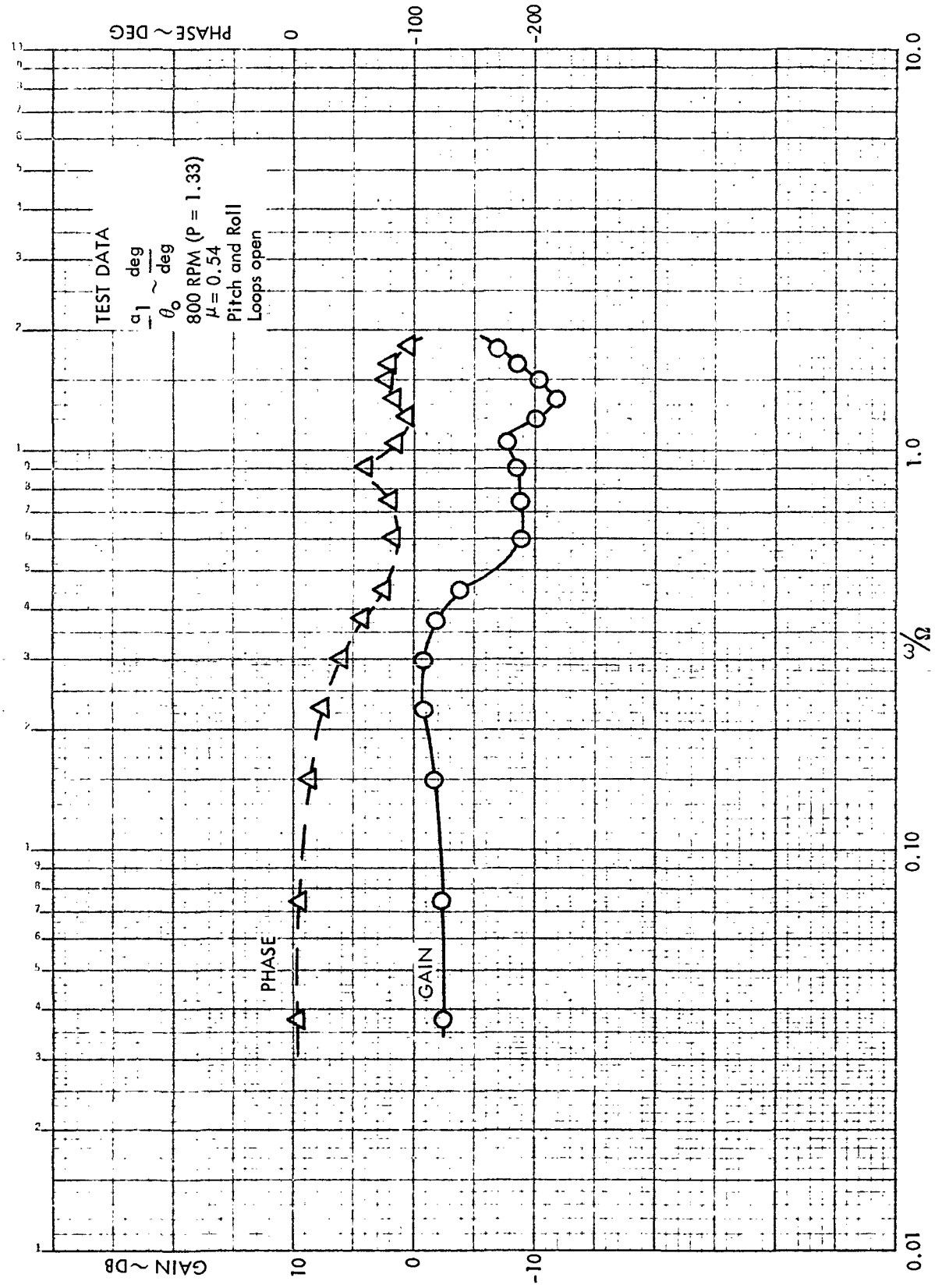

Figure 38. Rotor Longitudinal Frequency Response to Collective Pitch, μ = 0.54, 800 rpm (P = 1.33)

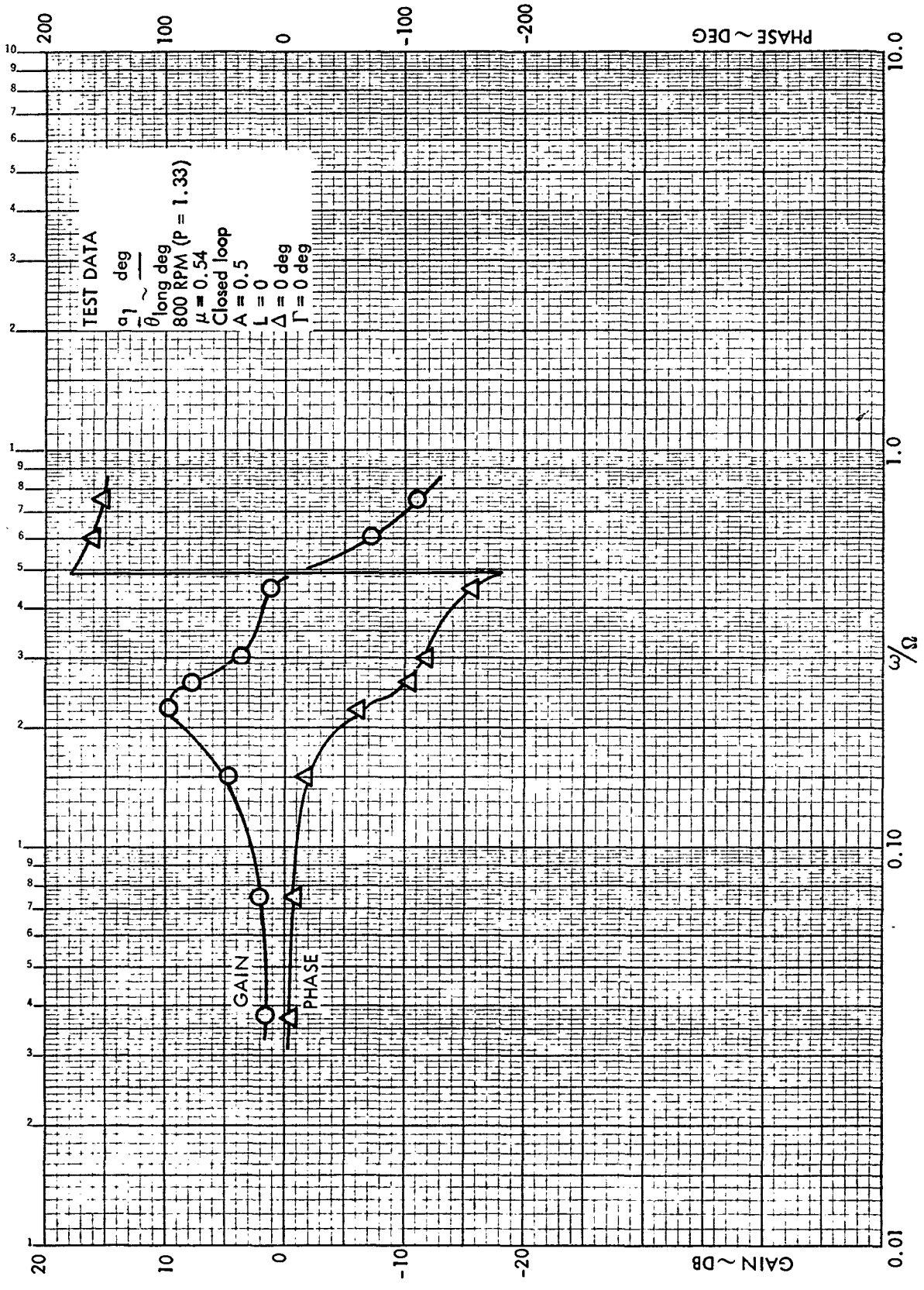

Figure 39. Closed Loop Rotor Longitudinal Frequency Response to θ_{long}, μ = .54, 800 rpm (P = 1.33), A = 0.50, L = 0, Δ = 0 deg

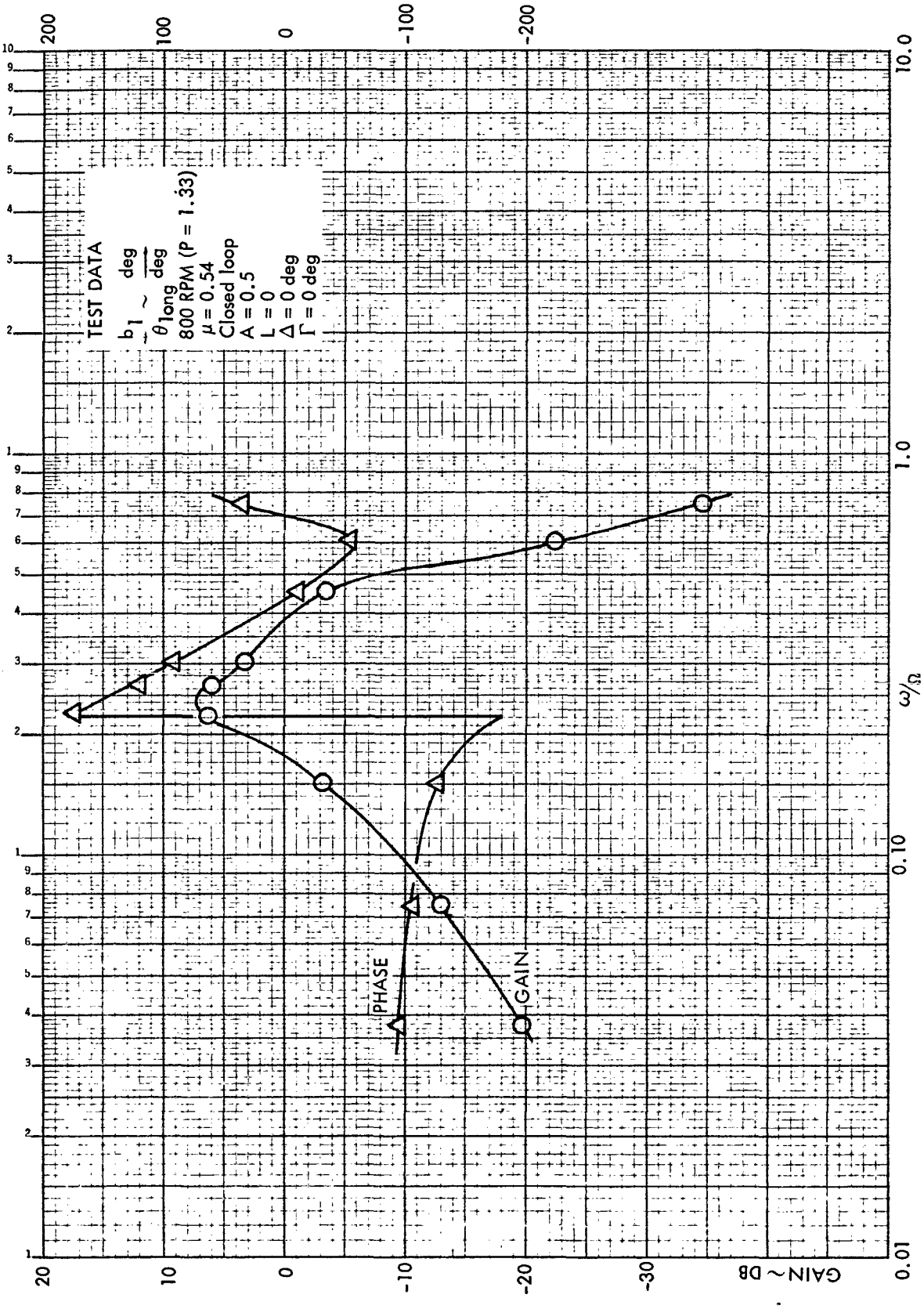

Figure 40. Closed Loop Rotor Lateral Frequency Response to θ_{long}, $\mu = .54$, 800 rpm (P = 1.33), A = 0.50, L = 0, Δ = 0 deg

the rotor also increases and significant pitch roll coupling is generated. These two features are highly undesirable and reemphasize the need for control system optimization with respect to transient response. Such frequencies would undoubtedly occur with normal control step inputs. Finally, it is observed that the rotor response falls off sharply as the frequency is increased further. This characteristic again demonstrates the ineffectiveness of the control system at high frequencies. However, in this case, it is a desirable feature.

The closed loop rotor frequency response to $\bar{\theta}_s$ is similar to that for θ_o. The moments generated by longitudinal cyclic pitch are treated as external disturbances and automatically compensated within the capabilities of the control system. In the same way, the response to a θ_{lat} command is analogous to that for θ_{long} with the pitch and roll response reversed. All of the closed loop frequency response data which were acquired during the test are documented in Appendix D. Table III contains a summary of the test conditions.

Steady State Closed Loop Response

The primary reason for the steady state closed loop test program was to determine the rotor response characteristics for various control system parameter combinations (A, L, Δ, Γ). Since the same characteristics are calculable from the Phase 1 rotor derivatives, the tests were designed to verify the known important characteristics rather than to be totally comprehensive.

The control system parameter combinations which were tested are conveniently separated according to whether $L = 0$ or $L \neq 0$. When $L = 0$ (and $A \neq 0$) the control system transfer functions represent pure integrators and the steady state rotor response derivatives are constant for all test conditions $(V, \Omega R)$ and rotor definitions (γ, P). Specifically the rotor pitching and rolling moment responses to α and θ_o are zero, the fore-aft moment response to θ_{long} and the lateral moment response to θ_{lat} are identical to each other and equal

to $2K_\theta$ and the lateral response to θ_{long} and the longitudinal response to θ_{lat} are both equal to zero. Since there is no response to α the phase angle Δ is not required. Similarly, with no roll response to θ_{long} generated, the phase angle Γ is not required. However, in order to maintain pure pitch response to θ_{long} and pure roll response to θ_{lat}, Δ and Γ must be equal to zero. These response characteristics are summarized below in Table V.

TABLE V

STEADY STATE CLOSED LOOP ROTOR RESPONSE CHARACTERISTICS

$(L = 0, \quad \Delta = 0°, \quad \Gamma = 0°)$

a_{1_α}	=	0	INDEPENDENT OF γ, P, μ, $A \neq 0$
b_{1_α}	=	0	
$a_{1_{\theta_o}}$	=	0	
$b_{1_{\theta_o}}$	=	0	
$a_{1_{\theta_{long}}}$	=	1	
$b_{1_{\theta_{long}}}$	=	0	
$a_{1_{\theta_{lat}}}$	=	0	
$b_{1_{\theta_{lat}}}$	=	1	

It is tacitly assumed for the above characteristics that the value of A is selected such that the closed loop system is dynamically stable.

When $L \neq 0$, the excellent response characteristics shown in Table V are compromised. The control system is no longer able to completely alleviate the rotor response to the external disturbances α and θ_o. Pitch/roll coupling is present for all excitations. Further, the magnitude of the rotor response derivatives with respect to the four excitations become functions of A/L, μ, P and γ.

When $L \neq 0$ the system can be optimized to some extent. For example, the phase angles Δ and Γ are available to decouple the pitch and roll response. The selection of the ratio A/L can do much to minimize the rotor response to external disturbances. However, since the rotor response is now a function of the advance ratio and the rotor definition (γ, P) it is not possible to have one system which is optimum for all conditions. In any practical application the optimization would undoubtedly be accomplished for one condition which was considered the best compromise over the anticipated advance ratio range.

The steady state closed loop tests were devised with optimization in mind. For example the criterion chosen for the selection of the phase angle Δ was

$$\frac{\partial L_R}{\partial \alpha} = 0$$

A sequence of tests were conducted to determine Δ as a function of μ and A/L. The test data used to achieve this are illustrated in Figure 41 where the rotor moment response is plotted versus Δ for 3 values of angle-of-attack. The test conditions are 800 rpm and $\mu = 0.29$. The nominal collective pitch setting was approximately 1 degree and the control system configuration was characterized by the ratio A/L = 2.5. For all of these Δ optimization tests, A was set equal to 0.5 and L adjusted to obtain the desired A/L ratio. This was done because the prior experimental analyses assured adequate closed loop stability for all anticipated test conditions when A = 0.5. From Figure

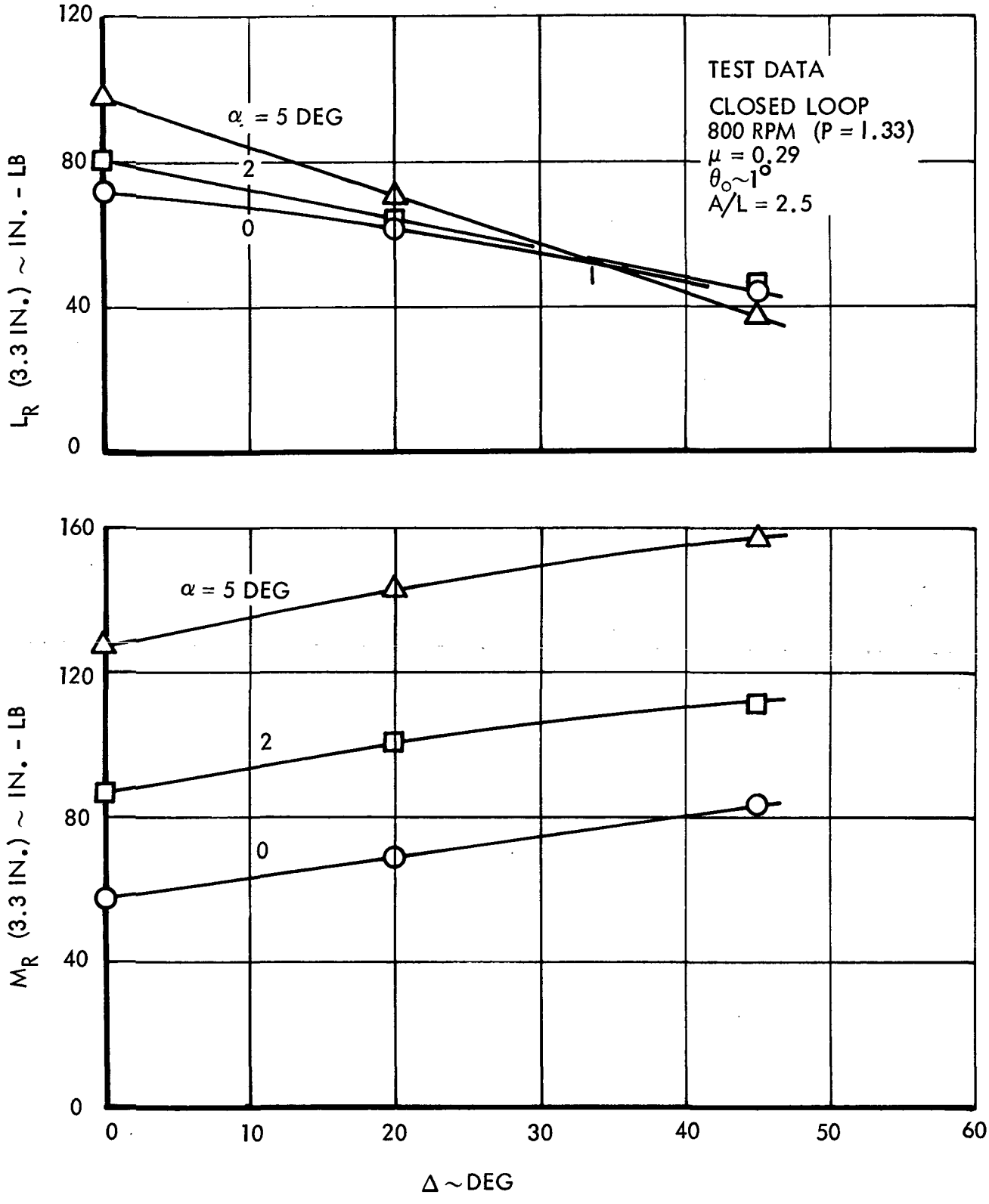

Figure 41. Closed Loop Steady-State Rotor Response to an α-Disturbance, μ = .29, 800 rpm (P = 1.33), A/L = 2.5

41 it is clear that when $\Delta \simeq 33$ degrees, the change in rotor rolling moment with a change in angle-of-attack is zero. It is noted that the initial values of L_R and M_R when $\Delta = 0$ degree are caused by the nominal θ_o and the effective rotor angle-of-attack caused by local airflow characteristics.

A summary of the required values of Δ versus μ and A/L are presented in Figure 42. (All of the test data used to determine Δ are plotted in Appendix E). It can be seen that the optimum Δ is highly dependent upon μ and mildly a function of A/L. It should be remembered that when $A/L = \infty$ and/or $\mu = 0$, the rotor does not respond to an α excitation thus precluding the need for Δ .

The forte of the tested hub moment feedback control system is its ability to alleviate rotor response to low frequency and steady external disturbances. It has been implied that the proficiency of the system depends upon the ratio A/L (the control system steady state gain). The degree to which the rotor response is automatically reduced is shown in Figure 43 as a function of μ and A/L. The response is expressed as a total rotor moment measured at the location of the strain gages

$$\text{MOMENT} \quad (3.3 \text{ in.}) = \sqrt{M_R^2 + L_R^2}$$

and a phase angle

$$\text{PHASE ANGLE} = \text{TAN}^{-1} \left(\frac{-M_R}{L_R} \right)$$

The range of A/L is from 0 to ∞ . A/L = 0 represents an open loop system and the derivatives were taken from Reference 1. The closed loop data (except for $A/L = \infty$) from which the other derivatives were deduced, are plotted in Appendix E. When $A/L = \infty$, the measured response was always zero within normal measurement tolerances (± 5 in-lb). Consequently these data have not been plotted in the appendix.

From Figure 43, it is obvious that the most desirable control system has A/L $= \infty$. While this ratio is achievable for an electrically implemented system

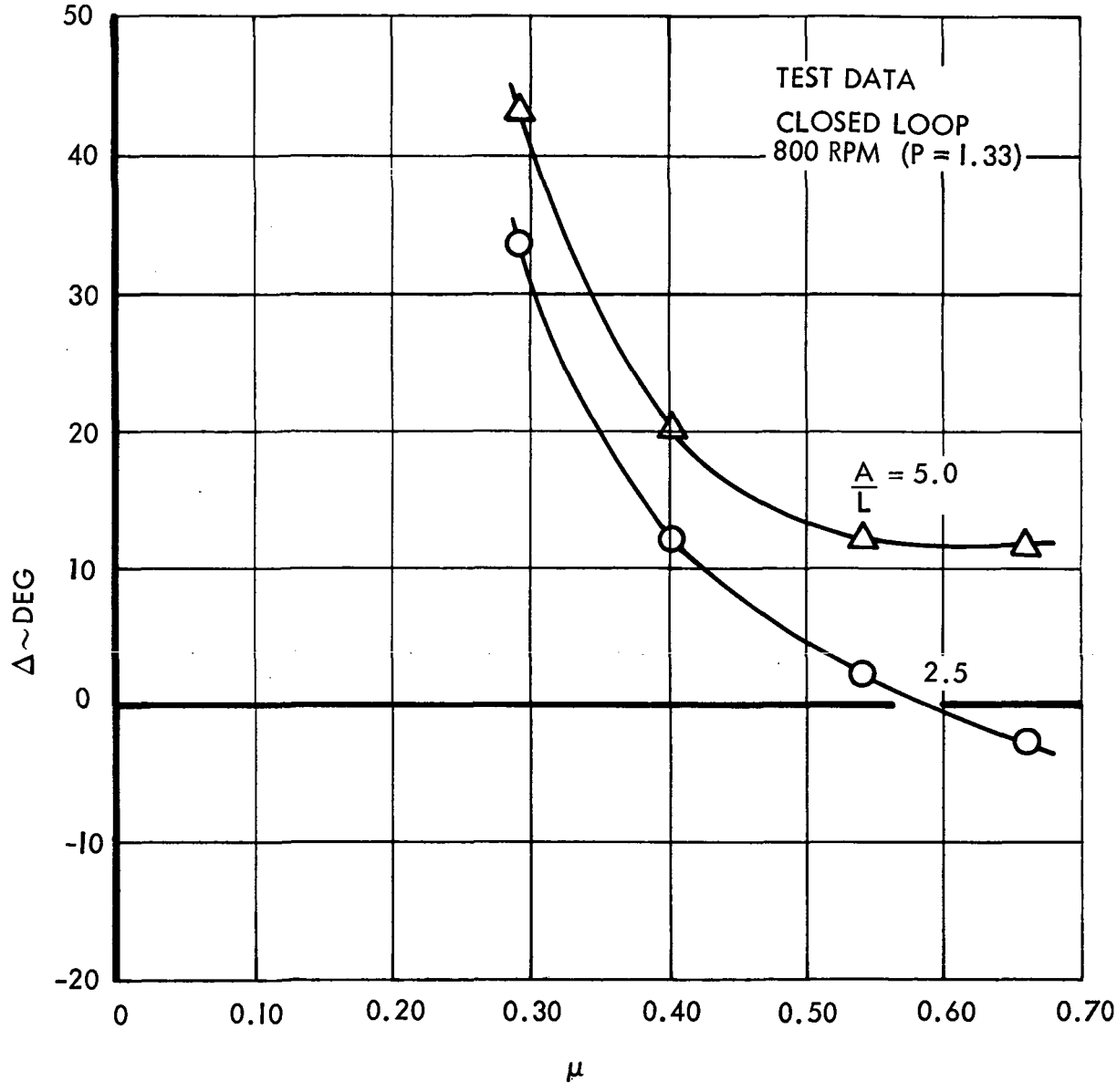

Figure 42. Summary of Optimized Phase Angle Δ, 800 rpm (P = 1.33)

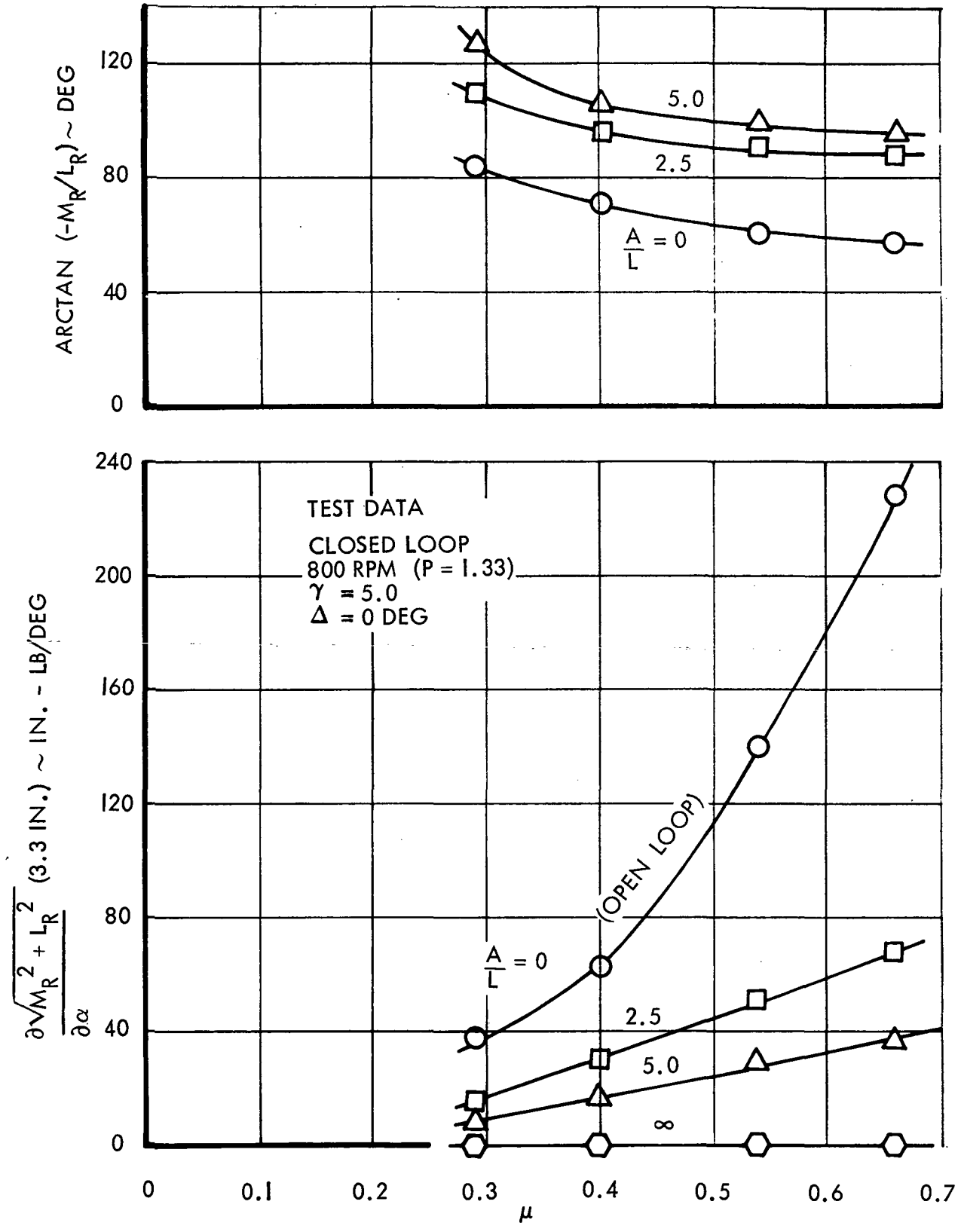

Figure 43. Closed Loop Steady-State Rotor Response to an Angle of Attack Excitation

such as the tested model, it is probably not possible to have L = 0 for a mechanical system because of friction and damping in the control device. The problem therefore would be to find the largest value of A for which the stability margins were satisfactory. For this situation some compromise between stability and response requirements is indicated.

The control system also treats the rotor moment response to θ_o as an external disturbance. Therefore, a compensating effect similar to that for an α disturbance is expected. Figure 44 presents test results which define the alleviation of the response to collective pitch. Three A/L ratios are shown, 0, 5 and ∞ with A/L = 0 data taken from Reference 1. As expected, the results are very similar to those for an angle-of-attack disturbance.

The criterion used to select the phase angle Γ was pure pitch response to a θ_{long} command or

$$\frac{\partial L_R}{\partial \theta_{long}} = 0$$

Since Δ is contained within the homogeneous system, its value influences Γ For the experimental determination of Γ, the values of Δ shown in Figure 42 were used. An example of the test results from which Γ was determined are shown in Figure 45. Steady data were recorded at several preselected values of Γ for θ_{long} = 0, 1°, and 1.5° (2°). For the selected case the optimum phase angle is approximately 3°.

The results of the tests to select Γ are summarized in Figure 46 where Γ is plotted versus μ for 2 ratios A/L.

A sequence of tests were conducted with the control system phase angles optimized for A/L = 5.0 at μ = 0.54 (800 rpm) The purpose was to define the response characteristics of the rotor at advance ratios where Δ and Γ are known to generate pitch/roll coupling. The results are presented in Figures 47 and 48

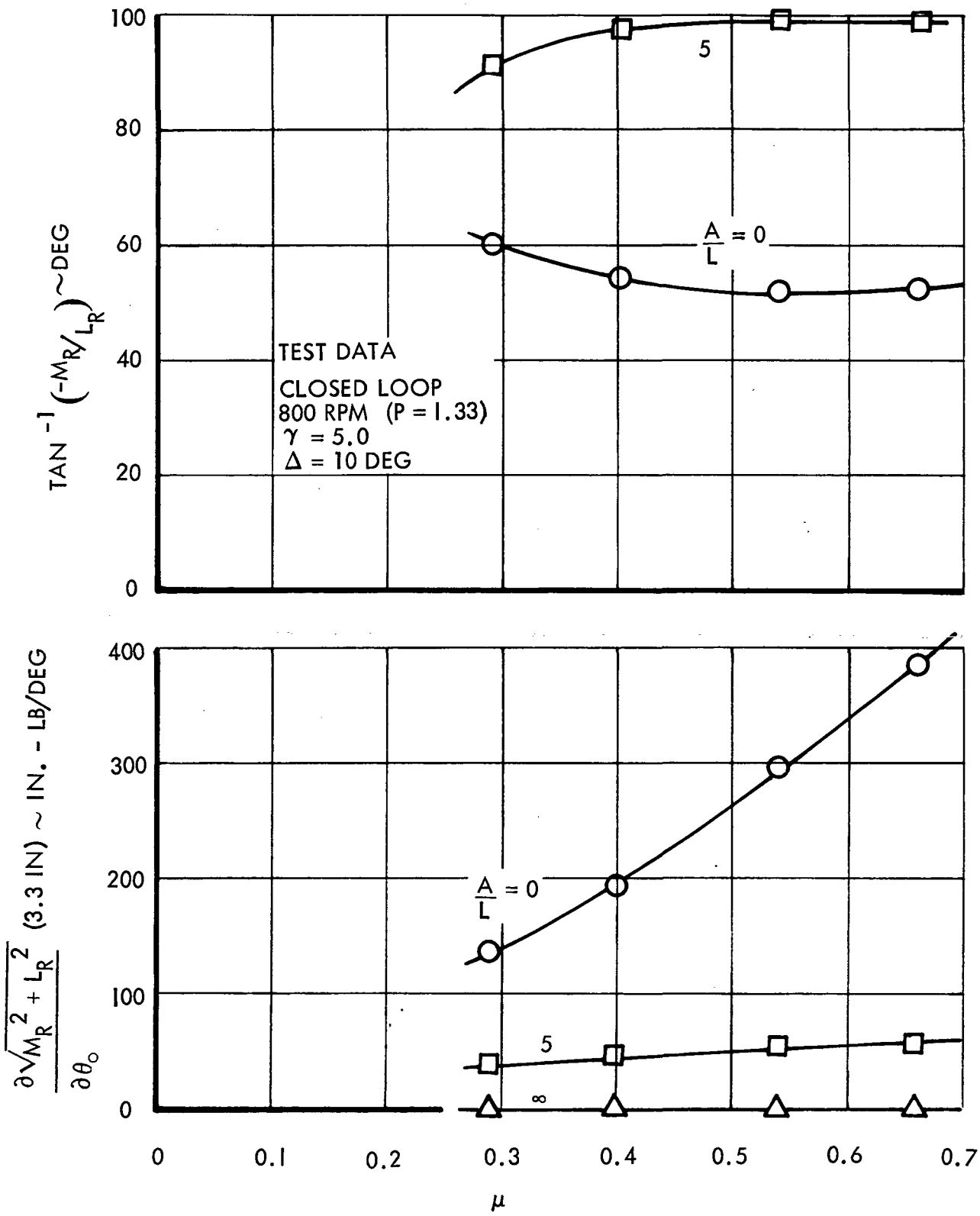

Figure 44. Closed Loop Steady-State Rotor Response to a Collective Pitch Excitation

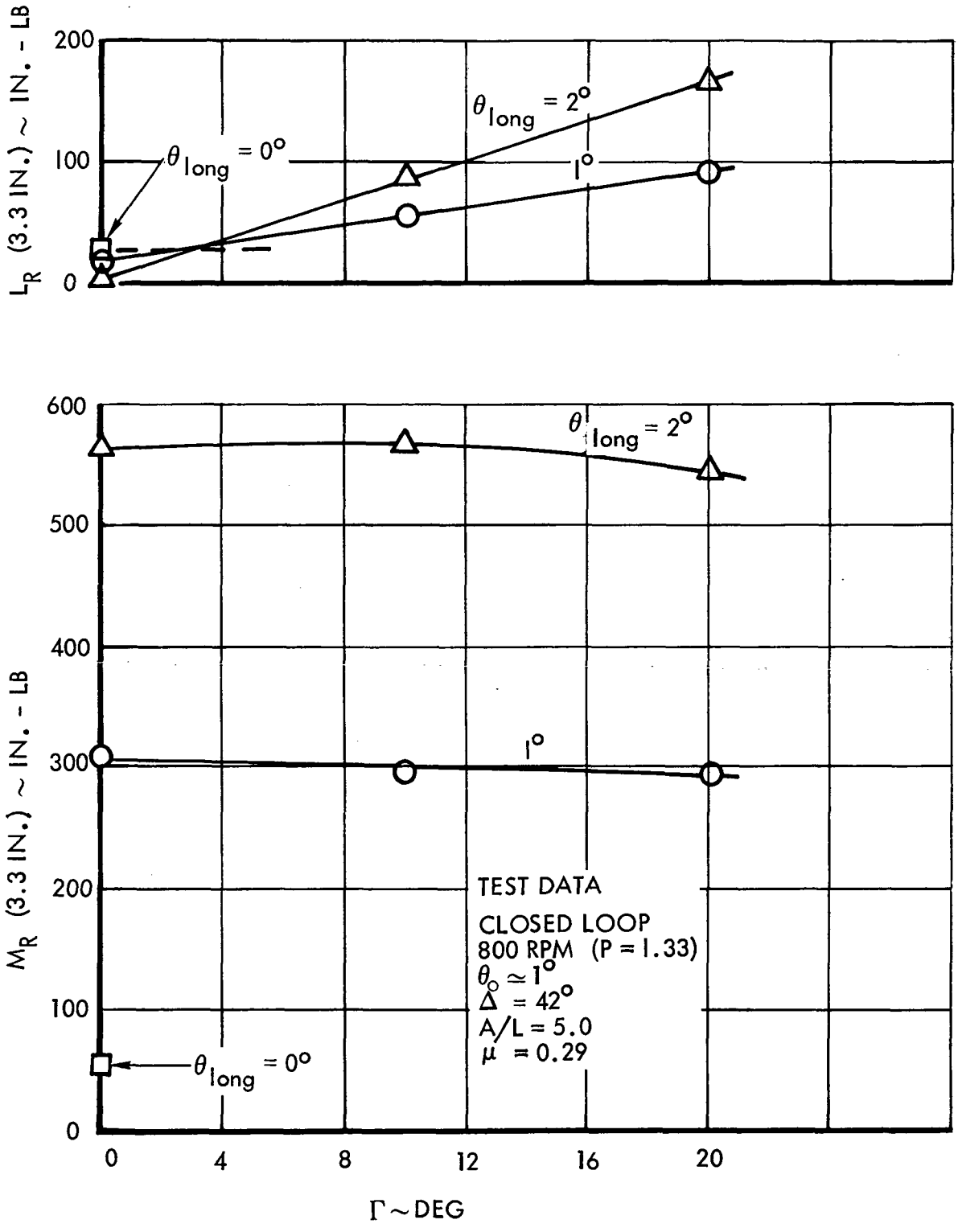

Figure 45. Closed Loop Steady-State Rotor Response to a Longitudinal Control Input (θ_{long}), μ = 0.29, 800 rpm (P = 1.33), A/L = 5.0, Δ = 42 deg

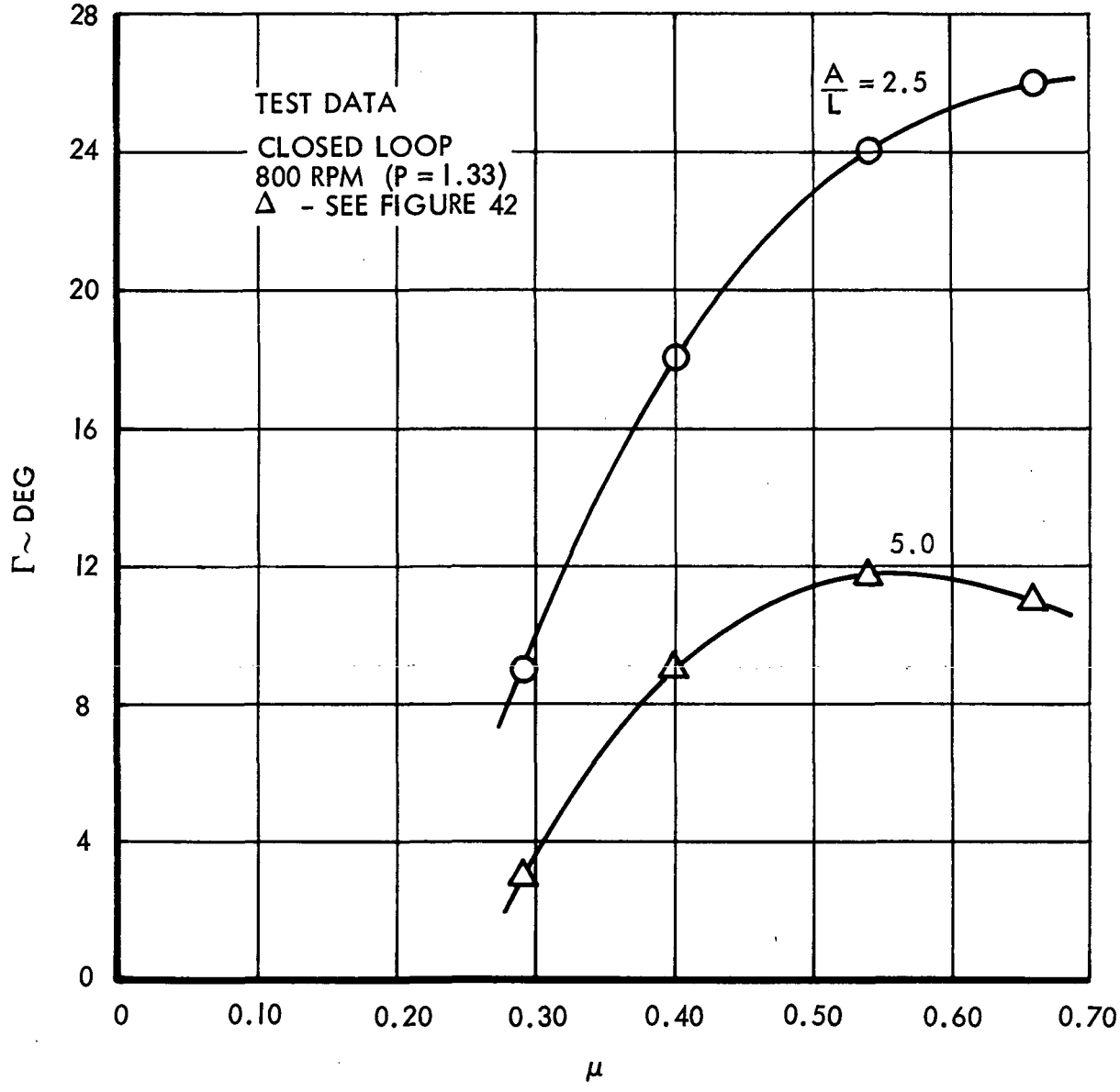

Figure 46. Summary of Optimized Phase Angle Γ, 800 rpm (P = 1.33)

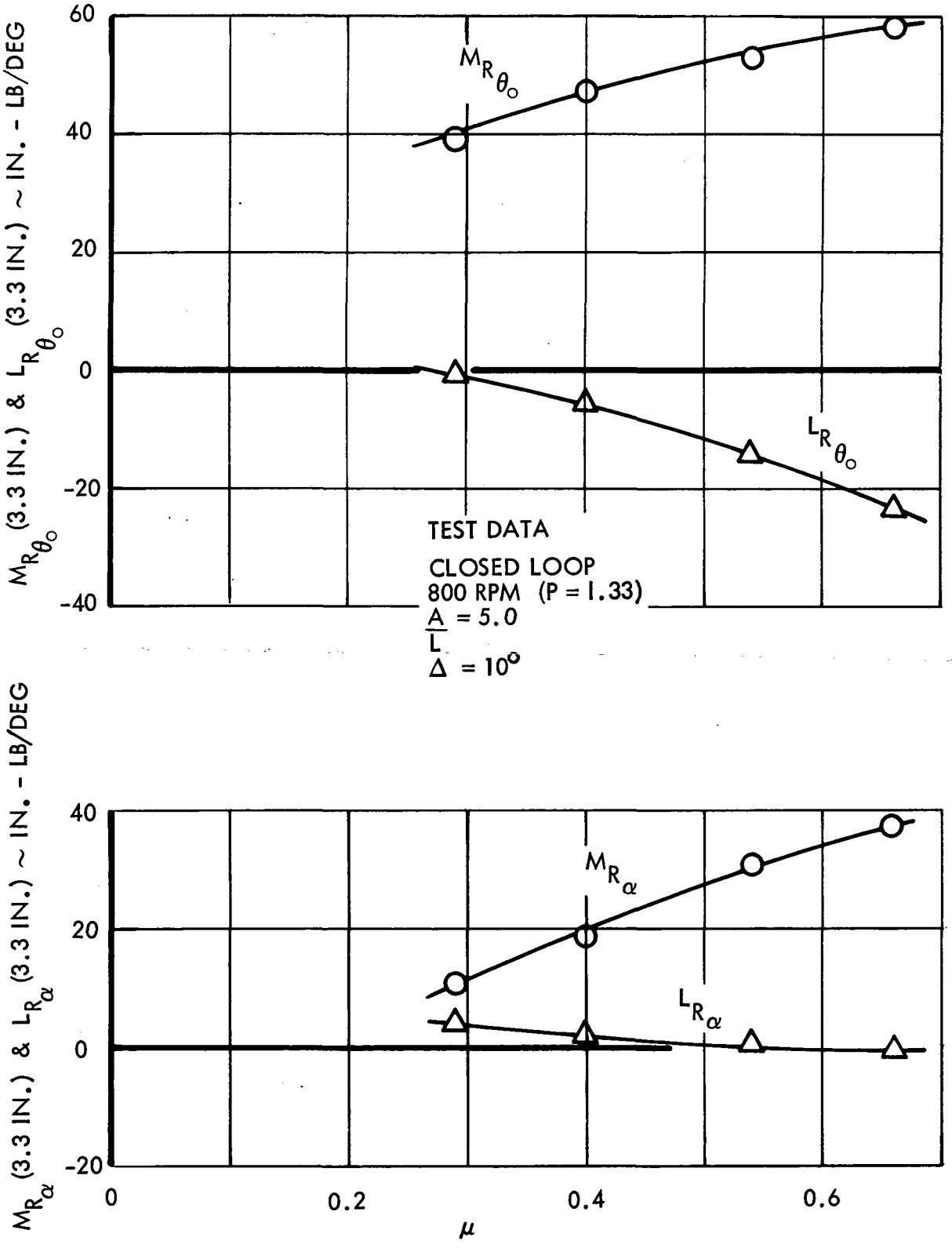

Figure 47. Closed Loop Steady-State Rotor Response Derivatives with Respect to θ_o and α, 800 rpm (P = 1.33), A/L = 5.0, Δ = 10 deg

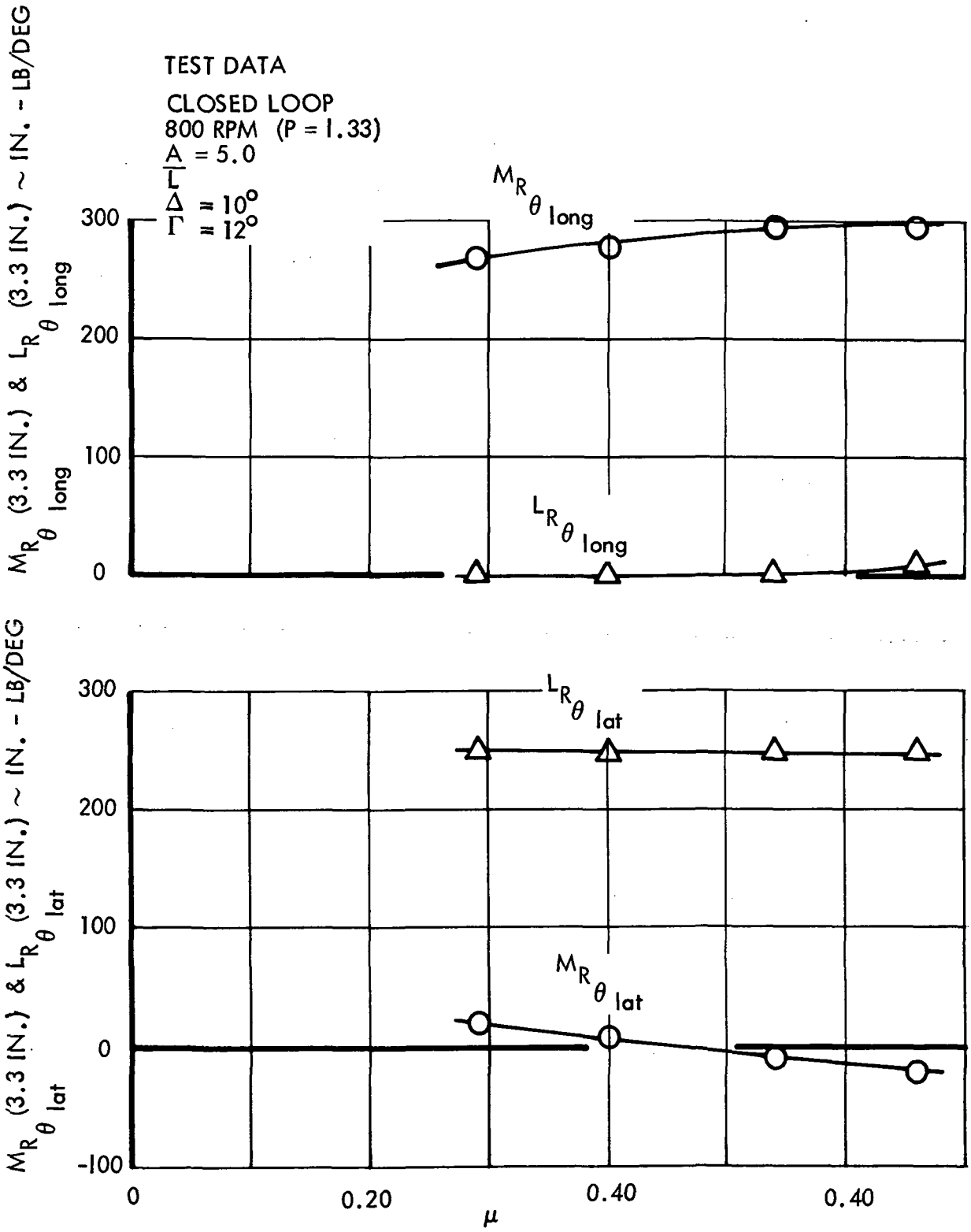

Figure 48. Closed Loop Steady-State Rotor Response Derivatives with Respect to θ_{long} and θ_{lat}, 800 rpm (P = 1.33), Δ = 10 deg Γ = 12 deg

where rotor pitching and rolling moment derivatives with respect to α, θ_o, θ_{long} and θ_{lat} are plotted versus μ. (The data from which these derivatives were calculated are plotted in Appendix E.) An examination of the curves shows that acceptable coupling characteristics may be achieved over a fairly wide advance ratio range with the system optimized at only one condition. If there is an exception, it is the roll response to θ_o at high advance ratios (See Figure 47). It is noted, however, that Δ could have been selected to eliminate roll response due to θ_o. It is likely, therefore, that some value of Δ could have been selected which would have produced acceptable response characteristics for both α and θ_o.

A series of closed loop steady-state tests were conducted at 300 rpm (P = 2.32) and advance ratios of 0.78, 1.07, and 1.44. Two sets of control system parameters were considered:

$$\left\{\begin{array}{lcl} A & = & 0.5 \\ A/L & = & 5 \\ \Delta & = & 0 \\ \Gamma & = & 0 \end{array}\right\} \qquad \left\{\begin{array}{lcl} A & = & 0.5 \\ A/L & & \infty \\ \Delta & & 0 \\ \Gamma & & 0 \end{array}\right\}$$

The results do not add anything to the previous discussion and will not be presented in this section. The data, however, are documented in Appendix E. For the configuration having $A/L = \infty$ the response characteristics of Table V were measured.

Open Loop Steady State Response

The tests were conducted at a rotor speed of 1200 rpm in order to obtain steady rotor moment derivatives with respect to α, θ_o, θ_s, and θ_c at a lower nondimensional flapping frequency (P) (with $\gamma = 5.0$) than that achieved during the Phase 1 program. At 1200 rpm, P = 1.17, advance ratios from 0.07 to 0.44 were tested. The rotor moment response and lift are presented in derivative form in Figures 49, 50, and 51. The data used to calculate the

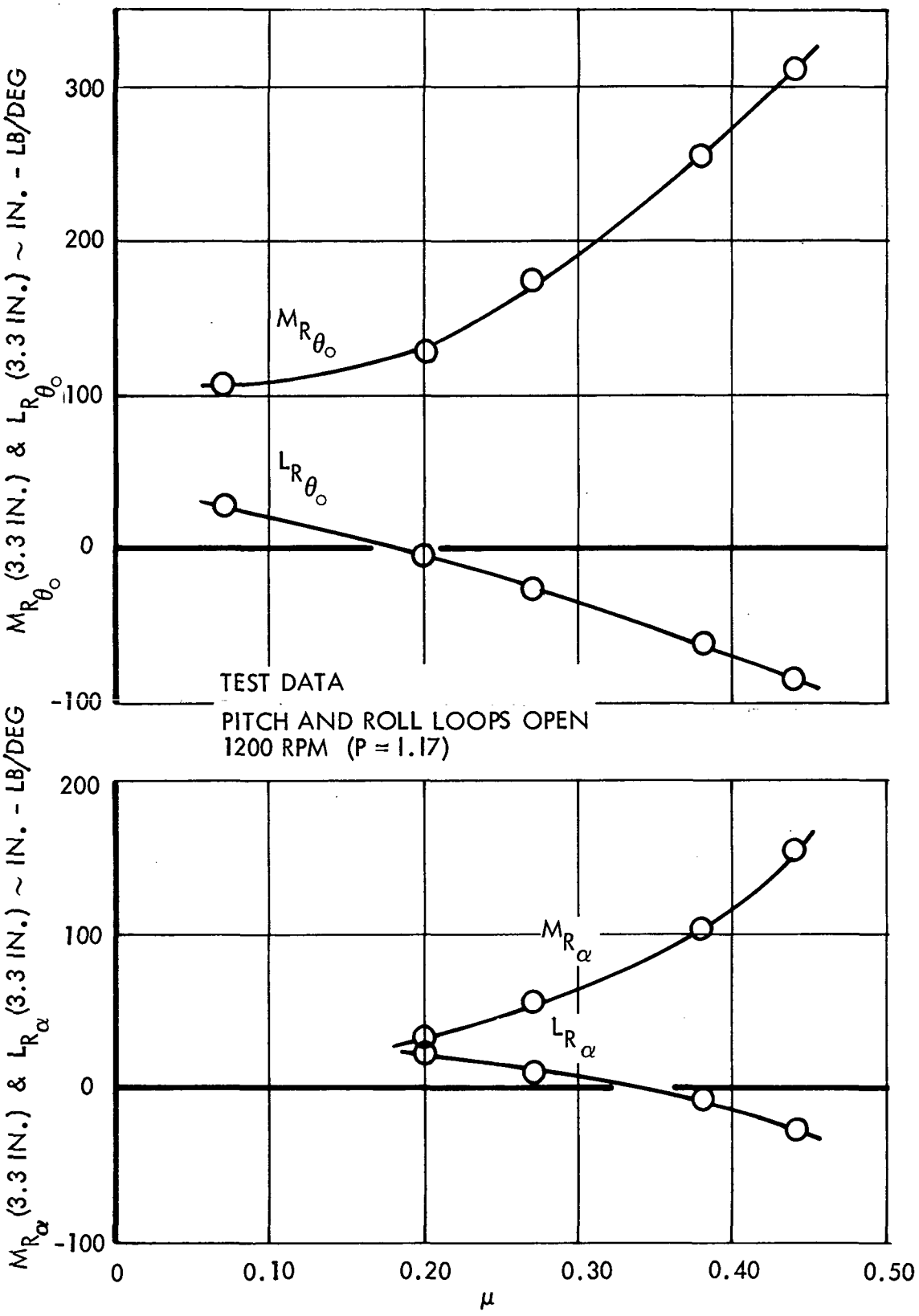

Figure 49. Open Loop Rotor Response Derivatives with Respect to θ_o and α, 1200 rpm (P = 1.17), γ = 5.0

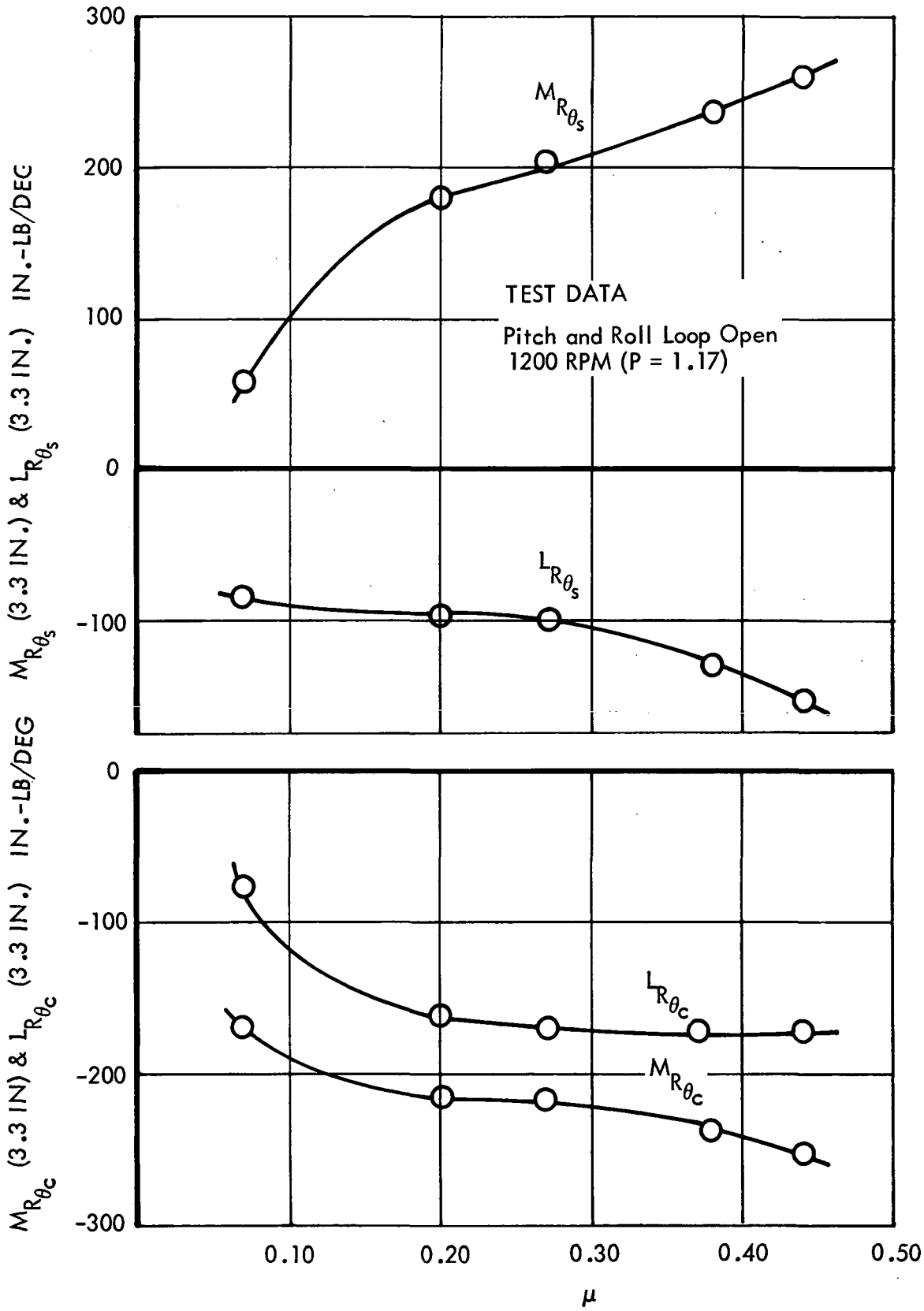

Figure 50. Open Loop Rotor Response Derivatives with Respect to θ_s and θ_c, 1200 rpm (P = 1.17), Y = 5.0

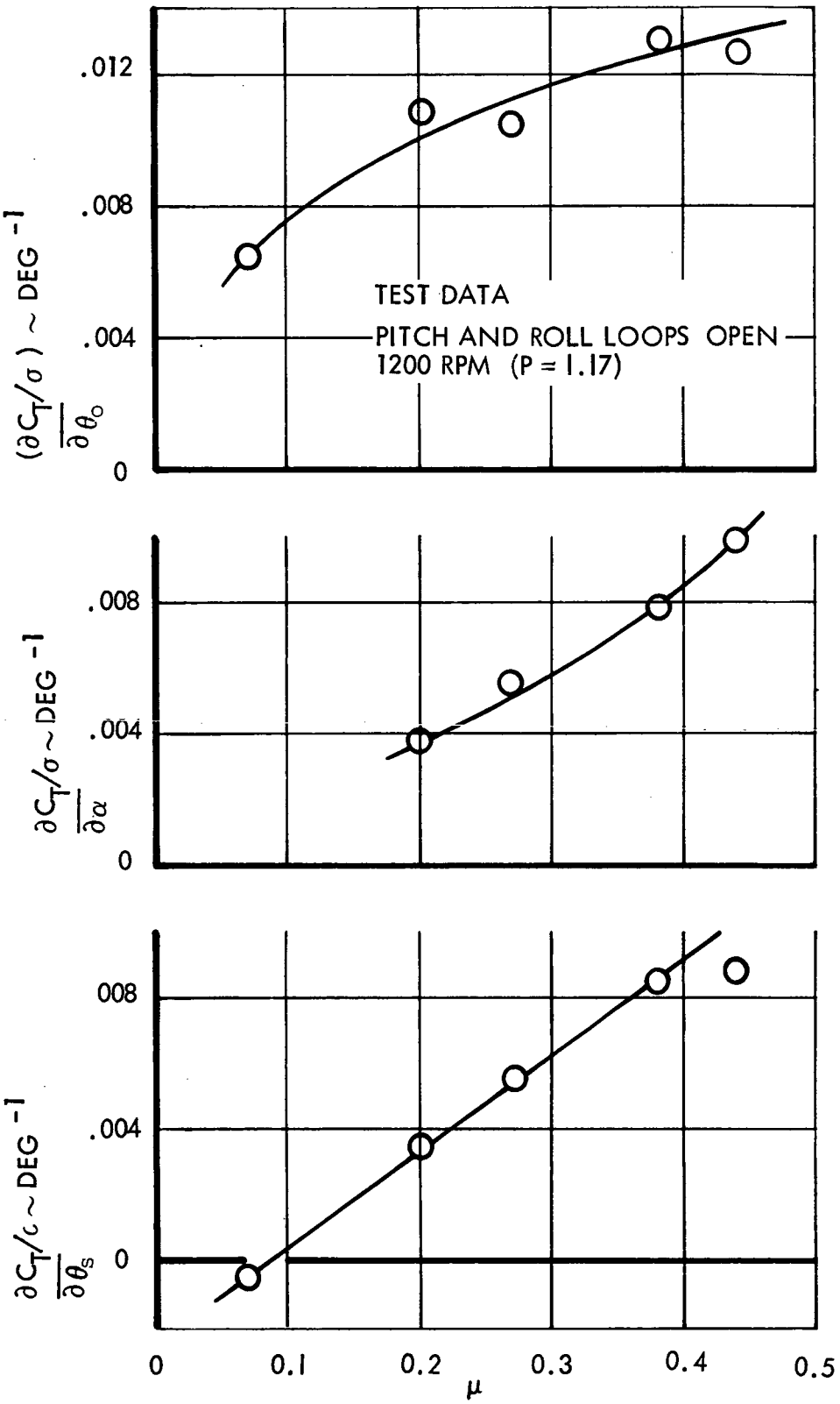

Figure 51. Open Loop Steady-State Rotor Lift Derivatives with Respect to θ_o, α and θ_s, 1200 rpm (P = 1.17), γ = 5.0

derivatives are plotted in Appendix F, and in general, the data have the same characteristics as the Phase 1 test results. The influence of induced velocity is more clearly seen however, because of the lower advance ratios. In order to present results which are consistent with the Phase 1 data bank, the moment derivatives (which were measured at rotor station 3.3 in.) have been adjusted to the center of rotation and listed below in Table VI. The adjustment procedure is described on Pages 80 - 84 of Reference 1.

TABLE VI

OPEN LOOP ROTOR STEADY STATE RESPONSE DERIVATIVES ADJUSTED TO THE CENTER OF ROTATION

RPM	P	μ	M_{R_α} $\frac{\text{in.-lb}}{\text{deg}}$	L_{R_α} $\frac{\text{in.-lb}}{\text{deg}}$	$M_{R_{\theta_o}}$ $\frac{\text{in.-lb}}{\text{deg}}$	$L_{R_{\theta_o}}$ $\frac{\text{in.-lb}}{\text{deg}}$	$M_{R_{\theta_s}}$ $\frac{\text{in.-lb}}{\text{deg}}$	$L_{R_{\theta_s}}$ $\frac{\text{in.-lb}}{\text{deg}}$	$M_{R_{\theta_c}}$ $\frac{\text{in.-lb}}{\text{deg}}$	$L_{R_{\theta_c}}$ $\frac{\text{in.-lb}}{\text{deg}}$
1200	1.17	0.07	-	-	139	36	74	-109	-235	-100
		0.20	44	33	166	-5	234	-127	-281	-210
		0.27	71	13	226	-35	264	-129	-284	-221
		0.38	133	-10	330	-79	306	-169	-309	-225
		0.44	201	-36	403	-110	345	-200	-329	-225

SECTION 7

THEORY

An extensive theoretical analysis was conducted in support of the wind tunnel test. The studies included both open and closed loop frequency response investigations and closed loop stability by matrix Floquet theory. The mathematical model consisted of the rotor flapping model described in the Phase I final report coupled with appropriate equations required to incorporate the hub moment feedback control system. The analytical studies were used to define a safe test envelope and were also instrumental in establishing the sequence of experiments.

In this section the mathematical model will be discussed as well as the methods by which the equations of motion were solved. A presentation of all the theoretical results is not the intended purpose of this discussion. Rather, a limited amount of theoretical and experimental data will be compared in order to assess the validity of those portions of the theory which do not exactly represent the physical system.

MATHEMATICAL MODEL

The mathematical model consists of four untwisted rigid blades which flap individually and inelastically about a centrally arranged flapping hinge. Each blade is restrained by a hypothetical spring which is selected so that the rigid blade flapping frequency is identical to the first flapping mode natural frequency of the elastic blade being represented. Rotor control may be exercised either directly, by positioning the swashplate, or indirectly through a first order lag moment feedback control system. The control signals are transmitted to the rotor through second order hydraulic actuators.

The eight degrees of freedom are:

4 rigid flapping angles

2 control system feedback signals

2 cyclic pitch actuator angles

The steady state aerodynamic theory used is classical; ignoring the effects of blade stall, mach number, and derivations from a uniform induced velocity field. The effects of reversed flow are totally accounted for resulting in theory which is applicable over the advance ratio range $\mu = 0 \rightarrow \infty$.

EQUATIONS OF MOTION

Flapping

The equation of motion for a single flapping blade expressed in rotating coordinates has been derived in Appendix A of Reference 1. By advancing the azimuth position ψ, flapping equations for four blades are obtained.

$$\frac{2}{\gamma}\ddot{\beta}_i + \Omega\,\dot{\beta}_i\,C\left[\psi+(i-1)\,\frac{\pi}{2}\right] + \Omega^2\,\beta_i\left\{\frac{2}{\gamma}P^2 + K\left[\psi + (i-1)\,\frac{\pi}{2}\right]\right\}$$

$$= \alpha\,\Omega^2\,m_\alpha\left[\psi + (i-1)\,\frac{\pi}{2}\right] + \Omega^2\left\{\theta_o + \dot{\theta}_s \sin\left[\psi + (i-1)\,\frac{\pi}{2}\right]\right.$$

$$\left. + \theta_c \cos\left[\psi + (i-1)\,\frac{\pi}{2}\right]\right\} m_{\theta_o}\left[\psi + (i-1)\,\frac{\pi}{2}\right] \qquad (1)$$

$$i = 1, 2, 3, 4$$

The periodic coefficients in the equation are of aerodynamic origin. Expressions for them in terms of μ and ψ can be found on Page 112 of Reference 1.

Feedback Control System Equations

The tested feedback control system evolved naturally as an improvement upon a gyroscope as a control device. As discussed in Reference 2, pure pitch and roll feedback control is obtainable by arbitrarily eliminating cross coupling terms in the gyro equations of motion. Since the model control system was electrical, this maneuver was easily implemented. The fundamental control system equations (Reference 2) are:

$$2\,\Omega\,\dot{\delta}_s + 2L\,\Omega^2\,\delta_s = \text{Pitch Feedback} \tag{2}$$

$$2\,\Omega\,\dot{\delta}_c + 2L\,\Omega^2\,\delta_c = \text{Roll Feedback} \tag{3}$$

For the model rotor system the feedback signals are the rotor pitching and rolling moments. Since the equations of motion are nondimensional, the feedbacks are therefore proportional to longitudinal and lateral rotor tilts. The rotor tilts are obtained by resolving the rotating blade flapping motions into stationary coordinates. The control system equations of motion including an adjustable gain A, and with the signs of the feedback signals selected to insure negative feedback (a stability requirement for all feedback control systems) can thus be written:

$$\dot{\delta}_s + L\,\Omega\,\delta_s = A\,\Omega\left\{0.5\left[(\beta_4 - \beta_2)\sin\psi + (\beta_1 - \beta_3)\cos\psi\right] + \theta_{long}\cos\Gamma - \theta_{lat}\sin\Gamma\right\} \tag{4}$$

$$\dot{\delta}_c + L\,\Omega\,\delta_c = A\Omega\left\{0.5\left[(\beta_3 - \beta_1)\sin\psi + (\beta_4 - \beta_2)\cos\psi\right] - \theta_{lat}\cos\Gamma - \theta_{long}\sin\Gamma\right\} \tag{5}$$

The terms θ_{long} and θ_{lat} are included to provide longitudinal and lateral control commands for the closed loop system. Recall that rotor moments generated by positioning the swashplate are treated as external disturbance by the feedback control system. Consequently, that method of control is no longer avialable. The phase angle Γ provides a measure of flexibility in decoupling the rotor pitch and roll response to longitudinal or lateral control commands.

Cyclic Pitch Actuators

From static test data it was determined that the actuators were approximately second order systems. With the driving functions expressed as linear combinations of the feedback control signals (δ_s, δ_c) and swashplate positioning commands ($\bar{\theta}_s$, $\bar{\theta}_c$) the actuator equations are:

$$\ddot{\theta}_s + 2\zeta\omega_n\dot{\theta}_s + \omega_n^2\theta_s = \omega_n^2\left(\bar{\theta}_s + c_2\delta_s\cos\Delta + c_2'\delta_c\sin\Delta\right) \quad (6)$$

$$\ddot{\theta}_c + 2\zeta\omega_n\dot{\theta}_c + \omega_n^2\theta_c = \omega_n^2\left(\bar{\theta}_c + c_2'\delta_c\cos\Delta - c_2\delta_s\sin\Delta\right) \quad (7)$$

where ζ is damping ratio and ω_n the natural frequency of the actuator. The phase angle Δ introduces arbitrary coupling of the pitch and roll control loops and c_2 and c_2' are respectively the pitch roll loop disable switches (i.e. 1 = closed loop, 0 = open loop).

SOLUTION OF EQUATIONS OF MOTION

Frequency Response

Open and closed loop frequency response was determined by two methods. The first involved a time history solution of the equations of motion coupled with a Fourier analysis of the steady state solution at the excitation frequency. This approach is exactly analagous to the test technique previously discussed. It required that the excitations $(\theta_o, \bar{\theta}_s, \bar{\theta}_c, \theta_{long}, \theta_{lat})$ be expressed as oscillating inputs, i.e:

$$\theta_o \sin\omega t$$

$$\bar{\theta}_s \sin\omega t$$

$$\bar{\theta}_c \sin\omega t$$

$$\theta_{long} \sin\omega t$$

$$\theta_{lat} \sin\omega t$$

For example, suppose that the frequency response derivatives $\frac{a_1}{\theta_o}$ and $\frac{b_1}{\theta_o}$ were desired. For a unit magnitude of θ_o and a fixed frequency ω the equations were solved (by a numerical integration process) until steady state

motion was reached. A Fourier analysis (with fundamental frequency ω) was then performed on the resolved flapping motions. The magnitude and phase angle of the first harmonic of the longitudinal rotor response relative to similar prescribed quantities for the excitation yielded the derivative $\frac{a_1}{\theta_o}$ in terms of gain and phase shift. In the same manner $\frac{b_1}{\theta_o}$ was determined from the time history of the lateral rotor response. This procedure was repeated for many discrete excitation frequencies yielding classical frequency response curves.

The principal advantage of the time simulation method of determining transfer functions is that an exact solution of the equations of motion is used. Traditional frequency response methods require that the equations of motion with periodic coefficients be transformed into a linear system with constant coefficients. This transformation forces both the responses and the periodic coefficients to be truncated. The most pronounced disadvantage of the time history method is the amount of computational time required. Numerical integration techniques require considerable CPU time and since many discrete frequencies must be considered, the cost of a comprehensive analysis is considerable.

The second analysis method used was the traditional frequency response technique. It became the primary theoretical tool when excellent agreement between the transfer functions determined by the two methods was realized. The flapping equations of motion were modified as follows in order to develop the required linear system with constant coefficients.

The flapping motion of blade 1 was assumed to be of the form

$$\beta_1 = a_o - a_1 \cos\psi - b_1 \sin\psi - a_2 \cos 2\psi - b_2 \sin 2\psi \qquad (8)$$

where the coefficients $(a_o, a_1, b_1, a_2, b_2)$ are functions of time. Further, all rotor blades were constrained to perform identical flapping responses.

$$\beta_2 = \beta_1 \left(\psi + \frac{\pi}{2}\right)$$

$$\beta_3 = \beta_1 \left(\psi + \pi\right) \tag{9}$$

$$\beta_4 = \beta_1 \left(\psi + \frac{3\pi}{2}\right)$$

This latter restriction makes it possible to define the rotor response by the motion of a single blade.

It was known from previous investigations (Reference 3) that the periodic coefficients were of the following forms:

$$C(\psi) = c_o + c_{1s} \sin\psi + c_{2c} \cos 2\psi + c_{3s} \sin 3\psi + c_{4c} \cos 4\psi + \ldots\ldots\ldots \tag{10}$$

$$K(\psi) = k_{1c} \cos\psi + k_{2s} \sin 2\psi + k_{3c} \cos 3\psi + k_{4s} \sin 4\psi + \ldots\ldots \tag{11}$$

$$m_{\theta_o}(\psi) = m_o + m_{1s} \sin\psi + m_{2c} \cos 2\psi + m_{3s} \sin 3\psi + m_{4c} \cos 4\psi + \ldots\ldots \tag{12}$$

It is noted that $m_\alpha(\psi)$ has the same form as $m_{\theta_o}(\psi)$. However, since frequency response with respect to α was not part of the program, the excitation α will not be carried through the ensuing development. After substituting equations 8, 10, 11 and 12 into equation 1 (with i = 1), expanding and equating the coefficients of the harmonics of ψ (up to 4ψ) to zero, the following linear system with constant coefficients describing the rotor is obtained.

$$\frac{2}{\gamma}\ddot{a}_o + \Omega c_o \dot{a}_o + \Omega^2 \frac{2}{\gamma} P^2 a_o + \Omega^2 \left(\frac{c_{1s}}{2} - \frac{k_{1c}}{2}\right) a_1 - \Omega \frac{c_{1s}}{2} \dot{b}_1$$

$$- \Omega \frac{c_{2c}}{2} \dot{a}_2 - \Omega^2 \left(c_{2c} + \frac{k_{2s}}{2}\right) b_2 - \Omega^2 \frac{m_{1s}}{2} \theta_s = \Omega^2 m_o \theta_o \tag{13}$$

$$\Omega\, c_{1s}\, \dot{a}_o + \Omega\, \frac{4}{\gamma}\, \dot{a}_1 + \Omega^2 \left(c_o - \frac{c_{2c}}{2} - \frac{k_{2s}}{2}\right) a_1 - \frac{2}{\gamma}\, \ddot{b}_1 - \Omega \left(c_o - \frac{c_{2c}}{2}\right) \dot{b}_1$$

$$+ \Omega^2\, \frac{2}{\gamma}\, (1 - P^2)\, b_1 + \Omega \left(\frac{c_{1s}}{2} - \frac{c_{3s}}{2}\right) \dot{a}_2 + \Omega^2 \left(c_{1s} - c_{3s} - \frac{k_{1c}}{2} + \frac{k_{3c}}{2}\right) b_2$$

$$- \Omega^2 \left(m_o - \frac{m_{2c}}{2}\right) \theta_s = \Omega^2\, m_{1s}\, \theta_o \qquad (14)$$

$$\Omega^2\, k_{1c}\, a_o - \frac{2}{\gamma}\, \ddot{a}_1 - \Omega \left(c_o + \frac{c_{2c}}{2}\right) \dot{a}_1 + \Omega^2\, \frac{2}{\gamma}\, (1 - P^2)\, a_1 - \Omega\, \frac{4}{\gamma}\, \dot{b}_1$$

$$- \Omega^2 \left(c_o + \frac{c_{2c}}{2} + \frac{k_{2s}}{2}\right) b_1 + \Omega^2 \left(c_{1s} + c_{3s} - \frac{k_{1c}}{2} - \frac{k_{3c}}{2}\right) a_2$$

$$- \Omega \left(\frac{c_{1s}}{2} + \frac{c_{3s}}{2}\right) \dot{b}_2 - \Omega^2 \left(m_o + \frac{m_{2c}}{2}\right) \theta_c = 0 \qquad (15)$$

$$\Omega^2\, k_{2s}\, a_o - \Omega \left(\frac{c_{1s}}{2} + \frac{c_{3s}}{2}\right) \dot{a}_1 - \Omega^2 \left(\frac{c_{1s}}{2} + \frac{c_{3s}}{2} + \frac{k_{1c}}{2} - \frac{k_{3c}}{2}\right) b_1$$

$$+ \Omega\, \frac{8}{\gamma}\, \dot{a}_2 + \Omega^2 \left(2\, c_o - c_{4c} - \frac{k_{4s}}{2}\right) a_2 - \frac{2}{\gamma}\, \ddot{b}_2 - \Omega \left(c_o - \frac{c_{4c}}{2}\right) \dot{b}_2$$

$$+ \Omega^2\, \frac{2}{\gamma}\, (4 - P^2)\, b_2 - \Omega^2 \left(\frac{m_{1s}}{2} + \frac{m_{3s}}{2}\right) \theta_c = 0 \qquad (16)$$

$$\Omega\, c_{2c}\, \dot{a}_o - \Omega^2 \left(\frac{c_{1s}}{2} - \frac{c_{3s}}{2} + \frac{k_{1c}}{2} + \frac{k_{3c}}{2}\right) a_1 + \Omega \left(\frac{c_{1s}}{2} - \frac{c_{3s}}{2}\right) \dot{b}_1$$

$$- \frac{2}{\gamma}\, \ddot{a}_2 - \Omega \left(c_o + \frac{c_{4c}}{2}\right) \dot{a}_2 + \Omega^2\, \frac{2}{\gamma}\, (4 - P^2)\, a_2 - \Omega\, \frac{8}{\gamma}\, \dot{b}_2$$

$$- \Omega^2 \left(2\, c_o + c_{4c} + \frac{k_{4s}}{2}\right) b_2 + \Omega^2 \left(\frac{m_{1s}}{2} - \frac{m_{3s}}{2}\right) \theta_s = \Omega^2\, m_{2c}\, \theta_o \qquad (17)$$

It is noted that retention of harmonics up to the fourth order of the periodic coefficients is required to be consistent with the assumed second order flapping solution.

The terms in the control system equations of motion which are functions of rotating flapping responses (β_i), must be modified to be consistent with equations 13 to 17. Specifically, the pitch and roll feedbacks reduce to

$$\frac{1}{2}\left[(\beta_4 - \beta_2)\sin\psi + (\beta_1 - \beta_3)\cos\psi\right] = -a_1 \tag{18}$$

$$\frac{1}{2}\left[(\beta_3 - \beta_1)\sin\psi + (\beta_4 - \beta_2)\cos\psi\right] = b_1 \tag{19}$$

and the equations become

$$\dot{\delta}_s + L\Omega\,\delta_s = A\Omega\left(-a_1 + \theta_{long}\cos\Gamma - \theta_{lat}\sin\Gamma\right) \tag{20}$$

$$\dot{\delta}_c + L\Omega\,\delta_c = A\Omega\left(b_1 - \theta_{lat}\cos\Gamma - \theta_{long}\sin\Gamma\right) \tag{21}$$

The equations of motion of the actuators are in an acceptable form since they contain only constant coefficients.

The nine equations of motion can be collected and expressed in matrix notation as

$$\left[D\right]\left\{\epsilon\right\} = \left[E\right]\left\{\eta\right\} \tag{22}$$

where $\left[D\right]$ is called the dependent variable matrix and $\left[E\right]$ the independent variable matrix. $\left\{\epsilon\right\}$ is a column matrix of the dependent variables.

$$\left\{\epsilon\right\} = \begin{Bmatrix} a_o \\ a_1 \\ b_1 \\ a_2 \\ b_2 \\ \delta_s \\ \delta_c \\ \theta_s \\ \theta_c \end{Bmatrix} \tag{23}$$

and $\{\eta\}$ is a column matrix of independent variables.

$$\{\eta\} = \begin{Bmatrix} \theta_o \\ \bar{\theta}_s \\ \bar{\theta}_c \\ \theta_{long} \\ \theta_{lat} \end{Bmatrix} \qquad (24)$$

In order to determine the frequency response of the system, equation 22 is first transformed into the La Place domain

$$[D(s)]\{\epsilon(s)\} = [E(s)]\{\eta(s)\} \qquad (25)$$

where s is the La Place operator and then into the frequency domain by substituting $j\omega$ for s. Table VII contains values of the Fourier coefficients of the periodic functions as a function μ. A tip loss factor of $B = 0.97$ has been assumed and the effects of reversed flow are accounted for.

Stability

The stability of the system was calculated from the results of the theoretical frequency response analysis using the techniques described in Section 6. Closed loop stability margins are directly measureable from the open loop frequency response curves.

Closed loop stability was also determined theoretically using matrix Floquet theory. Floquet theory leads to a method by which the roots of a linear system with periodic coefficients can be obtained. A description of the theory and the steps required to implement it can be found in Reference 4.

Both the frequency-analysis method and Floquet theory yield usable stability data. Each has its advantages and disadvantages. The Floquet solution considers equations with periodic coefficients and the damping and frequency

TABLE VII. VALUES OF FOURIER COEFFICIENTS FOR PERIODIC FUNCTIONS

Function	Coefficient	μ					
		0	0.4	0.8	1.2	1.6	2.0
C (ψ)	c_o	0.2213	0.2220	0.2342	0.2798	0.3447	0.4148
	c_{1s}	0	0.1200	0.2199	0.2596	0.2697	0.2742
	c_{2c}	0	-0.0010	-0.0171	-0.0753	-0.1427	-0.2055
	c_{3s}	0	0.0006	0.0100	0.0409	0.0617	0.0727
	c_{4c}	0	0.0003	0.0043	0.0142	0.0061	-0.0079
K (ψ)	k_{1c}	0	0.1223	0.2547	0.4225	0.6487	0.9374
	k_{2s}	0	0.0366	0.1335	0.2538	0.3692	0.4805
	k_{3s}	0	-0.0009	-0.0149	-0.0735	-0.1907	-0.3546
	k_{4s}	0	0.0005	0.0085	0.0411	0.0913	0.1425
m_{θ_o} (ψ)	m_o	0.2213	0.2582	0.3591	0.4960	0.6429	0.7931
	m_{1s}	0	0.2448	0.5100	0.8460	1.2980	1.8750
	m_{2c}	0	-0.0366	-0.1335	-0.2537	-0.3695	-0.4810
	m3s	0	-0.0006	-0.0100	-0.0490	-0.1269	-0.2363

of all natural modes are calculated. Results are also quickly and economically obtained which allows a thorough assessment of all parametric variations. The disadvantage lies in the use of the results at the test site. It is generally difficult to extract comparable modal dampings and frequencies from test data. Consequently, an immediate measure of the experimental degree of stability of the model which can be compared with analysis is not available during the test. The frequency-analysis method, on the other hand, is conducted in exactly the same manner for either theoretical or experimental analyses. Therefore, a comparison of theory and test results is immediately possible. The method has several mild disadvantages however. The equations of motion must be simplified to remove periodicity of the coefficients, only the stability of the least stable mode is identified and a thorough analysis of a multiple loop system is lengthy.

COMPARISON OF THEORETICAL AND EXPERIMENTAL RESULTS

It is clear that of the eight equations of motion representing the model, only the rotor description is subject to verification. The control system is precisely defined and the actuator equations, while not exact, represent the hardware quite accurately. Any disagreement can be easily quantified and appropriate corrections made to the theoretical results. It is correct, therefore, to state that the total system mathematical model is as valid as the rotor model. With this in mind, several representative comparisons of theoretical and experimental rotor transfer functions will be shown. The implication is that, if agreement exists, theoretical closed loop results calculated for the same conditions $(V,\Omega R)$ are valid. If the theory and test data do not agree, the analytical closed loop results, again at the same conditions, are also suspect.

The next eight figures present comparisons of theoretical and experimental rotor frequency response data. The selected conditions are representative of the agreement obtained for all the data. Figures 52 and 53 show the rotor transfer functions with respect to θ_o at $\mu = 0.40$ and 800 rpm. The longitudinal response $\frac{a_1}{\theta_o}$ correlates well except at those frequencies where the test data are suspect. The theoretical and experimental lateral response derivatives $\frac{b_1}{\theta_o}$ generally exhibit the same trends with frequency, again with the exception of the test data which are affected by the stand shake. The magnitudes, however, do not correlate well particularly at low excitation frequencies. It is noted that the same disagreement was also observed in a similar correlation of the steady state $(\omega=0)$ Phase 1 data.

Figures 54 and 55 present the correlation of transfer functions with respect to θ_c also at $\mu = 0.4$ and 800 rpm. Generally good agreement is noted. More peaking of the lateral response is seen in the experimental data than the theory. The inference is that the theory is conservative from a stability point of view. As noted earlier, the support stand appears to be excited only mildly by lateral cyclic pitch and therefore to have a reduced effect on the test data.

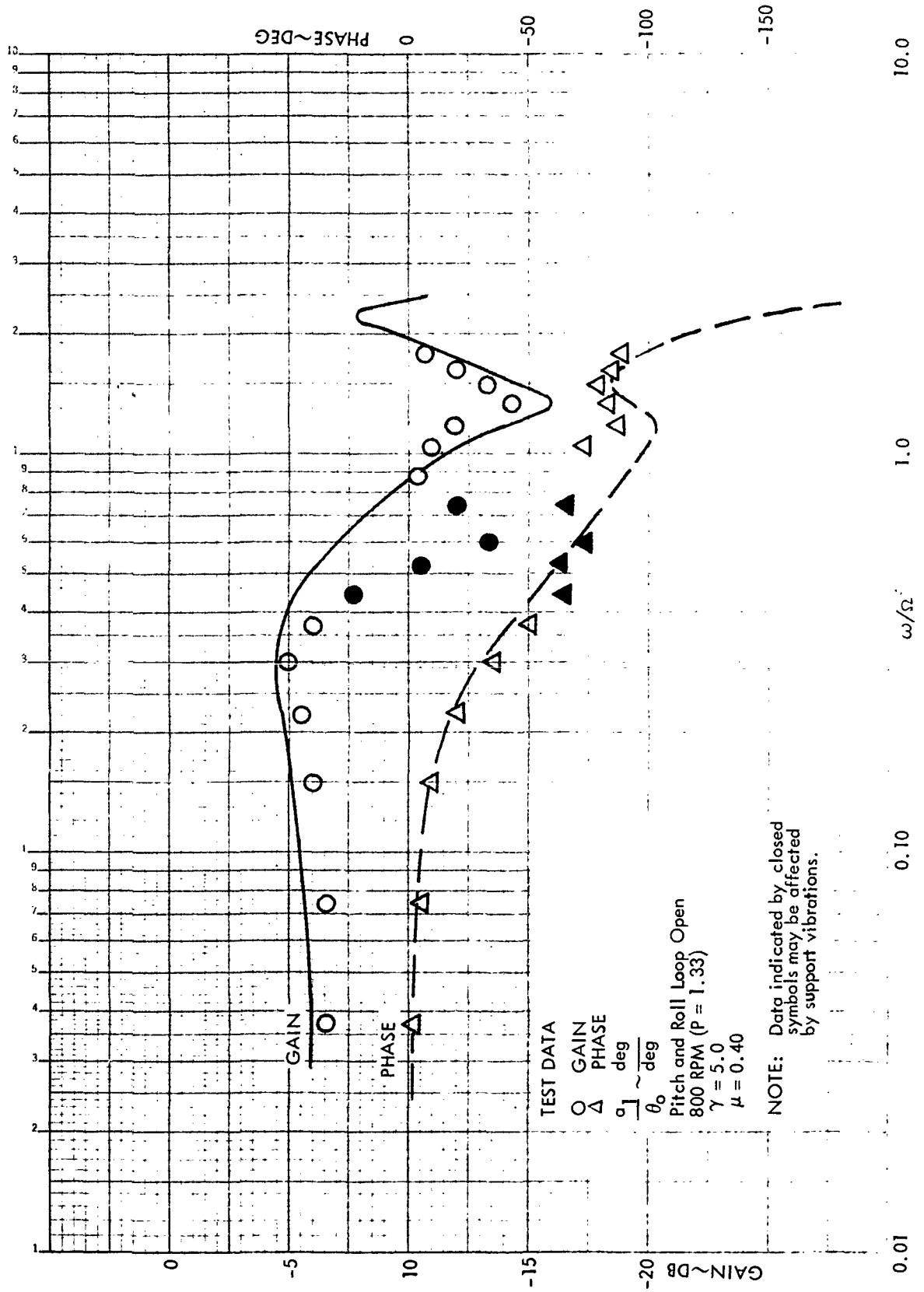

Figure 52. Comparison of Theoretical and Experimental Rotor Transfer Functions, Longitudinal Frequency Response to θ_o, $\mu = .40$, 800 rpm ($P = 1.33$), $\gamma = 5.0$

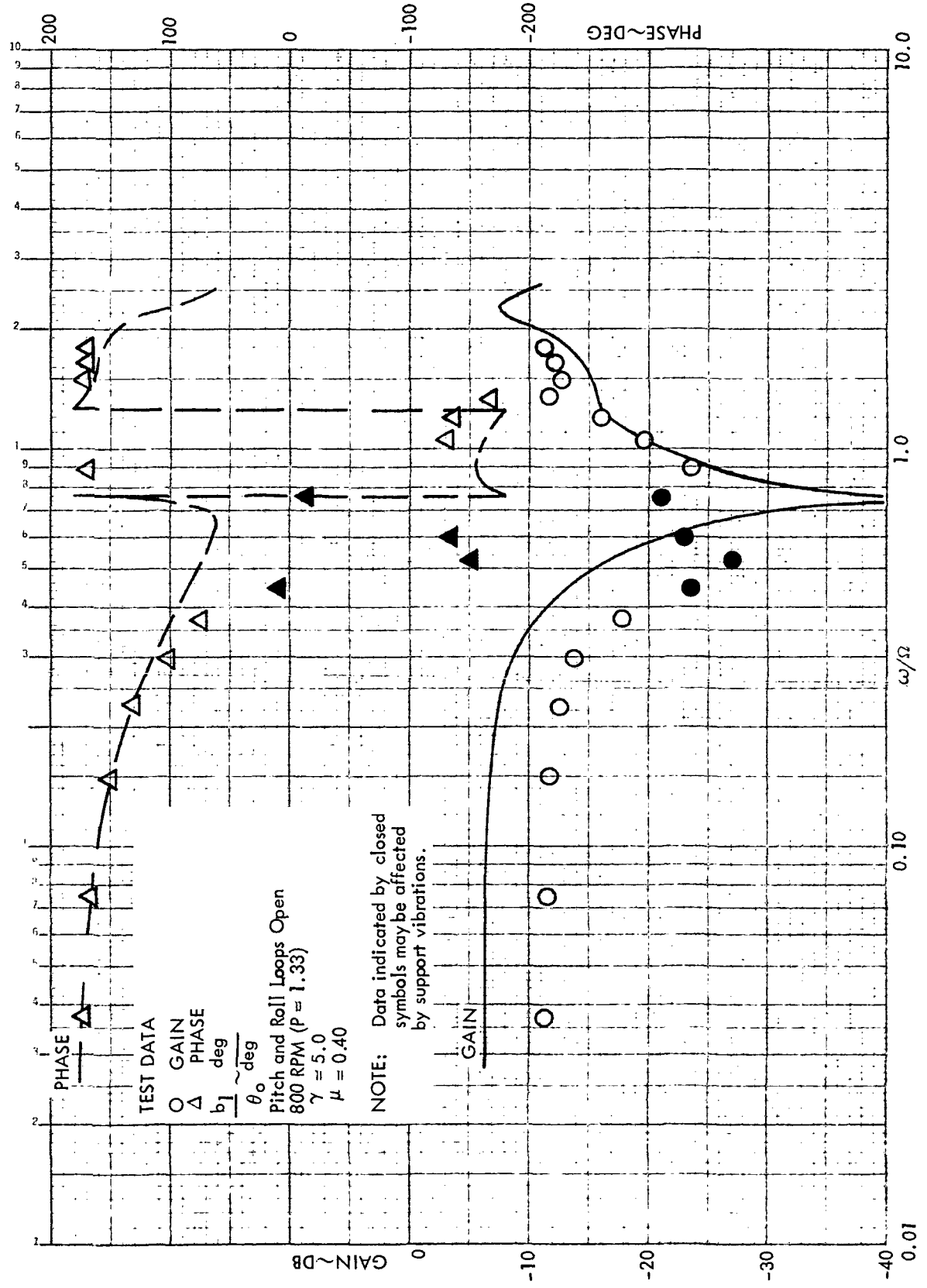

Figure 53. Comparison of Theoretical and Experimental Rotor Transfer Functions, Lateral Frequency Response to θ_o, μ = .40, 800 rpm (P = 1.33), γ = 5.0

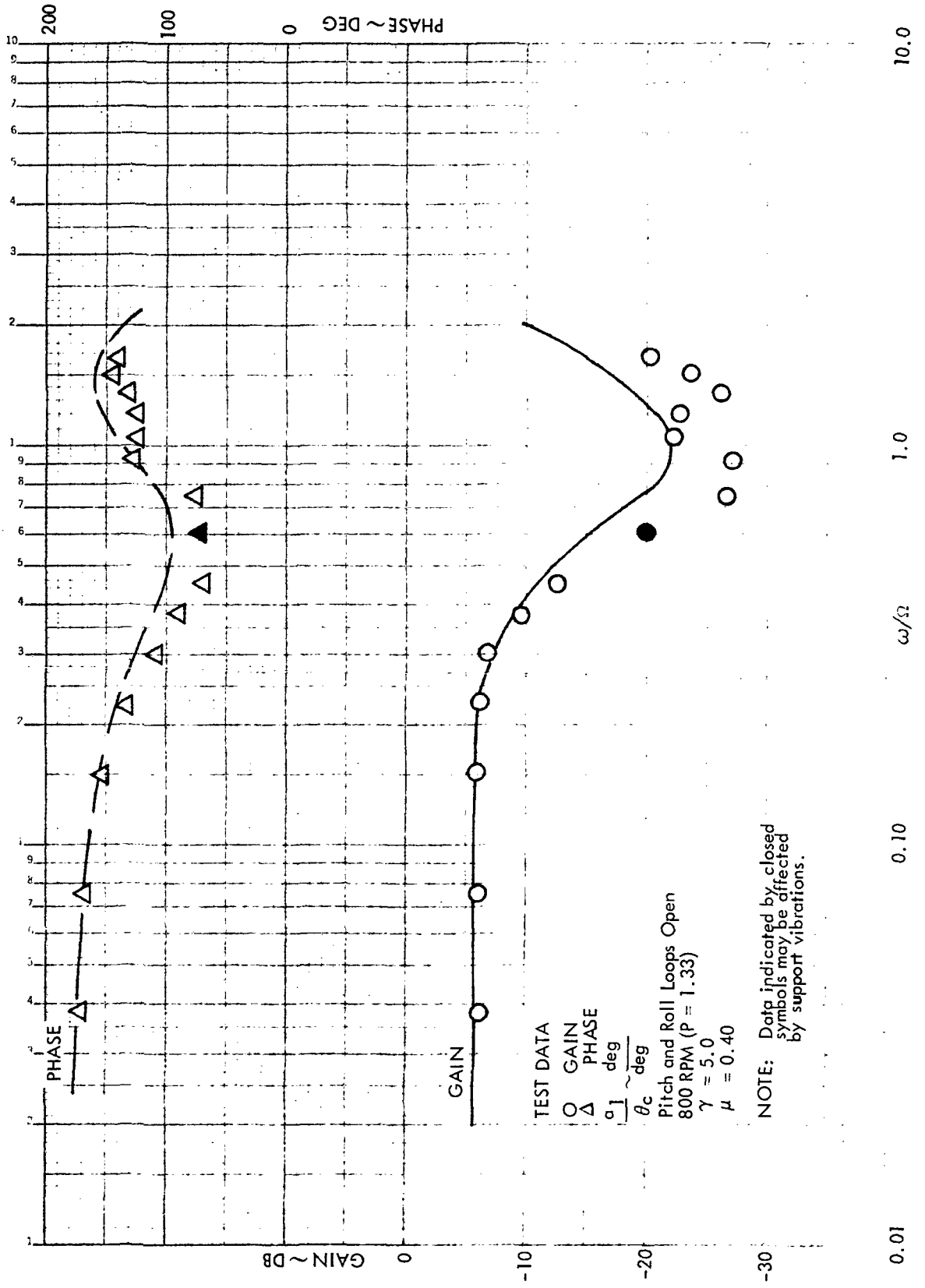

Figure 54. Comparison of Theoretical and Experimental Rotor Transfer Functions, Longitudinal Frequency Response to θ_c, μ = .40, 800 rpm (P = 1.33), γ = 5.0

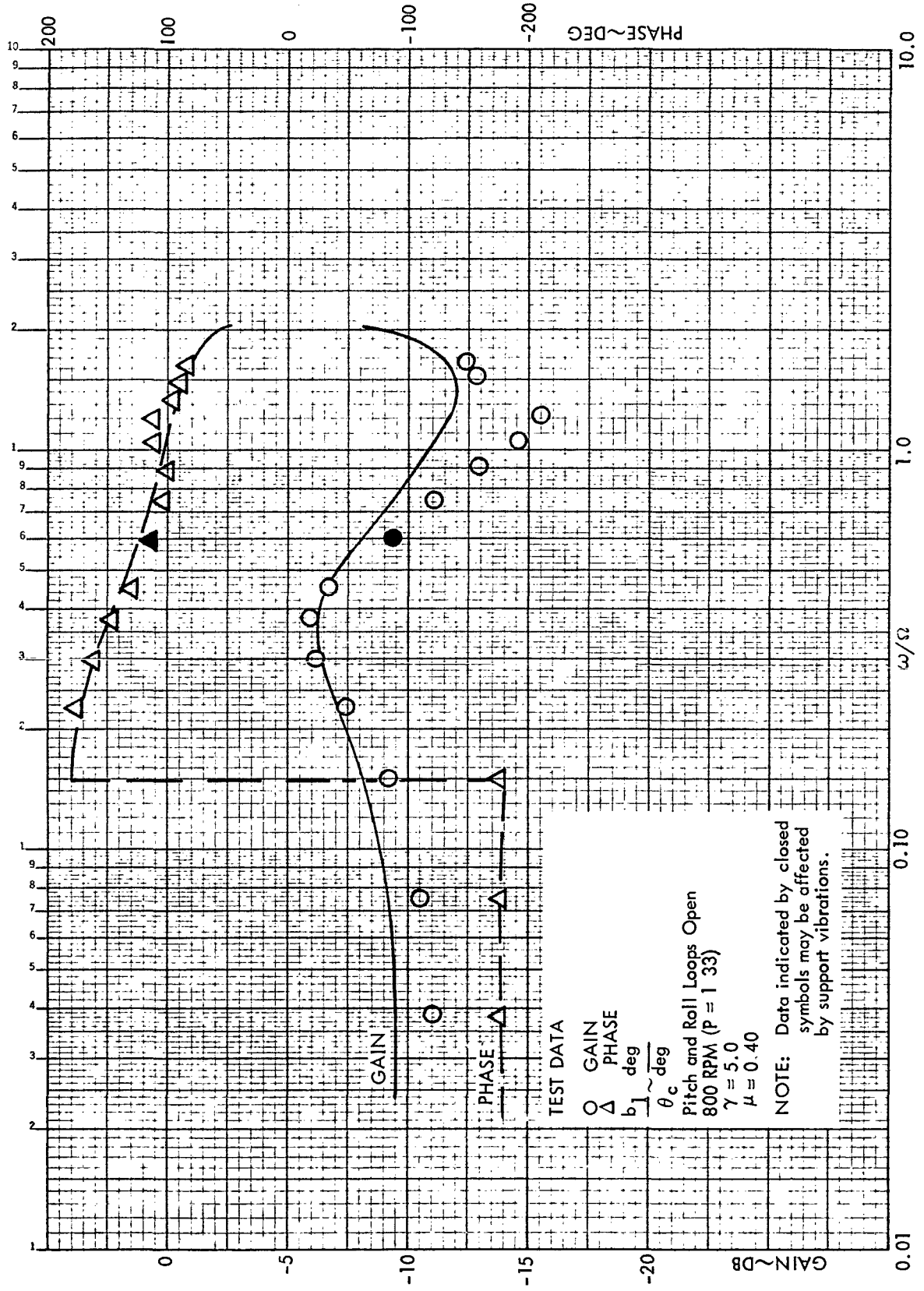

Figure 55. Comparison of Theoretical and Experimental Rotor Transfer Functions, Lateral Frequency Response to θ_c, μ = .40, 800 rpm (P = 1.33), γ = 5.0

Figures 56 to 59 show typical correlations of rotor frequency response at lower rotor speeds. Without discussing each curve separately, the following observation is offered. The agreement between theory and test data is markedly improved at the lower rpms. The probable reason is the apparent stiffening of the rotor flapping restraint (P).

One final observation is offered regarding the experimental stability margins presented earlier in the report. The correlation of theoretical and experimental rotor transfer functions at 800 rpm (P=1.33) reveals that the gross effect of the support stand vibrations is to reduce the magnitude of the rotor response over a certain frequency range. It happens that the depression in the gain curve occurs at frequencies where gain margins are determined. Therefore one would expect the gain stability of the rotor which was determined experimentally, to be greater than that which would be calculated theoretically. Since phase margins are generally ascertained at frequencies well below the range where the vibration is influential, they are unaffected. It is important to recognize that the experimental stability data are peculiar to the tested model and of necessity include the effect of the dynamic response of the support stand.

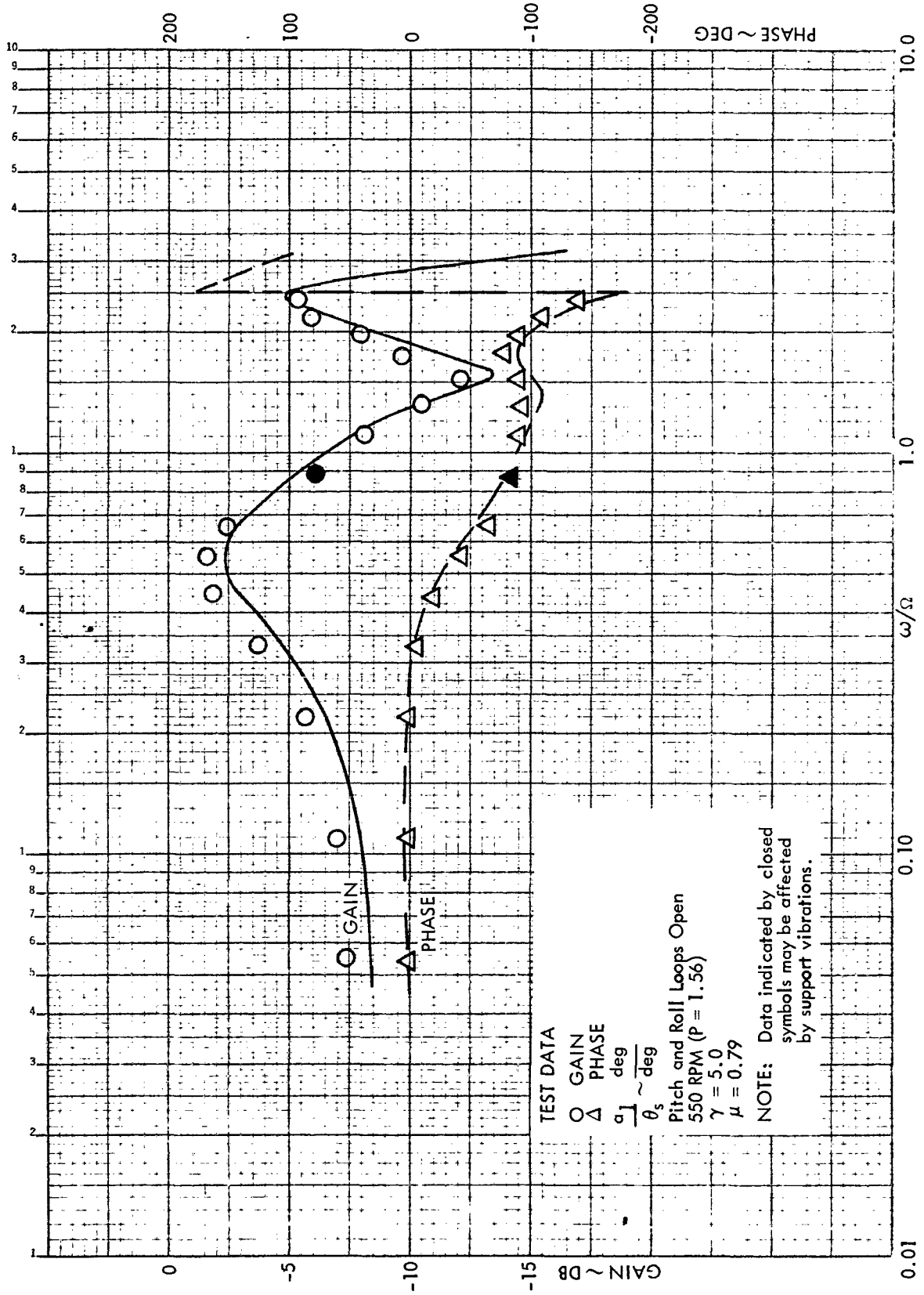

Figure 56. Comparison of Theoretical and Experimental Rotor Transfer Functions, Longitudinal Frequency Response to θ_s, μ = .79, 550 rpm (P = 1.56), γ = 5.0

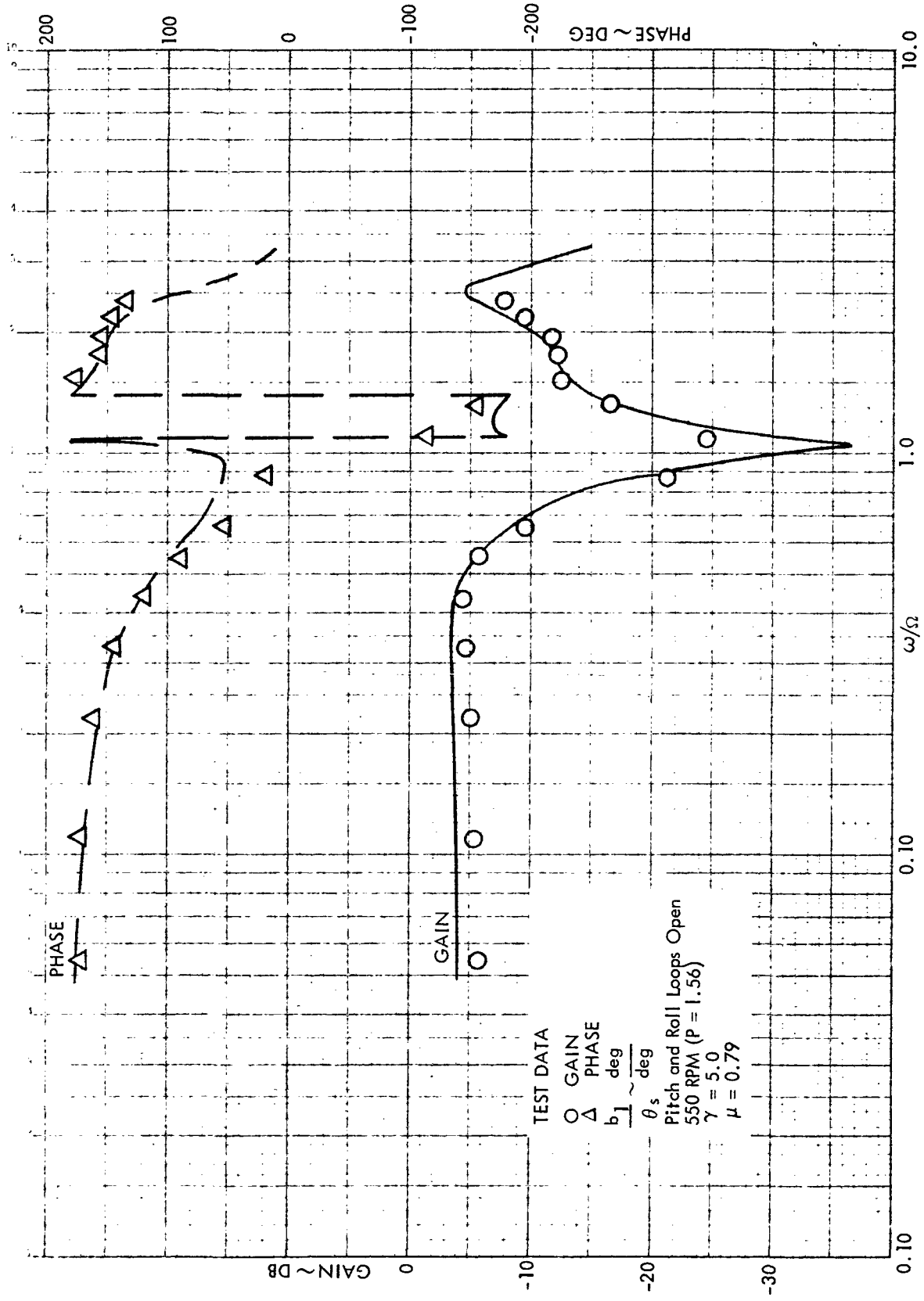

Figure 57. Comparison of Theoretical and Experimental Rotor Transfer Functions, Lateral Frequency Response to θ_s, μ = .79, 550 rpm (P = 1.56), γ = 5.0

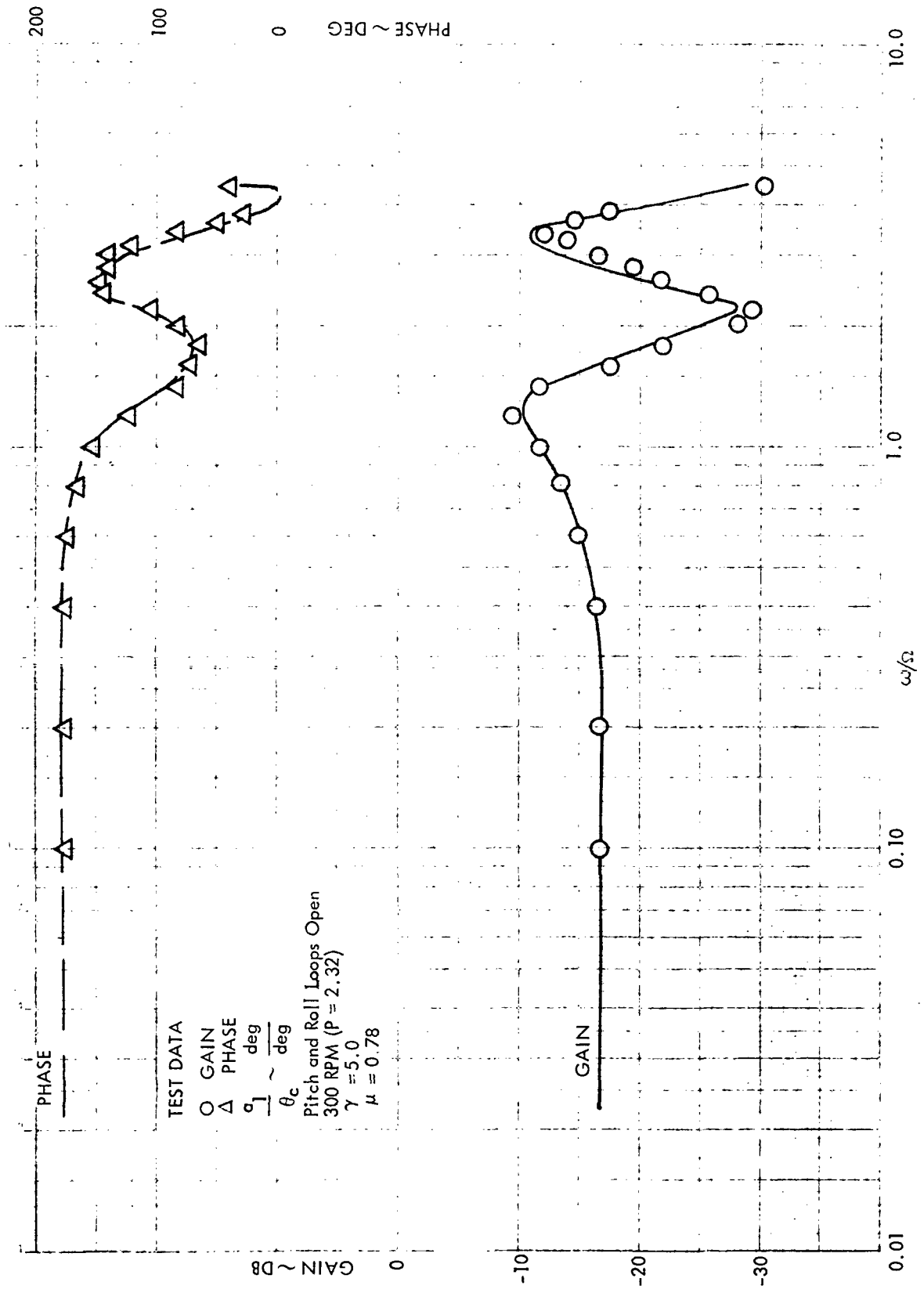

Figure 58. Comparison of Theoretical and Experimental Rotor Transfer Functions, Longitudinal Frequency Response to θ_c, μ = .78, 300 rpm (P = 2.32), γ = 5.0

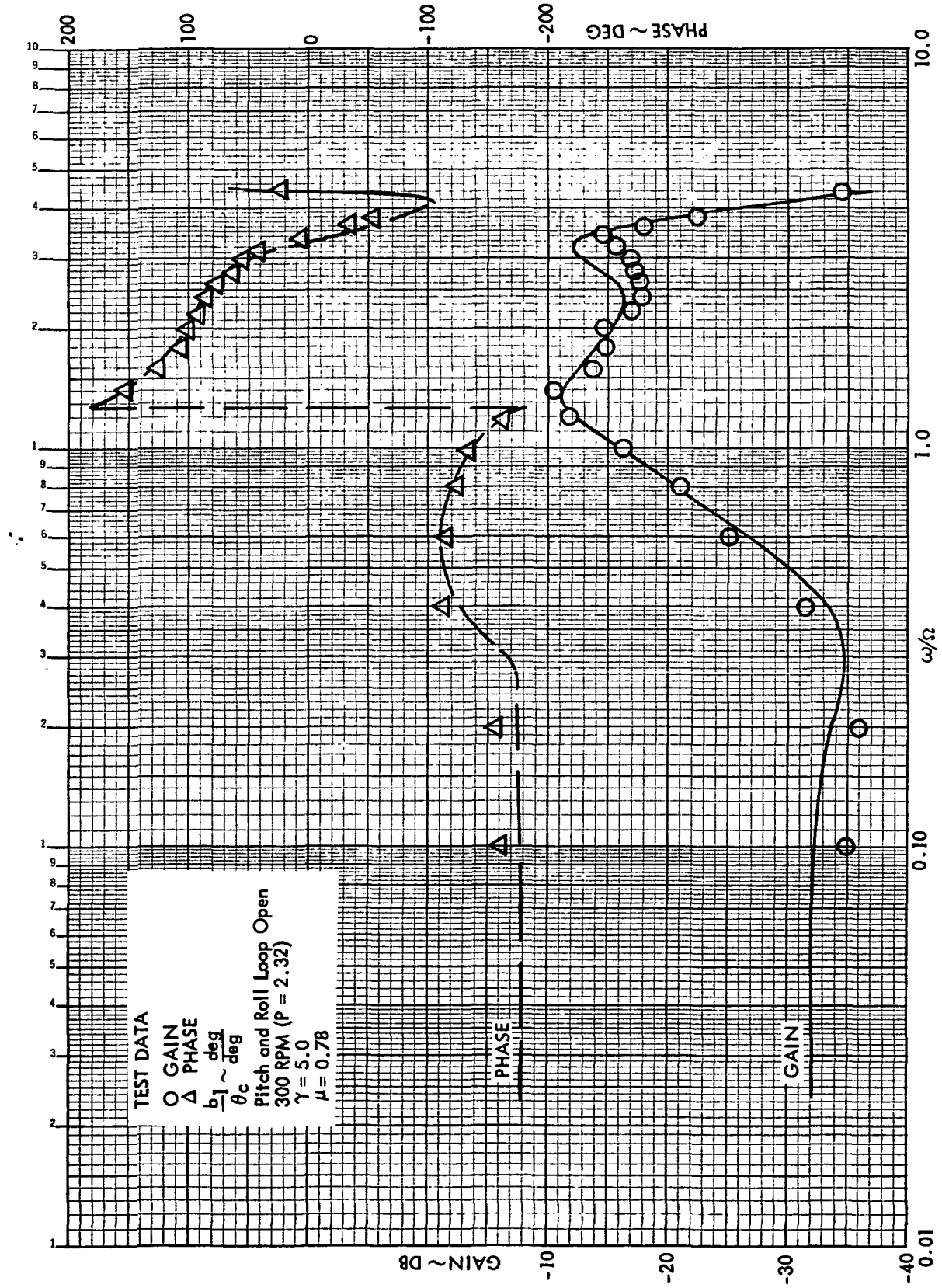

Figure 59. Comparison of Theoretical and Experimental Rotor Transfer Functions, Lateral Frequency Response to θ_c, μ = .78, 300 rpm (P = 2.32), γ = 5.0

LOCKHEED CALIFORNIA COMPANY

SECTION 8

CONCLUDING REMARKS

The second phase of the Lockheed/AMRDL High Advance Ratio Research Program has been successfully completed. The study is marked by the following achievements.

A hingeless rotor model equipped with an electrical first order lag hub moment feedback control system was tested at advance ratios from 0 to 1.44 and flapping frequencies which ranged from 1.33Ω to 2.32Ω. The response characteristics of the system were determined for several control system parameter combinations including the ideal case where the control filters have infinite time constants and therefore provide total alleviation of response to steady external disturbances. Both the stability and response characteristics of the closed loop system have been examined. A need for optimization of the control system (type) with respect to transient response characteristics has been identified.

The hingeless rotor data bank initiated by the Phase 1 test results has been expanded in two ways. First, additional steady-state rotor response derivatives with respect to α, θ_o, θ_s and θ_c have been obtained at a rotational speed of 1200 rpm. These data lower the nondimensional flapping frequency where experimental data are available at a Lock number of 5.0 to P = 1.17. Second, the data bank has been expanded by the acquisition of rotor longitudinal and lateral response transfer functions with respect to θ_o, θ_s and θ_c. These data were obtained for a Lock number of 5.0 at flapping frequencies from 1.30Ω to 2.32Ω and advance ratios ranging from 0 to 1.44. The frequency response data may be used for an immediate evaluation of control systems other than the type selected for the Phase 2 program.

The correlation of the theoretical and experimental rotor frequency response data has shown the rigid flapping mathematical rotor model to be quite adequate particularly at higher flapping frequencies.

The third phase of the High Advance Ratio Research Program will further enhance the hingeless rotor data bank already established. Softer flexures will be tested at higher advance ratios thereby expanding the μ/P envelope of data. Rotor frequency response to shaft pitching and rolling oscillations will be also acquired for the first time.

SECTION 9

REFERENCES

1. W. A. Kuczynski, G. J. Sissingh, "Research Program to Determine Rotor Response Characteristics at High Advance Ratios," NASA CR114290, February 1971

2. G. J. Sissingh, "Review and Discussion" of "On the Dynamics of Lifting Rotors with Thrust or Tilting Moment Feedback Controls," Journal of the American Helicopter Society, 15(1) 54-58 (January 1970)

3. G. J. Sissingh, "Dynamics of Rotors Operating at High Advance Ratios," Journal of the American Helicopter Society, 13(3) 56-63 (July 1968)

4. W. A. Kuczynski, D. L. Sharpe, "Hingeless Rotor Characteristics at High Advance Ratios," presented at the AIAA 4th Fluid and Plasma Dynamics Conference, June 21 - 23, 1971, Palo Alto, California

APPENDIX A

ANALYSIS OF FREQUENCY RESPONSE DATA

The initial analysis of the digitized FM data was conducted with the Fast Fourier Transform (FFT) program (Cooley-Tukey Algorithm). This method was used because a residue rotor frequency response (see Appendix B) was anticipated at many sum and difference frequencies. It was immediately discovered that while the technique clearly identified the frequencies at which the response occurred, the calculated magnitudes and phases were only approximately determined. This is due to the fact that the FFT calculates the transform at discrete frequencies which are not necessarily exactly the same as those at which the response occurs. The error was a function of the number of cycles of data analyzed (i.e., record length) and the discrepancy in the frequency. The situation is illustrated by the following example.

Consider the function

$$f(t) = \sin \Omega t \tag{A1}$$

If the frequency Ω were unknown and a harmonic analysis performed, the coefficients of the first harmonic response of f(t) are defined as:

$$A_1 = \frac{\omega}{\pi N} \int_0^{\frac{2\pi N}{\omega}} \sin \Omega t \cos \omega t \, dt \tag{A2}$$

$$B_1 = \frac{\omega}{\pi N} \int_0^{\frac{2\pi N}{\omega}} \sin \Omega t \sin \omega t \, dt \tag{A3}$$

where N is the number of cycles of data and ω the prescribed harmonic analysis frequency.

Evaluating the integrals yields

$$A_1 = \frac{1}{\pi N} \frac{\nu}{\nu^2 - 1} \left[\cos\left(\frac{2\pi N}{\nu}\right) - 1\right] \tag{A4}$$

$$B_1 = \frac{1}{\pi N} \frac{\nu^2}{1-\nu^2} \sin\left(\frac{2\pi N}{\nu}\right) \tag{A5}$$

where $\nu = \frac{\omega}{\Omega}$

It is noted that (by L'Hospital's Rule)

$$\lim_{\nu \to 1} A_1 = 0 \tag{A6}$$

$$\lim_{\nu \to 1} B_1 = 1 \tag{A7}$$

which of course is the known correct solution.

The magnitude

$$MAG = \sqrt{A_1^2 + B_1^2} \tag{A8}$$

and phase

$$PHASE = ARCTAN \left(\frac{B_1}{A_1}\right) \tag{A9}$$

are plotted in Figure 60 as a function of ν and N. The curves clearly show that the calculated harmonic content of f(t) is in error if $\nu \neq 1$ and the percentage error increases with an increase in the number of cycles of data analyzed.

Even though the FFT analysis introduced errors in the magnitude and phase angle of the data, it was still capable of calculating correct linear transfer functions. The reason, of course, was that all signals analyzed at a specific frequency were incorrect by the same percentage. Consequently, the errors were totally compensated when the ratios of the magnitudes and differences in phases were taken. Since for residue frequency response two

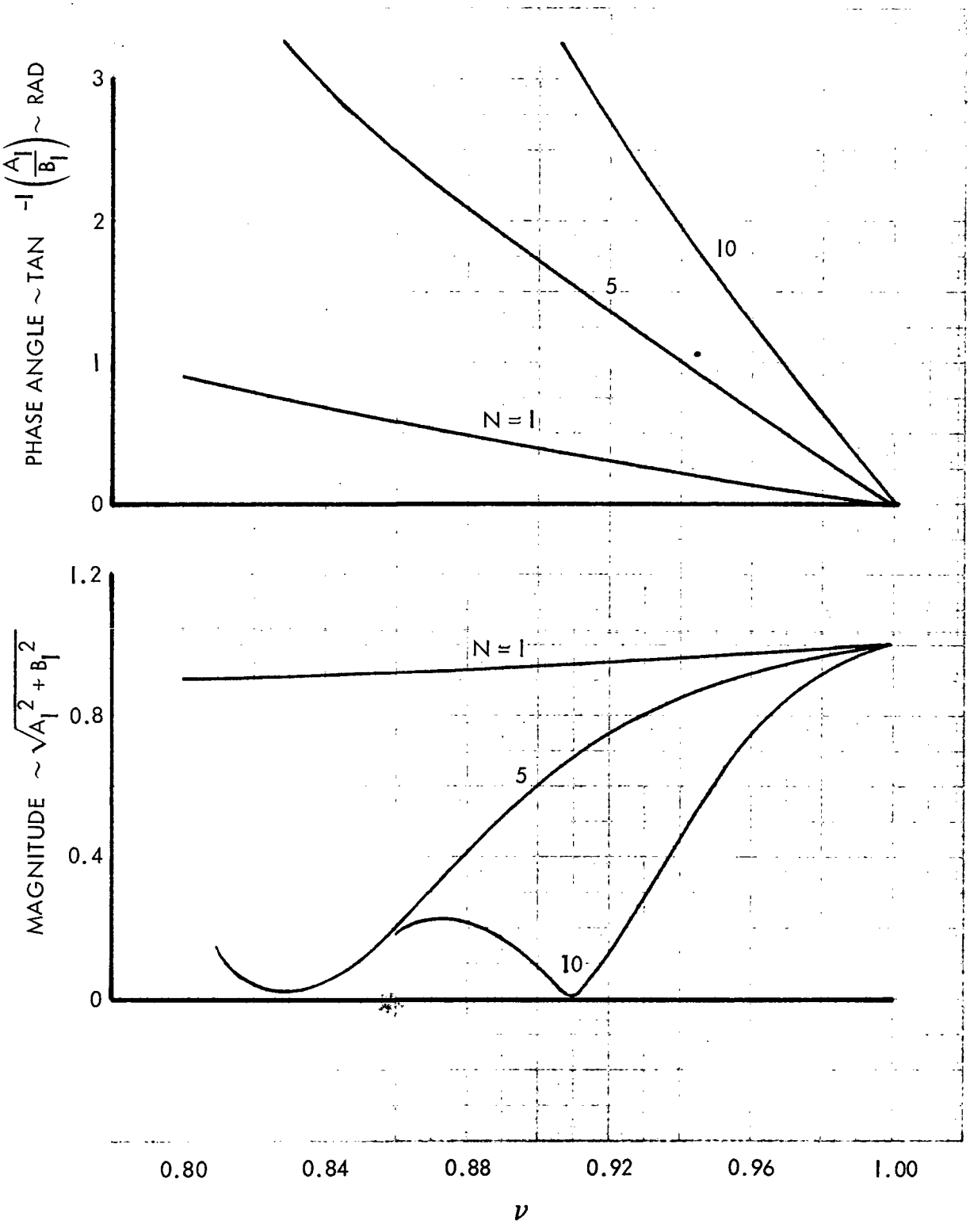

Figure 60. Harmonic Analysis Error Generated by Incorrect Frequency Selection

different frequencies are associated, the FFT was unsuited for these calculations. With only linear transfer functions obtainable from the FFT program, its further use was unjustifiable from an economic standpoint and the following more direct analysis approach was taken.

Both the oscillator output and a one-per-rev signal were recorded and digitized. Therefore the rotational and excitation frequencies could be determined directly from the test data. Once these were known, it was a simple matter to Fourier analyze the data of interest at combinations of ω and Ω. Sufficient data were analyzed at the sum and difference frequencies to verify the FFT results pertaining to the residue frequency response. Thereafter, the discrete Fourier Transform program was used to determine linear transfer functions. Either 13 seconds or 100 cycles of data were analyzed in order to minimize the effects of tunnel turbulence and other sources of noise. It is interesting to note that an automatic check of the accuracy of ω is provided by the Fourier analysis. Since approximate magnitudes of the excitations $\left(\theta_o, \theta_s, \theta_c\right)$ were known from the test log, errors in ω are indicated by large discrepancies between the known and calculated values. With 100 cycles of data analyzed, a very small error in ω generated a very large error in the magnitude of the excitation. For most of the data the values of ω determined from the test data were exact.

APPENDIX B

A DISCUSSION OF THE ROTOR 'RESIDUE' FREQUENCY RESPONSE

The term 'residue', as used in the following discussion, refers to the response of the rotor at the sum and difference frequencies $(n\Omega \pm \omega)$ $n > 0$. This characteristic is not generated by classical nonlinear excitations but rather by the periodic aerodynamic coefficients and forcing functions in the linear system. It is emphasized that all of the frequency response data presented in the main body of this report are linear. This discussion is offered to familiarize the reader with the fundamental mechanism which generates the nonlinear motion.

Consider, as an example, the nondimensional excitation of the flapping motion by longitudinal cyclic pitch. An oscillatory θ_s input

$$\theta_s \sin \omega t \tag{B1}$$

produces a blade feathering motion

$$\theta = \theta_s \sin \omega t \sin \Omega t \tag{B2}$$

$$\theta = \frac{\theta_s}{2} \left[- \cos (\Omega + \omega) t + \cos (\Omega - \omega) t \right] \tag{B3}$$

which in turn generates an excitation of blade flapping of the form

$$\begin{aligned} \theta m_{\theta_o}(\psi) &= \theta_s \sin \omega t \sin \Omega t \; m_{\theta_o}(\psi) \\ &= \frac{\theta_s}{2} \Big[2n_o \sin \omega t - r_{1s} \cos (\Omega + \omega) t \\ &+ n_{1s} \cos (\Omega - \omega) t + n_{2c} \sin (2\Omega + \omega) t \\ &+ n_{2c} \sin (2\Omega - \omega) t + n_{3s} \cos (3\Omega + \omega) t \\ &- n_{3s} \cos (3\Omega - \omega) t + n_{4c} \sin (4\Omega + \omega) t \\ &+ n_{4c} \sin (4\Omega - \omega) t + \ldots \ldots \end{aligned} \tag{B4}$$

The coefficients (n_o, n_{is}, n_{ic}) are calculable from the Fourier coefficients for $m_{\theta_o}(\psi)$ (see Table VII). Since a linear system will respond at the frequencies with which it is excited, the blade can be expected to flap at the frequencies

$$|n\,\Omega \pm \omega| \qquad n = 0, 1, 2, 3, 4, \ldots \tag{B5}$$

If all blades are assumed to flap identically, it can be shown that the rotor moments obtained by resolving rotating flapping moments occur at the driving frequency ω only. However, there is no reason to expect the rotor blades to flap identically for all conditions. This is particularly true of the flapping response to high frequency excitations. If dissimilar flapping motions do occur, residual nonrotating rotor moments will be generated at the sum and difference frequencies ($n\Omega \pm \omega$). The strength of the moments will depend upon the magnitudes of the high frequency aerodynamic excitations and the variance in the flapping of the four blades.

In order to examine the experimental residue rotor frequency response, a spectral analyses of the following digitized time history data were performed.

- Rotating Blade Feathering Angle
- Rotating Blade Flapping Moment
- Nonrotating Rotor Pitching Moment
- Nonrotating Rotor Rolling Moment

The Fast Fourier Transform (FFT) program (Cooley-Tukey Algorithm) was used. It provided the approximate magnitude (and phase) of the responses at 1023 discrete frequencies over the range 0.5113 → 523.09 rad/sec.

Figures 61 and 62 illustrate the results of the analysis at a low excitation frequency. The magnitudes of the Fourier transforms of the four responses are presented. For the selected case, the rotor is excited by longitudinal cyclic pitch. The excitation frequency ω is 25.15 rad/sec and magnitude of θ_s is 1.35 deg. The rotor rotational frequency Ω is ~ 83.78 rad/sec (800 rpm) and $\mu = 0.66$. As discussed above the frequencies of interest are:

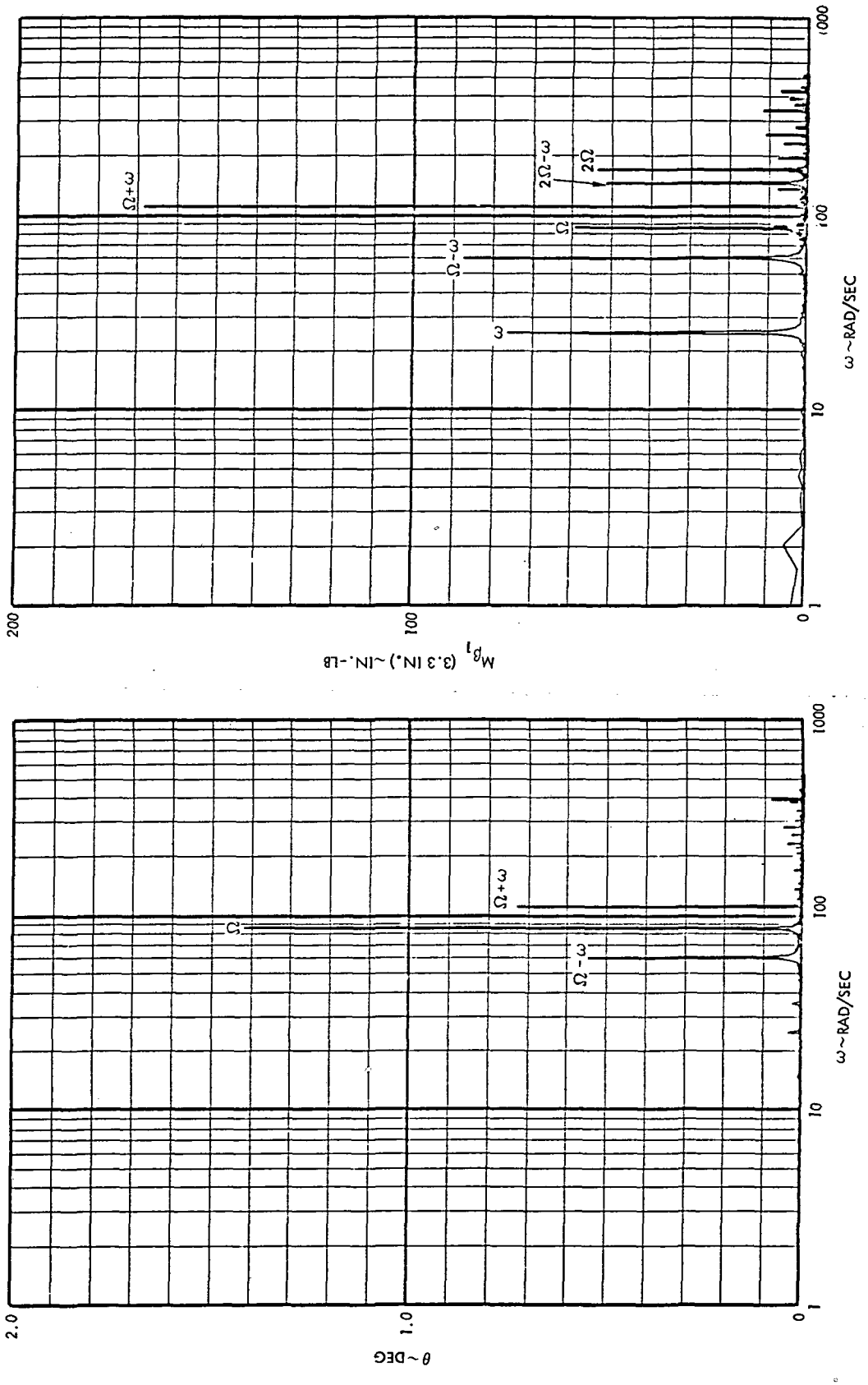

Figure 61. Magnitudes of the Fourier Transforms of Blade Flapping Moment and Blade Feathering Angle, θ_s - Excitation, 800 rpm (P = 1.33), μ = 0.66, Excitation Frequency = 25 rad/sec

LOCKHEED CALIFORNIA COMPANY

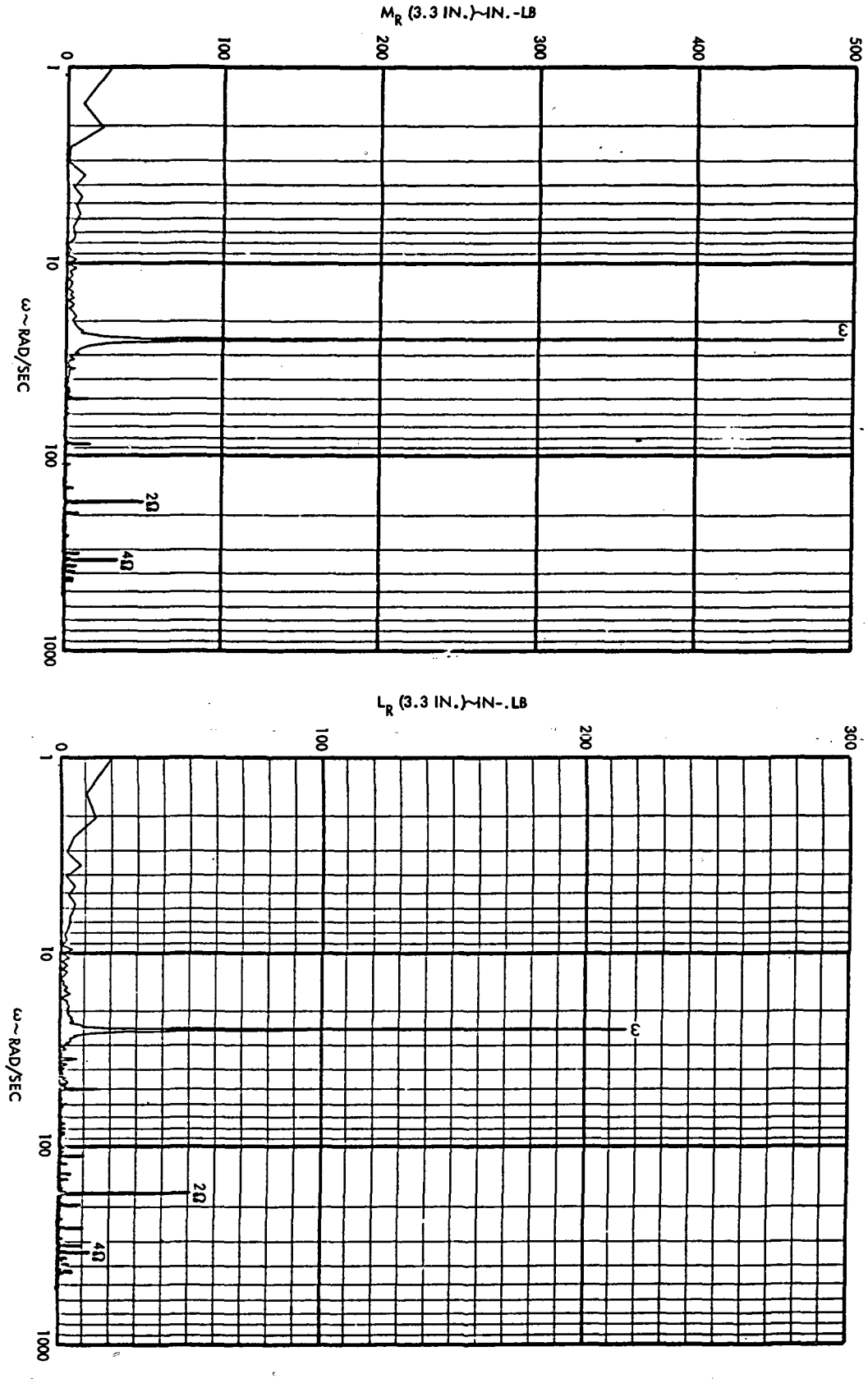

Figure 62. Magnitudes of the Fourier Transforms of the Rotor Pitching and Rolling Moments, θ_s - Excitation, 800 rpm (P = 1.33), μ = 0.66, Excitation Frequency = 25 rad/sec

LOCKHEED CALIFORNIA COMPANY

$$\omega = 25.15 \text{ rad/sec}$$

$$\Omega - \omega = 58.63 \text{ rad/sec}$$

$$\Omega + \omega = 108.93 \text{ rad/sec}$$

$$2\ \Omega - \omega = 142.41 \text{ rad/sec}$$

$$2\ \Omega + \omega = 192.71 \text{ rad/sec}$$

$$3\ \Omega - \omega = 226.19 \text{ rad/sec}$$

$$3\ \Omega + \omega = 276.49 \text{ rad/sec}$$

$$4\ \Omega - \omega = 309.97 \text{ rad/sec}$$

$$4\ \Omega + \omega = 360.27 \text{ rad/sec}$$

Responses at harmonics of the rotor frequency Ω will also occur which are generated by nonoscillatory excitations and are to be anticipated.

Figure 61 presents the transform of rotating blade feathering motion. Peaks in the response are noted at $\sim$ 110 rad/sec and $\sim$ 60 rad/sec. These frequencies correspond respectively to the sum and difference frequencies $\Omega + \omega$ and $\Omega - \omega$. A peak is also observed at $\sim$ 85 rad/sec. This reflects the steady cyclic pitch required to trim the rotor before the oscillating input was applied. The other small peaks are spurious noise, the largest of which occurs at $\sim$ 60 cps (377 rad/sec).

The blade flapping response is also shown in Figure 61. As predicted, response occurs at

$$\sim 25 \text{ rad/sec}, \ \omega$$

$$\sim 60 \text{ rad/sec}, \ \Omega - \omega$$

$$\sim 110 \text{ rad/sec}, \ \Omega + \omega$$

$$\sim 140 \text{ rad/sec}, \ 2\Omega - \omega$$

Significant peaks are also noted at $\sim$ 85 rad/sec and $\sim$ 170 rad/sec. The response at 85 rad/sec is one-per-rev flapping and indicates the rotor was slightly out of trim. The response at 2Ω ($\sim$ 170 rad/sec) is generated by

the trim cyclic pitch and the steady external disturbances. Other small peaks can be seen at the higher sum and difference frequencies. However, since they are of the same order of magnitude as the noise, they are not expected to generate measurable rotor moment responses.

The rotor moment responses are plotted in Figure 62. The curves clearly show that in the process of resolving the rotating blade moments into stationary signals only the response at the excitation frequency ω persists. The smaller peak at $\sim$ 330 rad/sec is normal 4-per-rev vibration and the response at $\sim$ 170 rad/sec (2Ω) is caused by minor rotor mistrack.

Consider now, a case exactly the same as the previous one except with an excitation frequency of ω = 124.67 rad/sec. The frequencies of interest are now:

$$\omega = 124.67 \text{ rad/sec}$$
$$\omega + \Omega = 208.45 \text{ rad/sec}$$
$$\omega - \Omega = 40.89 \text{ rad/sec}$$
$$2\Omega - \omega = 42.89 \text{ rad/sec}$$
$$2\Omega + \omega = 292.23 \text{ rad/sec}$$
$$3\Omega - \omega = 126.67 \text{ rad/sec}$$
$$3\Omega + \omega = 376.01 \text{ rad/sec}$$
$$4\Omega - \omega = 210.45 \text{ rad/sec}$$
$$4\Omega + \omega = 459.79 \text{ rad/sec}$$

Figures 63 and 64 show the magnitudes of the four Fourier transforms. As expected the feathering angle responds at the frequencies Ω, $\omega - \Omega$ and $\omega + \Omega$. Anticipated peaks in the flapping response at Ω , 2Ω , ω , $\omega + \Omega$, $\omega - \Omega$, $2\Omega - \omega$ and $3\Omega - \omega$ are also noted. For this case, however, the moments (Figure 64) have a significant response at the frequency $\omega + \Omega$ as well as at ω . As indicated earlier this residual response is caused by dissimilar flapping motions of the four blades.

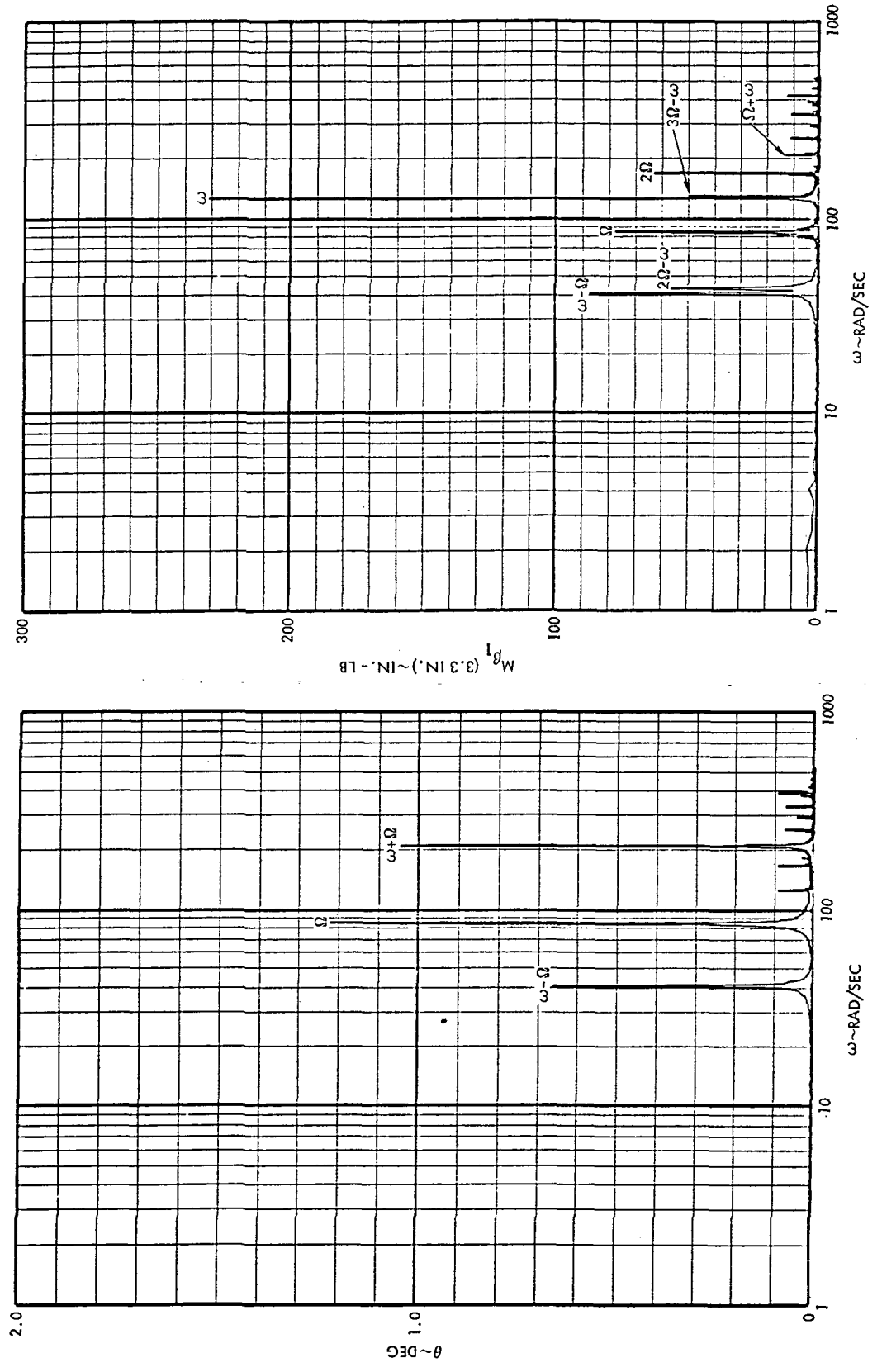

Figure 63. Magnitudes of the Fourier Transforms of Blade Flapping Moment and Blade Feathering Angle, θ_s - Excitation, 800 rpm (P = 1.33), μ = 0.66, Excitation Frequency = 125 rad/sec

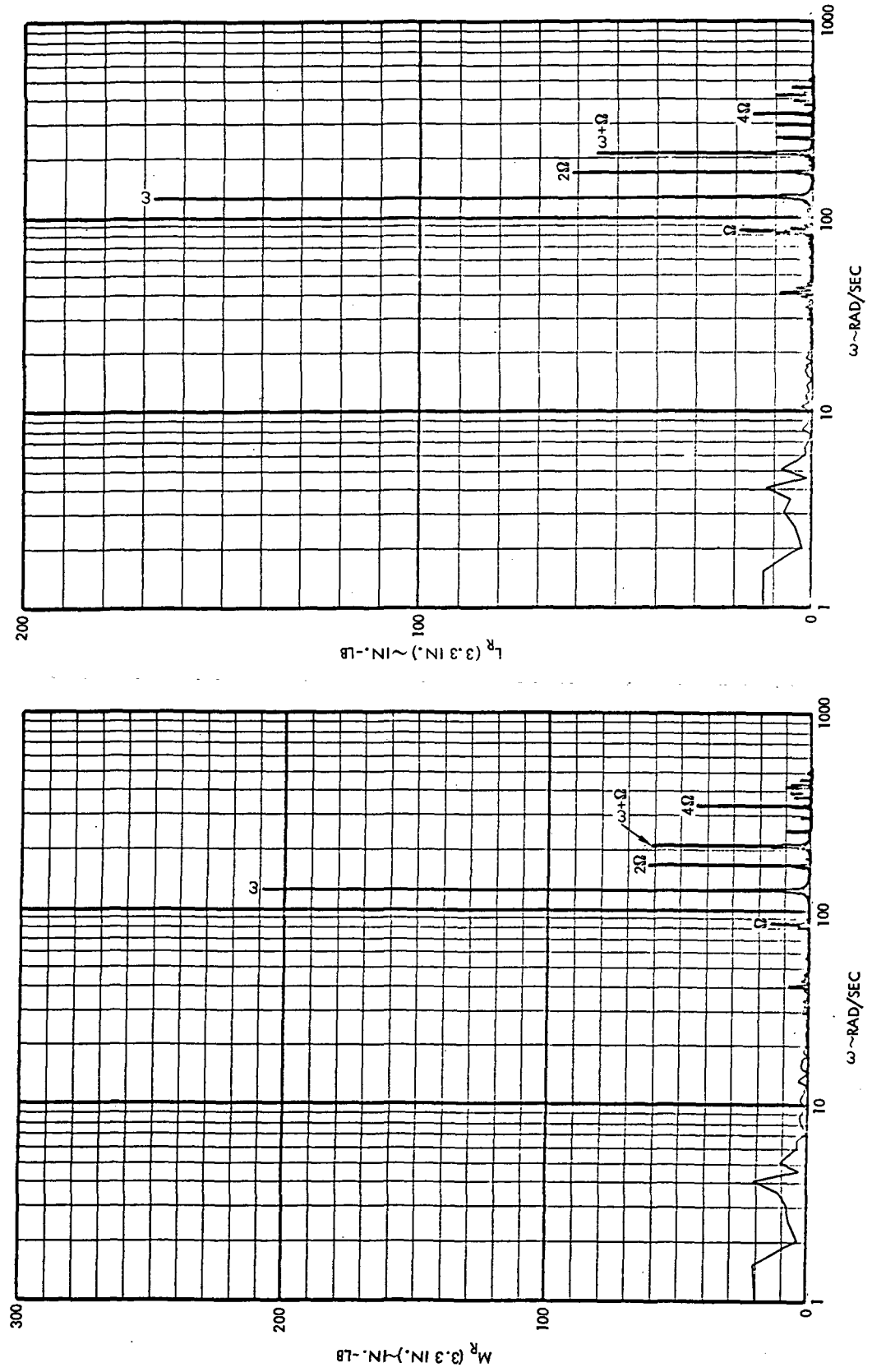

Figure 64. Magnitudes of the Fourier Transforms of the Rotor Pitching and Rolling Moments, θ_s - Excitation, 800 rpm (P = 1.33), μ = 0.66, Excitation Frequency = 125 rad/sec

LOCKHEED CALIFORNIA COMPANY

From the examples and discussion presented it is clear that a residue frequency response does occur and that its strength depends upon the magnitude of the higher harmonic aerodynamic forcing functions in combination with the frequency of the excitation. It is important to recognize, however, that while a residue frequency response may exist, it does not affect the linear transfer functions. By the principle of superposition, the total response of the rotor is simply a linear combination of the responses at the sum and difference frequencies and the excitation frequency.